J. R. Boer 4907361

Control section of prestressed members without shear reinforcement

Improvements to the next generation of Eurocode 2 around intermediate supports

Delft University of Technology

Control section of prestressed members without shear reinforcement

Improvements to the next generation of Eurocode2 around intermediate supports

by

J.R. Boer

to obtain the degree of Master of Science
at the Delft University of Technology,
to be defended publicly on Friday May 16, 2025 at 11:00.

Faculty of Civil Engineering and Geoscience
Track Structural Engineering

Student number:	4907361	
Thesis committee:	Dr.ir. Y. Yang	TU Delft, chairman
	Prof.dr.ir. J. G. Rots	TU Delft, supervisor
	M. S. Ibrahim	TU Delft, Supervisor
	Dr.ir. N. Ramos	Rijkswaterstaat, External supervisor

An electronic version of this thesis is available at *https://repository.tudelft.nl/*

Preface

Before you lies the report that marks the end of my journey as a MSc student Civil Engineering, with a specialisation in structural engineering at Delft University of Technology. In this thesis, the location of the critical crack of prestressed continuous beams has been investigated using a variety of methods.

Roughly six and a half year ago I started my bachelor Civil Engineering in Delft. Since then, I have encountered many complex topics that seemed impossible to understand. At first I was disheartened, but I gradually developed patience and the mindset required to study effectively. Strangely enough, as I reach the end of this journey, I am grateful for these challenges. Their difficulty pushed me to grow in ways I never could have imagined.

I would like to thank my main supervisors, Yuguang Yang and Mohammed Ibrahim for guiding me through this project. Their support was indispensable in overcoming difficulties and understanding unexpected results. I would also like to thank my other Committee members; Jan Rots for helping me better understand the results found with the Finite Element Method and Nathalie Ramos for providing comments to improve my work. Apart from the thesis committee members I would like to deeply thank Beyazit Aydin, who spend many hours helping me outside his work hours. Finally, I would like to express my heartfelt gratitude to my family and friends for their support and encouragement. Their kindness and understanding helped me find my way when I felt lost, and I am deeply grateful to them.

Jesper Boer
Delft, May 2025

Abstract

Currently a new Eurocode is in development where the shear capacity will be based on the Critical Shear Crack Theory (CSCT), rather than a purely empirical model. The newly introduced formulae provide good results overall and include the effects of bending moments on the shear capacity. However, the formulae are known to be too conservative for prestressed continuous beams with low amounts of shear reinforcement and severely underestimate the shear capacity. If these formulae are applied, many existing structures would therefore no longer meet the code requirements. New structures with prestressed continuous elements would also require more material and it may become difficult to design efficient concrete members that meet the new code requirements.

To prevent substantial costs, emissions and time investments, it was questioned if the design capacity of prestressed beams near intermediate supports could be increased by changing the location of the control section from 1d away from supports to the critical cross section. The location of the control cross section greatly influences the shear resistance according to the CSCT calculation. However, it is unclear how the critical cross section can be determined accurately.

In this thesis the location of the critical cross section near intermediate supports was investigated for prestressed continuous beams with less than the minimum required shear reinforcement. A small number of models and experiments from literature were compared. Additionally, multiple Finite Element Analyses have been performed with a variety of settings, assuming different shear behaviour. A plasticity approach was also investigated, where the critical cross section is found at the location where the cracking load equals the ultimate load of a crack.

This thesis found that the reinforcement ratios, prestressing stress, shear span and effective depth (as well as the concrete strength in lesser amount) influence the location of the critical cross section. The experiments and models found in literature, as well as the results found using the plasticity approach, indicate that the critical cross section for prestressed beams may be moved from 1d to 1.5d away from intermediate supports. However, due to the limitations and assumptions of the models it would not be safe to apply this change without further validation. It is therefore recommended that experiments are done on prestressed continuous beams with low amounts of shear reinforcement before any changes are made to the location of the control section.

Table of contents

Nomenclature

Symbol	Definition	Unit
A_c	Cross sectional area of concrete	mm^2
A_{sl}	Cross sectional area of longitudinal reinforcement	mm^2
A_{sw}	Cross sectional area of transverse reinforcement	mm^2
a	Shear span	mm
a_{cs}	Effective shear span with respect to the considered control section	mm
a_{eff}	Effective shear span	mm
a_v	Mechanical shear span	mm
b	Width of an element	mm
b_w	Smallest width of a concrete member transferring shear	mm
$C_{Rd,c}$	Design safety factor for shear, recommended value is equal to 0.12	-
c	Depth of the compression zone	mm
d	Effective depth	mm
d_{dg}	Roughness parameter of the crack, taking into account the aggregate sizes. D_{dg}= 16mm +D_{lower} <=40 mm for concrete f_{ck}<= 60 MPa	mm
d_f	Vertical distance between the tip of the crack and the longitudinal reinforcement	mm
d_g	Maximum aggregate size	mm
d_{lower}	Smallest value of the upper sieve size D, for the coarsest aggregates used in the concrete	mm
d_{nom}	Nominal value of the effective depth	mm
d_p	Effective depth of the prestressing steel	mm
d_s	Effective depth of the reinforcement steel	mm
d_v	Effective shear depth according to AASHTO LRFD	mm
E_c	Modulus of elasticity concrete	MPa
E_p	Modulus of elasticity prestressing steel	MPa
E_s	Modulus of elasticity steel	MPa
e_p	Eccentricity of the axial forces from the centroid of the element	mm
F_{po}	Modulus of elasticity of prestressing tendons multiplied with strain difference between concrete and prestressing tendons.	MPa
f_1	Principal tensile stress	MPa
f_2	Principal compression stress	MPa
f_c	Concrete compressive strength	MPa
f_{cd}	Design concrete compressive strength	MPa
f_{ck}	Characteristic concrete compressive strength	MPa
f_{cm}	Mean concrete compressive strength	MPa
f_{ct}	Concrete tensile strength	MPa
f_{ctm}	Mean concrete tensile strength	MPa
f_u	Ultimate strength of the reinforcement	MPa
f_y	Yield strength of reinforcement	MPa
f_{yd}	Design yield strength of reinforcement	MPa
f_{yk}	Characteristic value of the yield strength of the reinforcement	MPa
G_c	Compressive fracture energy of concrete	N/mm
G_F	Tensile fracture energy of concrete	N/mm
h	Height of the concrete member	mm
k	Size factor for shear calculations in Eurocode2	-
k_1	Effectiveness factor of the prestressing term	-
k_n	Normal stiffness modulus	N/mm^3
k_t	Shear stiffness modulus	N/mm^3
k_{vp}	Coefficient considering the effects of axial forces	-

L	Length or span of the considered concrete member	mm
L_0	Length of the loading plate	mm
M	Acting moment (without design factors)	kNm
M_{cr}	Cracking moment	kNm
M_{Ed}	Design value of the acting moment	kNm
M_u	Factored acting moment according to AASHTO LRFD	kNm
N	Acting normal force (without design factors)	kN
N_{Ed}	Design value of the acting normal force	kN
N_u	Factored acting normal force according to AASHTO LRFD	kN
P	Prestressing force acting on the concrete	kN
P_{cr}	Cracking load	kN
P_u	Ultimate load	kN
q	Distributed loading	kN/m
r_f	Horizontal distance from the load introduction or intermediate support to the tip of the crack	mm
s	Stirrup spacing	mm
V	Acting shear (without design factors)	kN
V_a	Shear force transferred by aggregate interlocking	kN
V_c	Shear force transferred by inclined compression chord	kN
V_d	Shear force transferred by the dowel action	kN
V_{Ed}	Design value of the acting shear	kN
V_{exp}	Experimentally found shear capacity	kN
V_p	Component of the prestressing force in the direction of the shear force	kN
V_R	Shear capacity (without design factors)	kN
$V_{Rd,c}$	Design value of the concrete shear capacity	kN
$V_{Rd,max}$	Maximum design value of the shear capacity	kN
$V_{Rd,s}$	Design value of the steel shear capacity	kN
V_t	Shear force transferred by the residual tensile strength of the concrete	kN
V_u	Factored acting shear according to AASHTO LRFD	kN
v_{min}	Minimum shear capacity of a concrete element	MPa
w	Crack width	mm
x_a	Horizontal location of the onset of the crack	mm
x_f	Horizontal location of the tip of the crack	mm
x_L	Horizontal length of the crack	mm
z	Lever arm of internal forces	mm
α_{cw}	A Coefficient taking account of the stress state in the compression chord	-
β	Factor indicating the ability of cracked concrete to transfer tension	-
β_1	Crack angle measured between the locations where crack intersects the reinforcement and d/2 above the reinforcement	°
β_{AB}	Crack angle measured between the locations where crack intersects the reinforcement and the neutral axis	°
β_{BF}	Crack angle measured between the location where crack intersects the reinforcement and the crack tip	°
γ_v	Partial factor for shear, γ_v= 1.4 for persistent and transient design situations	-
ε	Strain at a depth of 0.6d from the most compressed fibre.	-
ε_1	Principal tensile strain	-
ε_s	Strain at the longitudinal reinforcement	-
θ	Crack angle	°
ν_1	A strength reduction factor for cracked concrete	-
ρ_l	Longitudinal reinforcement ratio	-
ρ_w	Transverse reinforcement ratio	-
$\rho_{w,min}$	Minimum transverse reinforcement ratio according to the Eurocode	-
σ_{cp}	Average compressive stresses in the concrete, caused by prestressing forces.	MPa

$\tau_{Rd,c}$	Design shear resistance of concrete	MPa
$\tau_{Rdc,min}$	Minimum design shear resistance of concrete	MPa
ϕ	Longitudinal reinforcement degree	-
$\omega_{w,ct}$	Mechanical reinforcement ratio related to concrete tensile strength	-

1. Introduction

Throughout the world, concrete has been commonly used in the design of structures such as bridges and buildings even though some of its behaviour, such as the shear behaviour, is still widely debated. This uncertain concrete behaviour means that many different codes with different underlying models can be found on the design and assessment of concrete structures. One of these codes, the Eurocode, is used in Europe and is currently undergoing changes to the calculations and underlying models. As a result, the formula for shear capacity of concrete without shear reinforcement will no longer be based on purely empirical models. The formula will instead be based on a more theoretical approach, the Critical Shear Crack Theory (CSCT), where the capacity is determined by multiple shear transfer actions that influence and are influenced by the critical crack. The important difference compared to the current model, is that the acting moment and forces influences the shear capacity. For this reason, iteration is required at multiple cross-sections to find the global shear capacity.

The location of the control cross section is an important parameter when determining the shear capacity with the newly proposed Eurocode. According to the proposed Eurocode, the control sections that must be investigated are located at a distance 1d from static and geometric discontinuities. However, for prestressed continuous beams with low amounts of shear reinforcement overconservative estimates are obtained, which may cause problems for both new and existing structures. It is questioned whether the control section should be moved. After all, the distance 1d is based on a 45-degree shear crack angle, while prestressed concrete with low amounts of shear reinforcement is expected to have smaller crack angles. With smaller crack angles the critical control section would be located at a distance x > 1d from the support, where the capacity is increased. However, it is still unclear how the critical crack angle and thus the critical control section can be determined accurately.

This research aims to determine the critical cross section for prestressed continuous beams with low amount of shear reinforcement, so that the design capacity may be increased. The research question of this thesis is: "How can the location of the first control section, around intermediate supports, be determined and implemented to improve the proposed Eurocode, for prestressed concrete elements with less than the minimum required shear reinforcement?"
The following question should be answered during this research:

- What are the differences between the old formula, and the proposed formulae? and why should the new formulae be improved?
- What methods can be used to estimate the shear crack angle or critical cross section?
- What is the expected location of the shear critical cross-section near intermediate supports for prestressed beams with less than the required amount of shear reinforcement.
- What are the limitations of the models/estimates of the critical shear crack location?
- Can the models/estimates be implemented in the proposed Eurocode without any other changes to the proposal in a safe manner?

This research aims to investigate the location of the critical shear crack. To achieve this a variety of methods have been used. A literature review has been conducted to investigate if current models or experiments could be used to develop a model for the shear crack, and what modelling techniques could be used otherwise. Afterwards it is investigated if smeared FEM can recreate accurate crack patterns that could serve as alternatives to experimental data. Discrete FEM and the plasticity approach have been used to find the critical crack location in the case the single critical crack governs the behaviour. These two methods clearly show the effects of the shear crack angle/location on the shear capacity. The plasticity method has also been used to identify the effects of different design parameters on the crack angle/location.

This research will consider prestressed reinforced concrete beams with shear reinforcement less than the minimum required amount according to the Eurocode. The focus of this research lies on cross sections close to intermediate supports and consider the effect of bending moment on the shear capacity. During this thesis only literature and software have been used that could be acquired without any cost or were available through the university. Effects related to temperature, dynamics, and alternative materials such as FRC and geopolymer will not be considered.

2. Theories, codes and modelling methods on shear in literature

In this chapter, literature on the shear capacity of concrete members is discussed. This chapter provides the reader with background knowledge and information of relevant theories and design codes. It should become clear why new Eurocode formulas are introduced and why the location of the control section in the proposed Eurocode should be investigated. Finally, a small number of modelling methods, that can be used to model concrete behaviour, are discussed. These modelling methods may be useful in determining the control section for prestressed continuous elements with low amounts of shear reinforcement.

2.1 Background

When shear calculations are done for concrete members, a difference is made between members with and without stirrups (shear reinforcement). When shear reinforcement is applied, the engineer determines the amount of reinforcement that is required to prevent yielding and ensures that the compression chord has enough capacity. Although different codes vary in their assumptions and safety factors the general concept idea of preventing yielding holds. Unfortunately, when no stirrups are applied, the problem becomes more difficult, there is no universally accepted theory to describe this problem. Different design codes therefore use different methods of determining the shear capacity of concrete beams without shear reinforcement.

In the upcoming Eurocode, the calculations will be done based on the Critical Shear Crack Theory (CSCT) instead of empirical formulas. In the CSCT, different shear transfer mechanisms in reinforced concrete together provide the capacity of a concrete element. Individual forces transferred by the shear mechanisms can be determined with complex expressions but are often approximated instead with a much simpler formula. The formula in the CSCT estimates the capacity of a single cross-section, this means that multiple control sections must be investigated. The locations of these control sections have been determined based on experiments with reinforced concrete and are located at a distance d from discontinuities such as supports, point loads and points of contraflexure.

It is important to know that the shear transfer mechanisms and the cracks in the concrete are influencing each other. This means that when the cracking behaviour, such as the slope or roughness, changes so does the capacity of the beam (through the changes of different shear transfer mechanisms) and the location of the critical cross section.

The CSCT is based on experiments without axial loads. Prestressing is considered as a pre-deformation that causes strain in the longitudinal reinforcement. By solving a moment equilibrium of a cross-section an extra factor k_{vp} is obtained and added to the formula used in the CSCT. This term however, assumes that the crack pattern remains the same and that only the strain changes. It is unlikely that the model remains accurate for prestressed element with only this change, as prestressing does influence the crack patterns; the shape and slope of the cracks are influenced.

In (Silva, Mutsuyoshi, & Witchukrangkrai, 2008) the effect of prestressing is investigated on simply supported beams; the crack patterns, and crack angles are recorded for each tested beam. The average crack angles of the reinforced beams are around 40° while those of prestressed beams with concrete compressive stresses of 3 MPa varied between 30 and 35 degrees. This shows that compressive stresses, introduced by prestressing, lower the crack angle. This effect is also observed in other experiments and theories as shown in chapter 3. Inclination of shear cracks in literature.

With different crack patterns, the loads transfer changes. This means the different shear transfer actions contribute differently and the total capacity changes. Additionally, the location of the critical cross-section that has been determined for reinforced concrete does likely not hold as the cracks may be located at different locations and under different angles.

A case study done by (Adviesbureau ir. J.G Hageman B.V., 2021) shows that the results at end supports differ from the results found at intermediate supports. Shear calculations around intermediate supports seem to be much more conservative and increase the unity check considerably. A suggestion has been done that placing a control section at 2d distance from the middle support instead of 1d, can partly reduce the big increase in U.C. and may improve accuracy.

2.2 Mechanical/shear models

The shear capacity of concrete members can be estimated in many ways as there are many different codes and theories describing shear. Many these models, however, are based on empirical data, or the Modified Compressive Field Theory (MCFT). For this reason, a short explanation is given on empirical models, MCFT, as well as the Critical Shear Crack theory (CSCT), which will be the basis of the upcoming Eurocode.

2.2.1 Empirical

The shear behaviour of concrete without stirrups is not yet fully understood. For this reason, models are often based on regression analysis. These empirical models are based on experimental data and can therefore not adequately explain the physics behind shear failure. This means that the empirical model might not consider all variables on which the shear capacity depends. Variables that have been considered, might do not necessarily have the correct relation to the capacity. Furthermore, due to the limited number of experiments, it is possible that the formula/models do not closely relate to reality for elements that differ from the experimental set-up.

However, even though empirical models are not based on physical meaning, they can still be used for design. One reason for this is that empirical models can be relatively accurate, especially for elements that are similar to the ones that have been tested. A second reason is that a lack of knowledge on the shear behaviour, limits the ability to create a simple yet accurate model based on physics (ZSUTTY, 1971). An empirical model, although not completely (physically) accurate, can result in a simple formula that can be used in a practical sense.

2.2.2 Critical shear crack theory (CSCT)

The critical shear crack theory is studied in the paper of (Muttoni & Ruiz, 2008) and will be summarized in this chapter. The critical shear crack theory is based on the reasoning that shear capacity is dependent on the critical shear crack width and its roughness. The angle of the shear crack is often assumed to be 45 degrees. The shear capacity according to CSCT is expressed in the formula:

$$\frac{V_R}{b_w d} = \sqrt{f_c} f(w, d_g)$$

In this formula, w is the critical shear crack width and d_g the maximum aggregate size.

Assuming plane sections remain plane, and linear elastic behaviour in compression, and taking the effects of the aggregate size, and crack width into account, the following expression is obtained:

$$\frac{V_R}{b_w d\sqrt{f_c}} = \frac{1}{6} * \frac{2}{1 + 120 * \frac{\varepsilon d}{16 + d_g}}$$

Without axial forces, the strain at the control depth can be determined:

$$\varepsilon = \frac{M}{b_w d \rho_l E_s (d - \frac{c}{3})} * \frac{0.6d - c}{d - c}$$

the depth of the compression zone, noted as c, can be expressed as:

$$c = d\rho_l \frac{E_s}{E_c}\left(\sqrt{1 + \frac{2E_c}{\rho_l E_s}} - 1\right)$$

According to (Muttoni & Ruiz, 2019) the critical shear crack can occur at any location and has a bilinear shape. To calculate the shear strength, the location of the critical crack must be assumed, and the crack opening iteratively be increased. Once the applied shear force equals the resisting shear force, the shear capacity has been found for that cracking location. The governing location of the crack will be the location that has the lowest capacity among the locations. (Cavagnis, Ruiz, & Muttoni, 2018) States that there are three potential positions for the critical shear crack: $x_a = d, x_a = 0.5a, and\ x_a = a - d$, where a is the shear span, and d is the effective height.

The main assumptions of CSCT according to (Muttoni & Ruiz, 2019) are as follows:

- Shear strength is governed by the shape and location of the critical shear crack
- Shear can be transferred by different actions: Residual tensile strength, Aggregate interlocking, dowel action and the cantilever action.
- Shear failure occurs when the shear load reaches the capacity. The capacity is equal to the sum of the potential shear transfer actions. $V_R = V_a + V_t + V_d + V_c$

Shear transfer actions

According to the CSCT the capacity of a concrete element is the combined strength of the so-called shear transfer actions. The shear transfer actions are separated into beam shear transfer actions and arching action. The beam transfer actions are cantilever action, aggregate interlock, dowelling action, and residual tensile strength of concrete. These beam transfer actions allow nonconstant forces in the flexural reinforcement and develop tensile stresses in transverse direction. The arching action instead keeps the force in the flexural reinforcement constant and does not require transverse tensile stresses to transfer shear. The thesis (Cavagnis F. , 2017) contains a chapter going further into detail regarding the shear transfer actions, the essentials are summarized below. For more detailed explanations or equations, the reader is advised to explore literature such as (Cavagnis F. , 2017).

Cantilever action

The flexural cracks cause teeth-like shape in the concrete. The concrete between cracks behaves as cantilevers, fixed at the top of the compression zone. The tensile forces in the longitudinal reinforcement changes between cracks, due to the varying moment at the two crack locations. If the cracks do not transfer loads, this means that an inclined compressive chord and an inclined tension tie must be present to create force equilibrium.

Aggregate interlock

The shear capacity introduced by the sliding of concrete, caused by an opening crack is called aggregate interlock. The capacity is obtained because aggregates from one side of the crack are making contact to the concrete (matrix) at the other side of the crack causing a resistance to movement/sliding. The aggregate interlocking enables cracks to transfer shear through cracks.

Dowelling action
Dowel action refers to the mechanism by which a steel reinforcing bar, resists shear forces through its own shear capacity. This action can transfer loads across cracks in concrete structures.

Residual tensile strength of concrete
When concrete reaches its maximum stress and cracks, concrete starts to show softening behaviour. This means that concrete still has a capacity after cracking, given that the crack width is small. It is assumed that crack openings larger than 0.2 mm can no longer transfer stress.

Arching action
Arching action of concrete can develop when the longitudinal reinforcement loses its bond to the concrete. The longitudinal reinforcement will start to function as a tensile chord while the concrete will have an inclined compression chord that directly transfers the load. The concrete and detached reinforcement will now function like an arch. The arch action can only function if no cracks interfere with the arch (e.g. the arch/strut does not go through cracks). Arch action functions as a strut and tie model.

2.2.3 Modified compression field theory (MCFT)
The modified compression field theory is proposed in the paper (Vecchio & Collins, 1986) and will be briefly summarized. In the MCFT cracked concrete is treated as a different material with its own stress-strain characteristics. This new material has its own equations for equilibrium, compatibility, and stress-strain relationships. All of which are based on the average stresses and strains. The theory is based on tests of elements in a membrane element tester and assumes a rotating smeared crack model (Sadeghian & Vecchio, 2018).

To explain the MCFT a membrane element is introduced, which contains a grid of reinforcement in x and y direction as can be seen in Figure 1. Axial loads are applied in x and y direction denoted as fy and fx. Shear loads are denoted as Vxy. It is assumed that the edges remain straight when the membrane deforms.

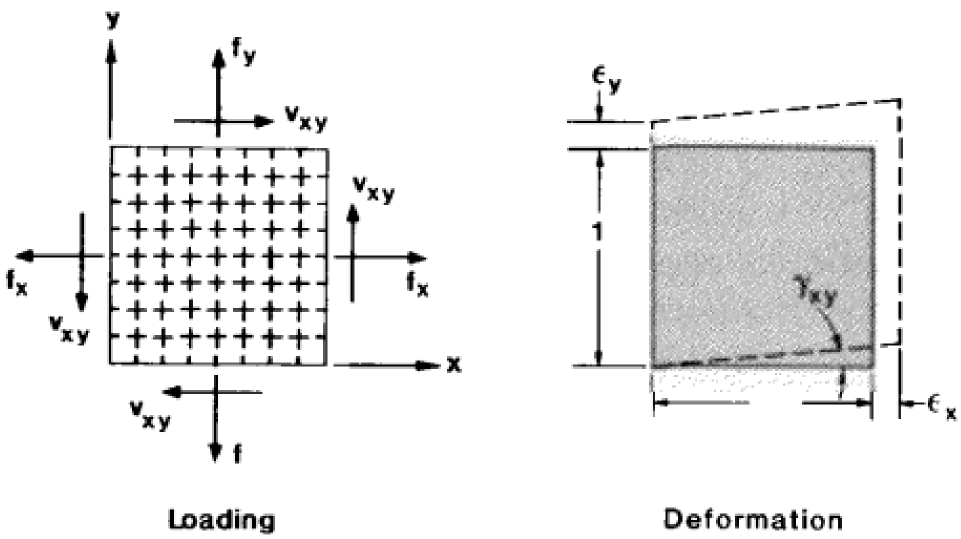

Figure 1 membrane element (Vecchio & Collins, 1986)

The following assumptions are made:

- Each strain corresponds to one stress state, there is no history dependency
- Stresses and strains are averaged when an area is considered where multiple cracks occur.
- No bond slip occurs, the reinforcement-concrete bond is perfect.
- Reinforcement is uniformly distributed in both the longitudinal and transversal direction.
- Edges of the deformed membrane remain straight and parallel

A summary of the MFCT equations has been given in (Collins, Bentz, Sherwood, & Xie, 2008) and is shown in Figure 2 MCFT equations. Equation 15 in this figure, was derived from aggregate interlocking experiments done by (Walraven J. , 1981) and describes the shear that can be transferred in a crack. In this formula a_g is the maximum aggregate size in mm, and the crack width equal to the principal tensile strain multiplied by the crack spacing w = ε_1* S_θ.

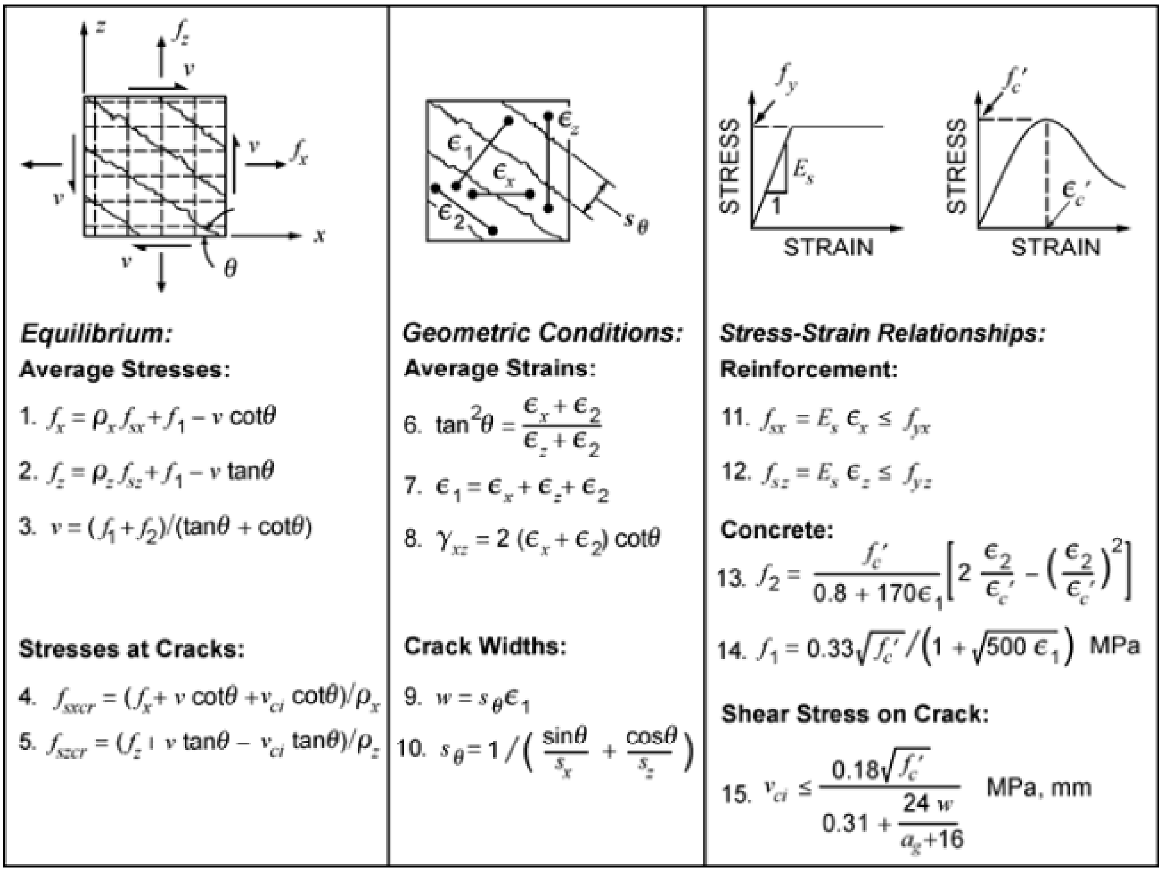

Figure 2 MCFT equations. (Collins, Bentz, Sherwood, & Xie, 2008)

2.3 Codes describing shear strength

Because there is a variety of shear strength models, design codes that are used throughout the world also differ from one another. Two important codes are the Eurocode2 and the AASHTO LRFD code. These two design codes, and the proposed Eurocode2, are briefly summarized in this chapter.

2.3.1 Eurocode 2

The Eurocode contains many formulae and design rules which apply to structures. Relevant for this research is the shear capacity for elements without stirrups (shear reinforcement). The formulae are found in (Eurocode2, 2015). The shear models are based on a regression analysis and are empirical models.

In (Yang & Roosen, 2023) It has been mentioned that there are 5 fundamental reasons to change the current Eurocode. These reasons are:

1. The size effect is underestimated in the current Eurocode
2. When axial tensile forces are applied the current Eurocode is too conservative
3. The aggregate size, and therefore roughness of the crack is not considered in the current Eurocode
4. The effect of shear slenderness is not considered, this means that the shear capacity can be overestimated (unsafe) for slender structures and underestimated (conservative) for non-slender structures.
5. The formula for shear capacity is based on a regression analysis. The formula may therefore not hold, and can even be unsafe, when parameters differ from the experimental setup

Without shear reinforcement

In the case that bending cracks have occurred and the design does not contain shear reinforcement. the design value for shear $V_{Rd,c}$ is given by:

$$V_{Rd,c} = \left[C_{Rd,c} * k(100 * \rho_l * f_{ck})^{1/3} + k_1\sigma_{cp}\right] * b_w d$$

The value of $V_{Rd,c}$ is at least equal to

$$V_{Rd,c} = \left[v_{min} + k_1\sigma_{cp}\right] * b_w d$$

In these formulae:

$k = 1 + \sqrt{\frac{200}{d}} \leq 2.0$ with d in mm.

$\rho_l = \frac{A_{sl}}{b_w d} \leq 0.02$ is the longitudinal reinforcement ratio.

$\sigma_{cp} = \frac{N_{Ed}}{A_c} < 0.2\ f_{cd}$ is the stress in the concrete due to an axial compressive force (Mpa).

$d = \frac{d_s^2 A_{sl} + d_p^2 A_p}{d_s A_{sl} + d_p A_p}$ is the effective height (mm).

The values used for $C_{Rd,c}$, v_{min} and k_1 depend on the county of the design and can be found in the national annex of countries. The recommended values are:

$$C_{Rd,c} = \frac{0.18}{\gamma_c}; k_1 = 0.15; v_{min} = 0.035 * k^{3/2} * \sqrt{f_{ck}}$$

The effect of prestressing or other axial forces are considered with the term $k_1\sigma_{cp}$. If the cross-sectional properties, including reinforcement and prestressing layout, remain constant the capacity does as well. The governing cross section would then be determined by finding the location with the highest shear stresses.

Members with shear reinforcement

For members with vertical shear reinforcement the shear capacity is the smaller value of

$$V_{Rd,s} = \frac{A_{sw}}{s} * z * f_{ywd} * cot\theta$$

And

$$V_{Rd,max} = \frac{\alpha_{cw} * b_w * z * v_1 * f_{cd}}{cot\theta + tan\theta}$$

for

$$1 \leq cot\theta \leq 2.5$$

Recommended values of v_1 and α_{cw} are given as follows:

$v_1 = 0.6$ $\quad for\ f_{ck} \leq 60\ MPa$

$v_1 = 0.9 - \frac{f_{ck}}{200} > 0.5$ $\quad for\ f_{ck} \geq 60\ MPa$

$\alpha_{cw} = 1 + \frac{\sigma_{cp}}{f_{cd}}$ $\quad for\ 0 \leq \sigma_{cp} \leq 0.25 f_{cd}$

$\alpha_{cw} = 1.25$ $\quad for\ 0.25 f_{cd} \leq \sigma_{cp} \leq 0.5 f_{cd}$

$\alpha_{cw} = 2.5\left(1 - \frac{\sigma_{cp}}{f_{cd}}\right)$ $\quad for\ 0.5 f_{cd} \leq \sigma_{cp} \leq f_{cd}$

2.3.2 Eurocode 2 proposal (prEN 1992)

New formulae have been proposed for the shear capacity of (prestressed) concrete elements without stirrups. These formulae are based on simplifications of the CSCT. There are two variants that will be considered in this research, and these will be denoted as D7-main and D7-alt as is done in (Adviesbureau ir. J.G Hageman B.V., 2021).

Control sections

Multiple control sections should be analysed in the proposed Eurocode, as the shear capacity is dependent on the shear forces and bending moments. The shear capacity also must be determined in an iterative way for each of the control sections. Locations of control sections are at determined to be at a distance 1d from a static discontinuity (supports, points of contraflexure and concentrated loads) or at distance d from geometric discontinuities (changing cross section). However, it is noted that for geometric discontinuities this does not always hold, for some examples it may be expected that also the location of the discontinuity itself should be inspected. Furthermore, a section at the edge of the supports might also need to be inspected (Adviesbureau ir.J.G. Hageman B.V., 2023).

The control section near the support is often called the 'first control section'. In the (FprEN 1992-1-1, 2023), this control section is located at a distance 1d from the support. This assumes that the shear crack angle is 45 degrees. For prestressed elements this assumption is however likely not accurate. This can be observed in documents like the RBK (Rijkswaterstaat, 2022b) where, for σ_{cp} > 5 N/mm^2 an angle of 30 degrees is estimated instead. For σ_{cp} between 0 and 5 N/mm^2 it is stated that a linear interpolation can be assumed. The angle of 30 degrees follows from the fact that for prestressed elements a smaller angle was found in experimental data but has not been determined precisely. For this reason, the location where the first control section should be remains uncertain, and a conservative angle of 45 degrees was assumed.

D7-main

The formula of D7-main is obtained by using a power law expression for the CSCT failure criterion that uses the strain at reinforcement level (instead of strain at 0.6d).

$$\frac{V_c}{b_w * d * \sqrt{f_c}} = k * \left(\frac{d_{dg}}{\varepsilon_s * d}\right)$$

In this formula the strain at reinforcement level can be determined by the expression:

$$\varepsilon_s = \frac{V * a_{cs}}{A_s * E_s * z}$$

By assuming values for E_s and z, introducing a safety factor and setting $V_E = V_c$, the formula for D7-main is obtained:

$$\tau_{Rd,c} = \frac{0.66}{\gamma_V}\left(100\rho_l * f_{ck} * \frac{d_{dg}}{d_{nom}}\right)^{1/3} \geq \tau_{Rdc,min}$$

$$\tau_{Rdc,min} = \frac{11}{\gamma_V}\sqrt{\frac{f_{ck}}{f_{yd}} * \frac{d_{dg}}{d}}$$

In members with an effective shear span a_{cs} smaller than 4d, the value for d_{nom} may be replaced by:

$$a_v = \sqrt{\frac{a_{cs}}{4} * d} \leq d$$

For reinforced concrete without axial force the effective shear span a_{cs} may be calculated as:

$$a_{cs} = \left|\frac{M_{Ed}}{V_{Ed}}\right| \geq d$$

Only the load case with maximum shear with the respective moment and the load case with maximum moment with the respective shear will need to be considered.

In the case that an axial force N_{Ed} is present (e.g. prestressing), d_{nom} or a_v should be multiplied by a factor k_{vp} and the capacity can be written as:

$$k_{vp} = 1 + \frac{N_{Ed}}{|V_{Ed}|} * \frac{d}{3 * a_{cs}} \geq 0.1$$

$$\tau_{Rd,c} = \frac{0.66}{\gamma_V}\left(100\rho_l * f_{ck} * \frac{d_{dg}}{k_{vp} * a_v}\right)^{1/3} \geq \tau_{Rdc,min}$$

When a compressive force is applied (negative N_{Ed}), k_{vp} lowers, and the shear capacity increases. The capacity is not constant, as it depends on the ratios between the shear force, bending moment and axial force. As the shear capacity is not constant, but dependant on the considered cross section, the shear crack angle will influence the capacity. With a smaller angle, the first control section will be further from intermediate supports. At this location the moment is lower and thus the shear capacity higher. Currently the shear crack angle is not implemented in the prEN 1992, a constant cross section located at 1d from discontinuities is used instead, but it should be clear that a different crack angle affects the capacity and should thus be investigated.

D7-alt

As an alternative to D7-main D7-alt was proposed in (FprEN 1992-1-1, 2023), which looks similar to the formula in the current Eurocode and contains a term for prestressing:

$$\tau_{Rd,c} = \frac{0.66}{\gamma_V}\left(100\rho_l * f_{ck} * \frac{d_{dg}}{d_{nom}}\right)^{\frac{1}{3}} - k_1 * \sigma_{cp} \geq \tau_{Rdc,min}$$

In this expression k_1 can be calculated with:

$$k_1 = \frac{0.5}{a_{cs,0}} * \left(e_p + \frac{d}{3}\right) * \frac{A_c}{b_w * z} \leq 0.18 * \frac{A_c}{b_w * z}$$

In (Adviesbureau ir. J.G Hageman B.V., 2021), a different expression was used to determine k1. In that report k1 is determined as:

$$k_1 = \frac{1.4}{\gamma_V}\left(0.07 + \frac{e_p}{4 * d}\right) \leq 0.15 * \frac{1.4}{\gamma_V}$$

Effects of new formulae

(Roosen, Yang, & Dieteren, 2023) shows that, based on 136 experiments, on average the determined shear capacity is slightly lower (conservative) for the D7-main on average compared to the current Eurocode. The experiments show that the experimental shear capacity on average was 1.34 times higher than the calculated shear capacity found with the current Eurocode. For the new Eurocode this is 1.41 times. The coefficient of variation however reduces from 27% in the current Eurocode to 18% in D7-main. The model D7-main also shows less of a trend when the ratio a_{cs}/d is compared to V_{exp}/V_{Rd}.

The report of Hageman (Adviesbureau ir. J.G Hageman B.V., 2021) mentions that the ease of use goes down with the proposed Eurocode. Different control sections must be considered, all of which may be governing. For all these cross sections, two load cases must be considered, maximum shear with corresponding moment, or maximum moment with corresponding shear. For moving loads, loads must be placed at different location for each control section until the governing situation is found. Because the cross-sectional properties are commonly not constant, the calculation is "unique" at each situation. Furthermore, to determine the maximum load at each control section, iterations must be done. This is the case because the shear capacity is based on the acting shear and moment on a cross section. It should be clear that the shear calculations according to the proposed Eurocode will no longer be feasible to do by hand.

In (Adviesbureau ir. J.G Hageman B.V., 2021) analyses have been done using D7-main, D7-alt and a third method known as “Valencia” by means of case studies. From these case studies it has become clear that the resulting capacities, and the locations of the critical cross section, vary wildly between models themselves, but also vary from the current Eurocode. Particularly at intermediate supports of prestressed beams, large differences are found between D7-main and the current Eurocode; D7-main (the proposed Eurocode) produces overly conservative results. A suggestion is made that the control section located at 1d from the support is moved to 2d, this would decrease the differences between the current Eurocode and D7-main significantly. It is however not yet clear if this is possible. Without knowing the shear crack angle, the location of the first control section, near intermediate supports, is unknown and cannot be moved. The model then remains overly conservative. For this reason, a model that can determine the location of the first control section, should be developed.

2.3.3 AASHTO LRFD

As a comparison to the Eurocodes an American code, AASHTO LRFD, is briefly discussed. In (AASHTO LRFD, 2007), there are multiple procedures to determine the shear resistance. In 5.8.3.4.2, the second method to determine the shear resistance, a way to determine the inclination angle of diagonal compressive stresses (θ) is shown. To determine this angle, tables are given for elements with and elements without transverse reinforcement. The table for elements without transverse reinforcement is given in Figure 3. Elements without prestressing, will use 45-degree angles according to 5.8.3.4.1.

s_{xe} (mm)	$\varepsilon_x \times 1000$										
	≤–0.20	≤–0.10	≤–0.05	≤0	≤0.125	≤0.25	≤0.50	≤0.75	≤1.00	≤1.50	≤2.00
≤130	25.4 6.36	25.5 6.06	25.9 5.56	26.4 5.15	27.7 4.41	28.9 3.91	30.9 3.26	32.4 2.86	33.7 2.58	35.6 2.21	37.2 1.96
≤250	27.6 5.78	27.6 5.78	28.3 5.38	29.3 4.89	31.6 4.05	33.5 3.52	36.3 2.88	38.4 2.50	40.1 2.23	42.7 1.88	44.7 1.65
≤380	29.5 5.34	29.5 5.34	29.7 5.27	31.1 4.73	34.1 3.82	36.5 3.28	39.9 2.64	42.4 2.26	44.4 2.01	47.4 1.68	49.7 1.46
≤500	31.2 4.99	31.2 4.99	31.2 4.99	32.3 4.61	36.0 3.65	38.8 3.09	42.7 2.46	45.5 2.09	47.6 1.85	50.9 1.52	53.4 1.31
≤750	34.1 4.46	34.1 4.46	34.1 4.46	34.2 4.43	38.9 3.39	42.3 2.82	46.9 2.19	50.1 1.84	52.6 1.60	56.3 1.30	59.0 1.10
≤1000	36.6 4.06	36.6 4.06	36.6 4.06	36.6 4.06	41.2 3.20	45.0 2.62	50.2 2.00	53.7 1.66	56.3 1.43	60.2 1.14	63.0 0.95
≤1500	40.8 3.50	40.8 3.50	40.8 3.50	40.8 3.50	44.5 2.92	49.2 2.32	55.1 1.72	58.9 1.40	61.8 1.18	65.8 0.92	68.6 0.75
≤2000	44.3 3.10	44.3 3.10	44.3 3.10	44.33 3.10	47.1 2.71	52.3 2.11	58.7 1.52	62.8 1.21	65.7 1.01	69.7 0.76	72.4 0.62

Figure 3 Values for theta and beta, for sections with less than minimum transverse reinforcement (AASHTO LRFD, 2007)

To find the inclination angle of the diagonal stresses ε_x and s_{xe} are required. Linear interpolation is allowed between values of ε_x and s_{xe} but this is not recommended for hand calculations.
For members without transverse reinforcement S_{xe} can be taken as follows:

$$S_{xe} = \frac{35}{a_g + 16} S_x \leq 2000\ mm$$

Where S_x is equal to the effective shear height d_v when less than the minimum transversal reinforcement is present as is visualized in Figure 4.

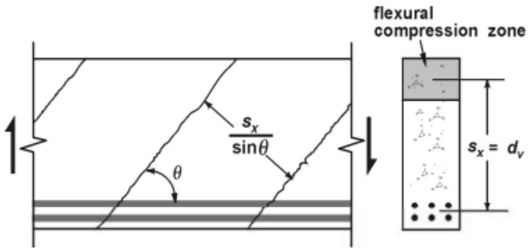

Figure 4 Member without transverse reinforcement and with concentrated longitudinal reinforcement (AASHTO LRFD, 2007)

ε_x is the largest calculated longitudinal strain in the web of a section is subjected to the forces and moments Nu, Mu, and Vu and can be calculated for elements without transverse reinforcement as is shown in Figure 5.

- If the section contains less than the minimum transverse reinforcement as specified in Article 5.8.2.5:

$$\varepsilon_x = \frac{\left(\frac{|M_u|}{d_v} + 0.5N_u + 0.5|V_u - V_p|\cot\theta - A_{ps}f_{po}\right)}{E_sA_s + E_pA_{ps}}$$

(5.8.3.4.2-2)

The initial value of ε_x should not be taken greater than 0.002.

- If the value of ε_x from Eqs. 1 or 2 is negative, the strain shall be taken as:

$$\varepsilon_x = \frac{\left(\frac{|M_u|}{d_v} + 0.5N_u + 0.5|V_u - V_p|\cot\theta - A_{ps}f_{po}\right)}{2\left(E_cA_c + E_sA_s + E_pA_{ps}\right)}$$

(5.8.3.4.2-3)

Figure 5 ε_x in the case less than minimum transverse reinforcement is present. (AASHTO LRFD, 2007)

The nominal shear resistance can be found based on θ and β as follows:

$$V_R = V_c + V_s + V_p \leq 0.25f_c'b_vd_v$$

$$V_c = 0.083\beta\sqrt{f_c'}b_wd_v$$

$$V_s = \frac{A_{sw}f_yd_v(cot\theta + cot\alpha)sin\alpha}{s}$$

Although the AASHTO LRFD calculations are quite different from the proposed Eurocode, some important similarities are observed. In both AASHTO LRFD and the proposed Eurocode the shear capacity is dependent on the normal forces, shear forces, moment, aggregate size and amount of longitudinal reinforcement at an investigate cross section. Although, an estimate for the crack angle can be done with AASHTO LRFD, it is expected that this estimate cannot be applied to the proposed Eurocode in an accurate manner. The reason for this is that the inclination angle is meant to be used as an intuitive and conservative design parameter for the shear capacity, rather than accurate representation of the crack angle.

2.4 Modelling methods

A variety of methods is available to model concrete behaviour. In this chapter an overview is given of several of these methods.

2.4.1 Finite Element Method (FEM)

Smeared cracking

A common approach to modelling cracks in concrete is to use a finite element analysis (FEA) with smeared cracking. In smeared FEM a mesh of quadrilateral or triangular elements is used to model the investigated member. When forces or displacements are applied to the model, stresses and strains are calculated in the integration points of the elements. When the allowed stresses are exceeded, the stiffness in the affected integration points gradually reduce. This causes a deformation of the element and creates smeared damage, where the elements are still physically connected but show smeared damage.

FEM can be used to find reasonable capacity estimates of concrete members, and it may be possible to obtain realistic estimates for the crack patterns. With the vast number of settings, a Finite Element Model can be made to reflect many of the assumptions that have been made. Unfortunately, this generally also means that many assumptions must be made, and the user could become lost, searching for optimal settings. This can mainly be a problem with settings such as the shear retention factor, which heavily influences shear behaviour and can be based on a variety of models. Fortunately, many of the settings are provided in a guideline (Hendriks & Roosen, 2022).

Discrete cracking

An alternative to using smeared cracking in FEM, is to use discrete cracking. In discrete cracking, the crack locations must be determined a priori and are put into the model. Cracks can no longer occur in every element and instead can only disconnect the predetermined elements when the strength is exceeded. In the case of continuous beams, where many flexural cracks may occur, a dilemma arises. Either all flexural cracks must be predicted and added to the model, or it must be assumed that the influence of the flexural cracks is minimal. On the other hand, the localised cracking of discrete cracks may give more realistic results than the smeared damage found in smeared FEM.

It should be noted that the shape (crack angle) of the critical crack is not known a priori. This means that for a single beam not one, but multiple numerical models must be set up, the number of models being equal to how many different crack angles are considered. These models can be created quickly, especially if smeared models of the same beam have already been created, but running multiple discrete models will take longer than running a single smeared model.

2.4.2 Extended Finite Element Method (XFEM)

Extended Finite Element Method (XFEM) as the name suggests, is an extension of FEM which offers other analysis methods. A few advantages of XFEM over FEM are found in (Rombach & Faron, 2019) and shortly explained below.

In FEM (smeared) cracks are modelled as regions with large strains and alter the shape and/or size of the finite elements, instead of creating actual discontinuities in the mesh. When discrete models are used, cracking occurs at the boundary of predetermined elements and the model is likely requires to re-mesh often and therefore increase the computational load. The cracking using the FEM may therefore create unrealistic and computationally expensive models.

XFEM can create discontinuities in the model while not being required to align with the mesh elements, XFEM also does not require remeshing. Furthermore, complex crack patterns can be modelled without the need for very fine meshes, and the computational cost of XFEM may be lower than regular FEM. However, (Vellwock & Libonati, 2024) notices several drawbacks of XFEM. The most important drawback relevant to this thesis is poor convergence behaviour. Additionally, the availability of (free) software capable of implementing XFEM should also be considered.

2.4.4 Plasticity theory

The Plasticity theory found in (Nielsen & Hoang, 1984) and the paper of (Zhang J. P., 1997) can be used to find critical cross sections for beams in shear. In this theory concrete is over-reinforced and behaves as a rigid plastic material according to the modified Mohr-Coulomb failure criterion. In this method there are two expressions based on the crack properties. One expression can be used to determine the ultimate capacity for given cracks at a location. The second expression is used to find the load required for a crack to occur at the given location. If the failure load of a crack at a location is exceeded but not the cracking load, there will be no failure as the crack that would fail has not formed yet. If the cracking load is exceeded but not the failure load, the crack has enough capacity to support the beam and will not fail. This means that only when both cracking and failure loads are exceeded failure will occur. In (Zhang J. P., 1997) it is shown that this occurs when the cracking load is equal to the failure load, which is the case at one location that can be solved for.

This method can be used to estimate the capacity and critical cross section for both reinforced and prestressed beams that are simply supported. It is also possible to extend this method to continuous beams by following the same steps as (Nielsen & Hoang, 1984) and (Zhang J. P., 1997). In this method, variations with different design parameters can be calculated in mere seconds and a clear influence of design parameters is shown on the critical crack and capacity.

2.4.5 Lattice modelling (LM)

In the lattice model the material is modelled as a lattice made of beam elements. Although rectangular grids are also common, triangular grids are less likely to show preferential crack directions. At the location where the capacity is exceeded a beam element breaks and is removed from the mesh. This way a crack is created or propagated. (Schlangen & Mier, 1992)

In (Aydin, Tuncay, & Binici, 2019) a rectangular grid, with grid size d, has been used when modelling reinforced concrete. The grid contains uniformly distributed nodes, and each node interacts with points within the horizon, a predetermined distance. Common horizon values are 1.5d and 3.01d, for which a node has 8 and 28 connected nodes respectively. This holds for nodes away from the boundaries, as at the boundaries this cannot hold due to the lack of nodes. It is said that the square grid is the easiest model for lattice modelling in terms of mesh generation and defining reinforcement. Unfortunately, as the reinforcement follows the grid nodes in a horizontal or vertical direction, curved reinforcement such as curved prestressing tendons are difficult to model. (Aydin, Tuncay, & Binici, 2019) states that even though some directional dependency will be present, using the 1.5d horizon gives accurate and relatively fast results for modelling shear in reinforced concrete. It is shown that lattice modelling is a viable method to simulate reinforced concrete but may not be suitable for prestressed concrete.

2.4.3 Sequential linear analysis (SLA)

The method of the SLA uses multiple linear analysis in a sequence as the name suggests. The tensile softening curve which has a negative slope is replaced with a saw-tooth curve. This curve only consists of positive slopes and jumps, making it look like teeth. SLA for shear critical concrete beams is discussed in (Slobbe, Hendriks, & Rots, 2012), and a short summary is given below.

Each analysis determines the critical integration point, where the highest stress/strength ratio is observed. The solution is then rescaled, and a stiffness and strength reduction is added to the critical integration point, according to saw-tooth constitutive laws. The previous steps are repeated until the damage has reached the desired location. This method can work well in cases where FEA is unable to give accurate/consistent results due to strong non-linearity and convergence problems.

This is because SLA consists of linear analysis without iteration. In case of prestressing this method becomes more complex, as the prestressing load should not be scaled.

2.4.6 Discrete element method (DEM)

In (Kaschube & Dieter, 2021) DEM is shortly discussed for RC. The concrete is modelled using spherical particles. The reinforcement is generally modelled as a line of particles, or truss or beam-like elements. By using interfaces parallel to the reinforcement line, the bond behaviour is modelled.

In (Shirzehhagh & Fakhimi, 2021) CA2, a 2D hybrid FEM-DEM software has been used to model RC beams. In this paper reinforcement is modelled using 1D linear cable elements while the concrete is modelled using discrete particles. The model was able to capture shear and flexural cracks as well as the capacity quite well.

2.4.7 Galerkin finite volume method (GFVM)

The Galerkin finite volume method (GFVM) has been used in soil, and computational fluid mechanics more frequently, but can also be used for modelling cracks (Sabbagh-Yazdi & Amiri, 2021). GFVM is a matrix-free method and therefore has reduced computational requirements. This means that the model runs faster than methods like FEM or XFEM. A variant of GFVM discussed by (Sabbagh-Yazdi & Amiri, 2021) is the Adaptive Galerkin Finite Volume Method (AGFVM), which increases the accuracy by automatically adapting an optimal mesh, while slightly increasing the computational load. The accuracy of AGFVM is like those of other methods such as FEM and XFEM, while the computational cost is lower.

2.4.8 Element-Free Galerkin (EFG)

As mentioned before, (Soparat & Nanakorn, 2008) states that FEM has difficulties in treating discontinuities that do not coincide with the original mesh. A common solution is the use of remeshing. However, this will be more computationally expensive.

The Element-Free Galerkin (EFG) method, uses moving least-square approximations, and does not use a finite element mesh. This avoids the need for remeshing or refining meshes. The moving least squares method approximates a function by using scattered data. Cracks are modelled using interface elements and grow by adding new interfaces in each incremental step (Soparat & Nanakorn, 2008). These interfaces allow cracks to propagate unrestricted by the mesh.

2.4.9 Selected models

Due to the time limitations of this thesis only a few of the methods have been used. A short overview is given to explain why methods have or have not been chosen.

Smeared FEM can be used to find reasonable capacity estimates of concrete members, and it may be possible to obtain realistic estimates for the crack patterns. This method is common, widely available and can be used to model prestressed concrete. For these reasons, smeared FEM is the first method that has been used in this thesis.

Although Discrete FEM has some important drawbacks, it is expected to have better local behavior compared to smeared FEM as damage will no longer be smeared. If the critical (discrete) crack governs the overall behavior of the investigated members, it may be possible to obtain more accurate results than smeared FEM. With the availability of smeared models and experience in FEM, discrete models could be created in a relatively short amount of time. For these reasons discrete FEM has also been used.

The XFEM was considered after smeared and discrete Finite Element Analyses had been conducted. This method is expected to provide better results but has ultimately not been used. It was decided that other types of methods should be investigated instead of focusing purely on different Finite element Models.

The plasticity theory can be used to estimate the capacity and critical cross section for both reinforced and prestressed beams. With this method, the crack angle or control section can be obtained within seconds, and a clear influence of design parameters is shown on the critical crack and capacity. This makes the plasticity theory an attractive choice and has therefore been used.

Lattice models have been briefly used to model the crack patterns in prestressed concrete. However, realistic prestressing behaviour could not be recreated in a timely manner. Due to the time constraints of this thesis this method was abandoned. The lattice models can be found in Appendix E. Lattice models.

The methods SLA, DEM, GFVM, EFG have not been used during this thesis. Compared to the other methods, not much literature is found on their use in modelling prestressed concrete and due to the limited time, the other methods were given priority.

3. Inclination of shear cracks in literature

In literature, information on crack angles is found that may be used to determine the critical cross section. In this chapter, models and experiments found in literature are reviewed, to find influences on the crack angle and how this angle may be determined. Once the crack angle is known, the control section may be estimated at a location cot(θ)*d away from the intermediate supports.

3.1 Crack angle estimations

Several models have been found that estimate crack angles or locations of governing cross-sections. The models reported in this chapter vary in complexity and investigated parameters. Some of the models consider only the amount of prestressing stress in the concrete, while other models include different variables and might not consider prestressing.

3.1.1 Cavagnis

The thesis (Cavagnis F. , 2017) discusses the critical shear crack and aims to improve the theory. To accomplish this, several experiments are investigated. The thesis contains valuable information such as detailed explanation of the CSCT and experimental findings.

Test setups

The experiments done were varied, so that different loading conditions and different boundary conditions were considered. The beams were rectangular (250x600) and had 2ϕ22 or 2ϕ28 as both top and bottom reinforcement. The reinforcement ratios were ρ=0.54% and ρ=0.89% respectively. The concrete cover was 30mm. concrete strength ranged between 31.2 MPa and 36.9 MPa. Maximum aggregate size d_g is equal to 16 mm. The average yield strength of the reinforcement was 713 MPa (ultimate strength 820 MPa) for ϕ28 and 760 MPa (ultimate strength 920 MPa) for ϕ22.

Critical Shear Crack Development types from flexural cracks.

In the Cavagnis thesis it has been observed that for primary flexural cracks, also referred to as crack type A, the distance between cracks at mid-height varies between 0.4d - 0.8d, with 0.56d on average. Between these primary flexural cracks, smaller cracks that do not propagate to half the effective depth may be present. The angle of the primary flexural crack from point A (location of reinforcement) to d/2 above point A can be estimated by the formula:

$$\tan(\beta_1) = 1 + 1.25 * \frac{M_A}{V_A * d} = 1 + 1.25 * \alpha_A.$$

Where M_A and V_A are the moment and shear at the location where the flexural crack intercepts the flexural reinforcement and α_A is defined as:

$$\alpha_A = \frac{M_{A(x)}}{V_{A(x)} * d}$$

The inclination of the crack reduces as it propagates. The angle between point A and the neutral axis point B (or the point where the stress reaches the tensile strength if the crack propagates below the neutral axis) can be estimated by:

$$\beta_{AB} = \frac{\pi}{4} + \frac{\pi}{12} * \alpha_A^{1/3} < \frac{\pi}{2}$$

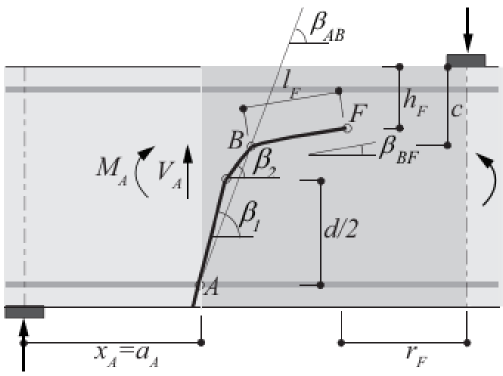

Figure 6 Geometry and definition of parameters investigated (Cavagnis F. , 2017)

The angle β_{BF} has a big scatter and therefore has no formula that can nicely fit the data. The angles were roughly between 8° and 35°, on average the angle was 22°. The angle β_{BF} and the corresponding length L_F have been assumed to be 22.5° and d/6 respectively in the Cavagnis report. The vertical distance of the tip of the crack to the longitudinal reinforcement can be calculated with the formula: $d_f = d - c + l_F * \sin(\beta_{BF})$, where d is the effective depth, and c is the height of the compressive zone. The geometry and definitions are visualized in Figure 6.

According to (Cavagnis F. , 2017) the primary flexural crack can turn into a critical shear crack in several ways. The different crack development types are listed below and are shown in Figure 7.

- Critical Crack Development Type (CCDT) 1 allows full arching action and has a compressive strut that is undisturbed by cracks
- CCDT 2, the flexural crack A develops a flat crack F in the compressive zone in a stable manner. It is possible for a secondary flexural crack C to merge with the primary crack and still develop crack type F in a stable manner.
- CCDT 3, the failure is caused by the loss of local aggregate interlocking. The aggregate interlocking crack E' propagates from the primary flexural crack.
- CCDT 4, a secondary crack C merges with the primary crack causing the cracks to open and triggering failure.

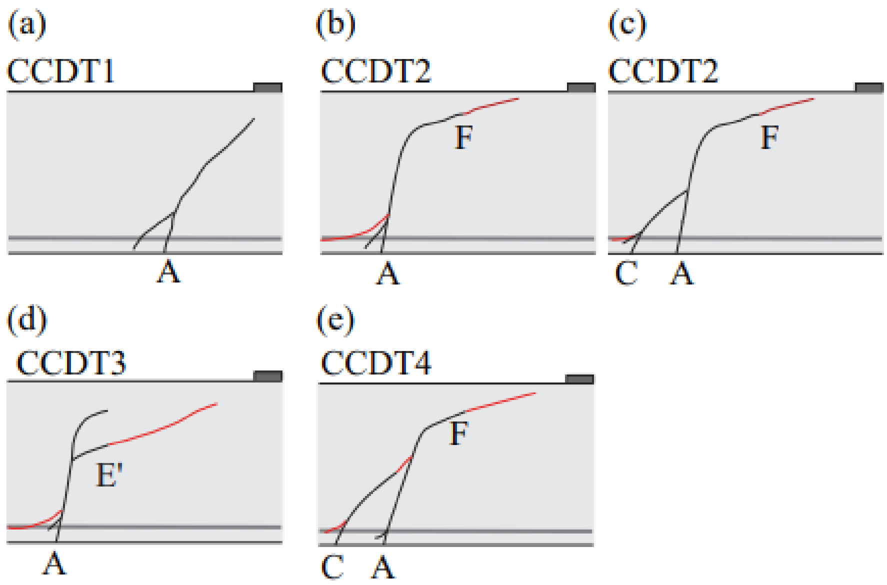

Figure 7 Critical Shear Crack Development types (Cavagnis F. , 2017)

Analysis of the shear transfer actions

In chapter 5 of (Cavagnis F. , 2017) an analysis is done on the shear transfer actions. The relevant conclusions are listed below:

- Cantilever action plays an important role before the critical crack forms. The cantilever action is seen to develop at loads much below the maximum loads
- Arching action may be the dominant shear transfer action under the condition that the critical crack grows toward a location above the intermediate support plate in a stable manner.
- The amount of aggregate interlocking depends on the geometry, kinematics and location of the critical crack. For cracks developing above or near the intermediate supports aggregate interlocking only plays a small part. However, if the crack is further away from the intermediate support, aggregate interlocking has a large contribution to the shear capacity.
- For slender elements the shear is transferred by the sum of beam transfer actions. From these actions aggregate interlocking is usually dominant.
- For concrete members subjected to uniform loads, the loads applied between intermediate supports and the critical shear crack can assumed to be transferred directly to the supports. From experiments it is observed that the critical shear crack meets the longitudinal reinforcement between d and 2.6d.
- The shear-transfer actions differ depending on shape and location of a crack, but the total shear capacity does not vary significantly. This means that the location of a shear crack could potentially vary largely between similar elements, but also that the shear capacity can be determined in one calculation instead of a sum of multiple contributions.

Closed-form equation

In the thesis of (Cavagnis F. , 2017) power-law failure criterion and the load-deformation relationships are combined, and a closed-form equation is obtained for the shear capacity at the control section:

$$V_c = k * \left(100 * \rho_l * f_c * \frac{d_{dg}}{a_{cs}}\right)^{\frac{1}{3}} * b_w * d$$

This closed-form expression is discussed for simply supported, cantilever and continuous beams. The closed-form expression in (Cavagnis F. , 2017) is known as Eq. (7.18) while a more refined calculation based on integration is known as (Eq. (7.3) + Eq. (7.7))

Simply supported beam under point loading

To show that the closed-from equation has similar results to the refined calculations, the shear capacity has been graphed as a function of several parameters in Figure 8. In the top left corner, noted as (a), the total shear resistance and the resistance of different shear transfer actions are shown for a varying location of the critical crack. For this reinforced beam with a span of 2.5m a 30% capacity difference is observed between the locations $0.2\frac{x_F}{a}$ and $0.6\frac{x_F}{a}$.

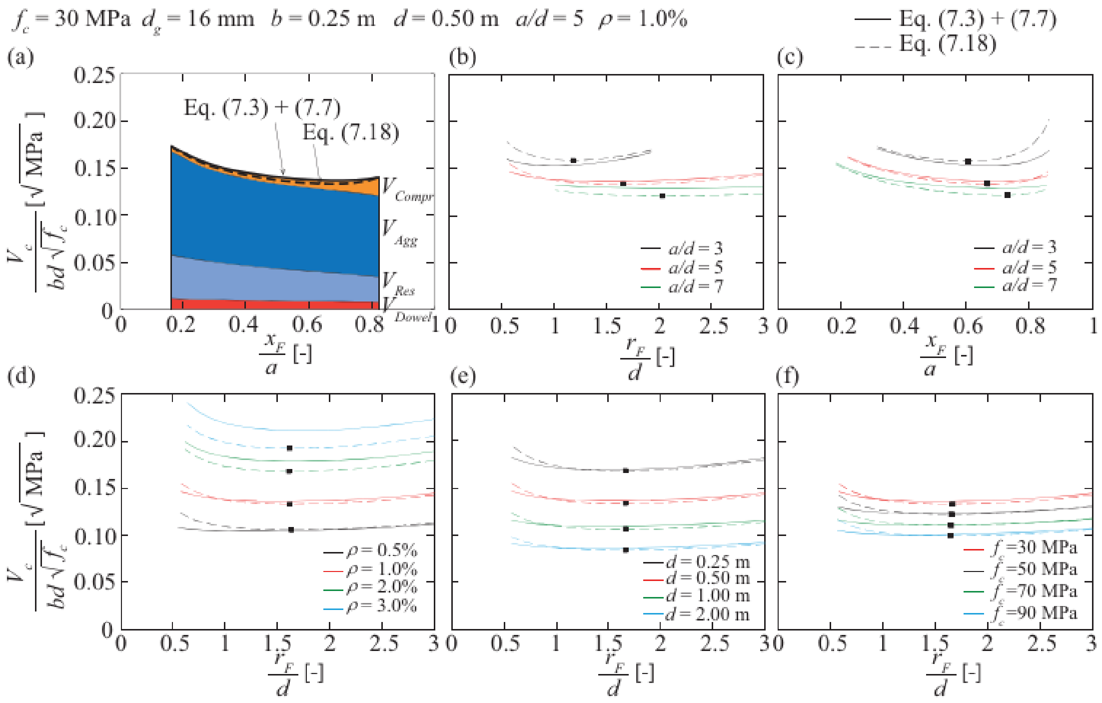

Figure 8 Shear capacity of simply supported beams under point loads for possible control sections and different parameters (Cavagnis F. , 2017)

Of the investigated parameters in Figure 8, only the a/d ratio seems to influence the location of the critical crack in a significant amount. However, as the curves are very flat (the different cross section locations have almost the same strength), it is said that only one of the sections needs to be checked. It is proposed by Cavagnis that this location is r_f = 1d from the support.

The closed form equation slightly overestimates the capacity for small (<3) a/d ratios and underestimates the strength of members with high (>7) a/d ratios or reinforcement ratios bigger than 2%. This is because of the assumption that the height of the compressive zone above the crack tip h_f is 0.3d (while in fact is lies between 0.2d and 0.4d based on reinforcement ratio) and a slight inaccuracy in a coefficient k, which influences the shear capacity.

Members with axial compression or prestressing, have a decreased effective shear span. The effective shear span for elements under central compression can be determined as follows:

$$a_{eff} = a + \frac{N}{V}\left(\frac{h}{2} - \frac{c}{3}\right) \cong a + \frac{N}{V} * \frac{d}{3}$$

Where N is the normal force (negative for compression), h is the beam height, c is the height of the compression zone. For prestressed elements this is visualized in Figure 9, the expression changes to:

$$a_{eff} = a - \frac{P}{V}\left(\frac{h}{2} - \frac{c}{3} + e_p\right) \cong a - \frac{P}{V} * \left(\frac{d}{3} + e_p\right)$$

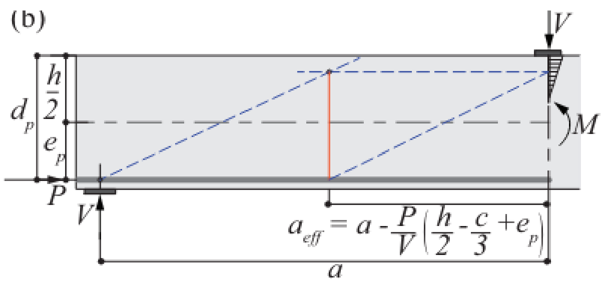

Figure 9 Equilibrium of internal forces and definition of a_{eff} for a reinforced concrete beam without shear reinforcement subjected to axial compression forces or prestressing (compressive forces in blue and tensile forces in red) (Cavagnis F. , 2017)

Simply supported beams under distributed loading

Elements with l/d < 10 are different than elements with l/d>10. From experiments it is concluded that for l/d>10 the beam-transfer actions lose capacity and fail while for l/d<10 crushing of concrete occurs above the crack tip. For this reason, only l/d >10 has been discussed in the thesis of Cavagnis.

The critical crack can start from a location between X_A= 0.5d-1.5d from a support for a simply supported beam under distributed load. For design purpose X_A=d is a reasonable assumption. The shear and moment should both be calculated at X_F. X_F is assumed to be $x_F \cong x_A + 0.5 = 1.5d$ which can also be observed from Figure 10. However, to keep the control section location the same for different conditions, x_F is once again chosen at 1d. This is accepted as the load capacity is almost constant in the interval x_F= 1d-1.75d.

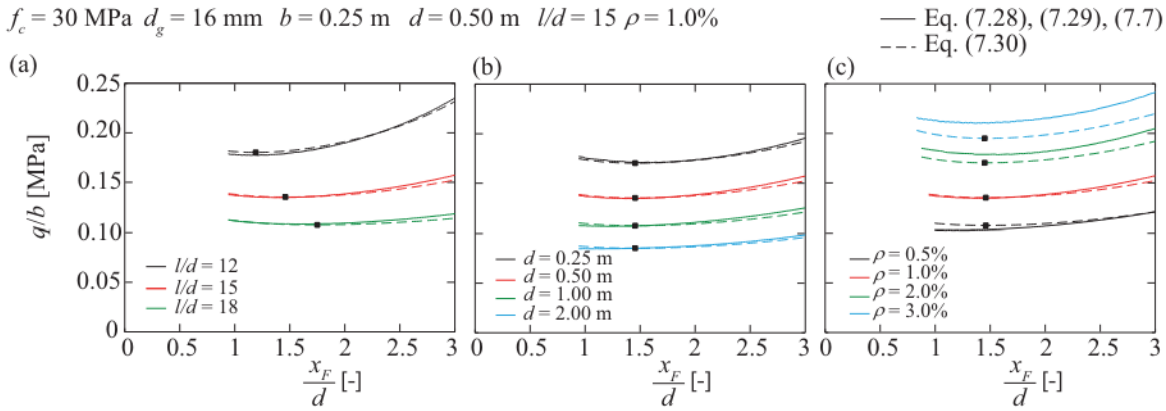

Figure 10 Shear capacity of simply supported beams under distributed loads for possible control sections and different parameters (Cavagnis F. , 2017)

The shear strength of beams under a distributed load is lower than the same beam under a point load, for simply supported beams. This is because the shape, location and governing shear transfer actions are different.

The coefficient k in the formula $V_c = k * \left(100\rho_l * f_{ck} * \frac{d_{dg}}{a_{cs}}\right)^{\frac{1}{3}} * b * d$ has different optimal values for point loads and distributed loads (for the most accurate results). 0.016 for distributed and 0.019 for point loads. It is therefore stated that the same formula can be applied regardless of boundary conditions and that the k value can be adjusted for the differences in shear transfer.

Cantilever beams under distributed loading

For cantilever beams, the shear capacity is shown in relation to l/d and the reinforcement ratio in the Figure 11. In the graphs it is shown that the critical location r_A lies between 1d-1.5d, but the thesis also mentions that another experimental investigation had observed a distance between 1d – 2.6d. Note that for larger l/d and ρ, the position moves further away from the supports in the graphs.

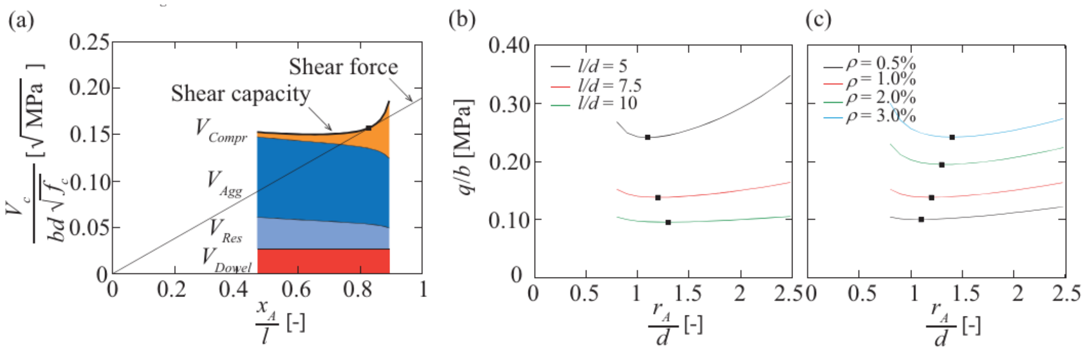

Figure 11 Shear capacity of cantilever beams under distributed loads for possible control sections and different parameters (Cavagnis F. , 2017)

For cantilever beams a reduction can be done on the applied shear loads. This reduction is applied because the moment to shear ratio is determined at x_f instead of x_a, and an increased dowel action is present. A reduction of $q * \Delta x$ can be done on the applied shear loads from x_a or $q * \Delta x_{tot}$ from x_f, where $\Delta x_{tot} = x_F - x_A + \Delta x$. This is shown in Figure 12.

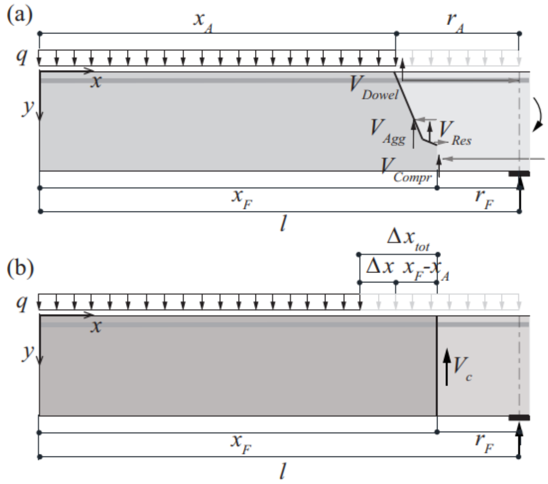

Figure 12 Cantilever subjected to distributed loading: (a) rigid body equilibrium and internal forces; (b) definition of Δx_{tot} (Cavagnis F. , 2017)

The values of $\Delta x_{tot}/x_F$ are plotted in Figure 13, together with locations of r_F. without great loss of accuracy $\Delta x_{tot}/x_F$ is estimated as 1/5 for all cases, which means $\Delta V = \frac{V_F}{5}$. This means that the shear capacity is increased by 25% (as only 80% of the load is carried by the crack.).

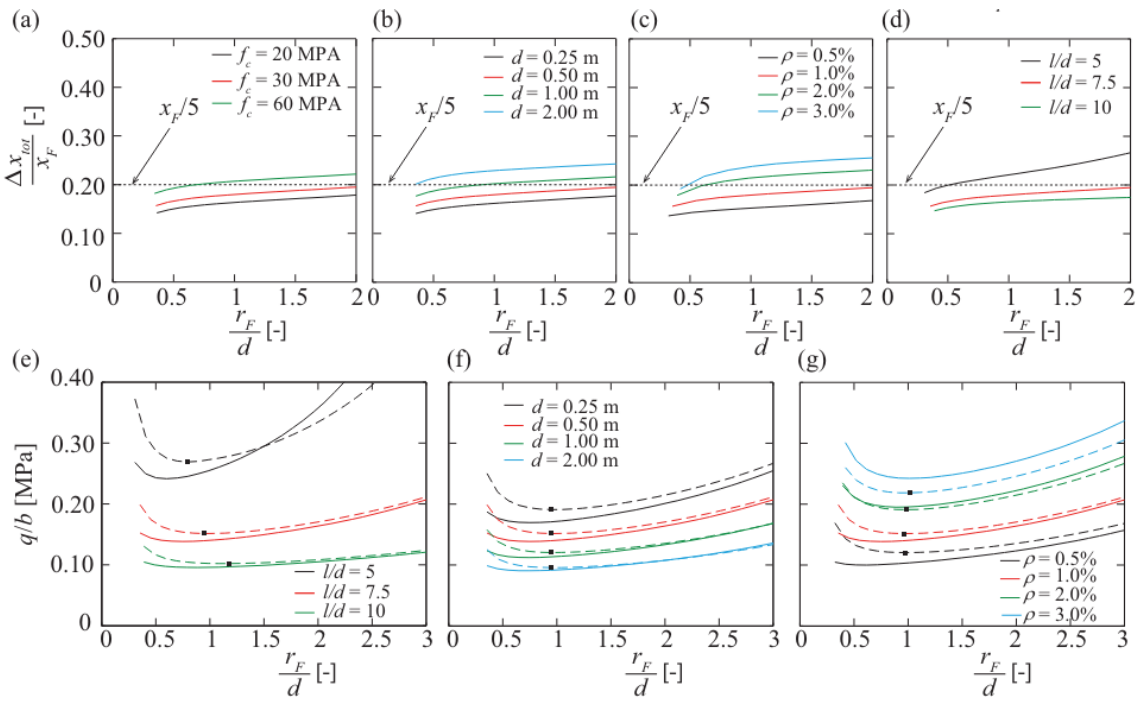

Figure 13 x_{tot}/x_F and the capacity of cantilever beams under distributed loads for possible control sections and different parameters (Cavagnis F. , 2017)

The effect of l/d, d and ρ on r_f/d is also shown in the graphs. The l/d ratio seems to be the only parameter affecting the location of r_f while location r_a also seems to be influenced by ρ as can be seen in Figure 11 and Figure 13. The minimum capacity is found when r_f=d for most cases and the graphs are relatively flat around this value, for this reason r_F =d (and thus x_F=l-d) has been determined as the control section for cantilever beams.

Continuous beams under distributed loading

For continuous beams under distributed loading, the critical control section is once again investigated. As is done before with the cantilever beam, a reduction is made on the applied shear forces of $\Delta V = \frac{V_F}{5}$, increasing the capacity. The minimum load capacity can be found at control sections r_F between 0.5d and 0.75d, and l/d seems to be the only parameter influencing this location as can be seen in Figure 14. Because low values of a_{cs}/d show overestimation of the capacity, and a consistent use r_f =d is preferred, a limit of $a_{cs} \geq d$ is introduced. With this limit the capacity has become almost constant after r_f =0.75d, thus allowing the use of r_f =d as critical cross section like cantilever and simply supported beams.

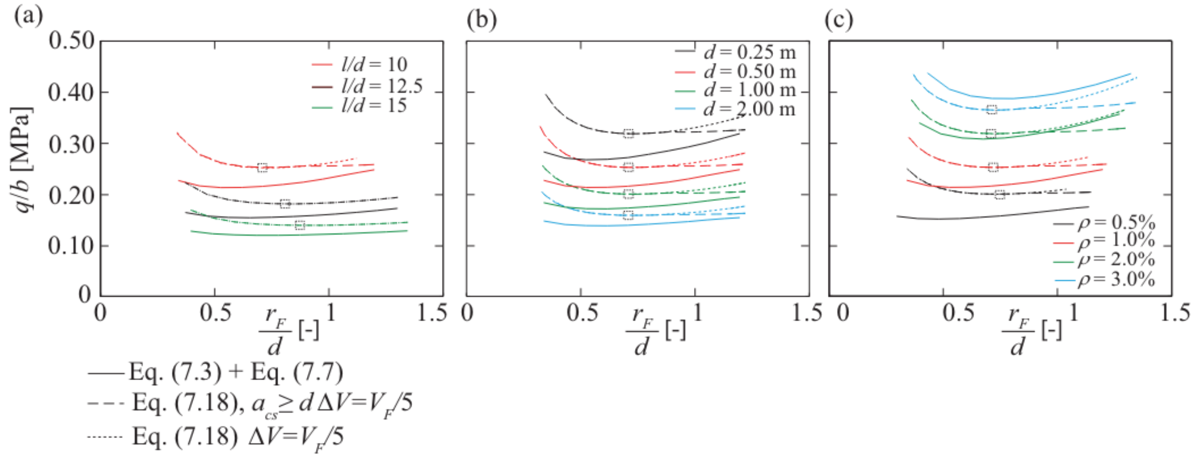

Figure 14 Shear capacity of continuous beams under distributed loads for possible control sections and different parameters (Cavagnis F. , 2017)

3.1.2 Hicks

(Hicks, 1958) contains a model for prestressed I-beams loaded by a concentrated load in a simply supported setup. The beam's prestressing was designed in such a way that the top fibre has zero stress and the bottom fibre a stress of -13.8 MPa. The beam did not contain transverse reinforcements. Different shear span-to-depth ratios (0.35-8.15) and concrete strengths (32-48 MPa) were investigated to study their influence on the capacity.

At low shear span-to-depth ratios (a/d < 1.5) shear distortion failures were observed, where cracks occur in the web. The crack angles for these failures varied between 48° and 32°. For higher shear span-to-depth ratios (1.5 < a/d < 5) diagonal compression failure was observed. When a/d was on the lower end of this range, failure resembled the shear distortion type. If a/d is on the higher side the failure resembles diagonal tension failure. For diagonal tension failure (4.5 < a/d < 9) no web cracking occurred before failure and a crack angle of 19° was found, which was roughly equal to the estimate of the principal stress theory.

The relation between the shear span-to-depth ratio and the crack angle is given in Figure 15. This graph also shows the relationship between the shear span-to-depth ratio and the principal tensile stresses at failure. According to the graph, the crack angle is close to 45° for very small a/d ratios and reduces significantly when a/d is increased. For a/d > 3.5, the crack angle seems to be constant around 18°.

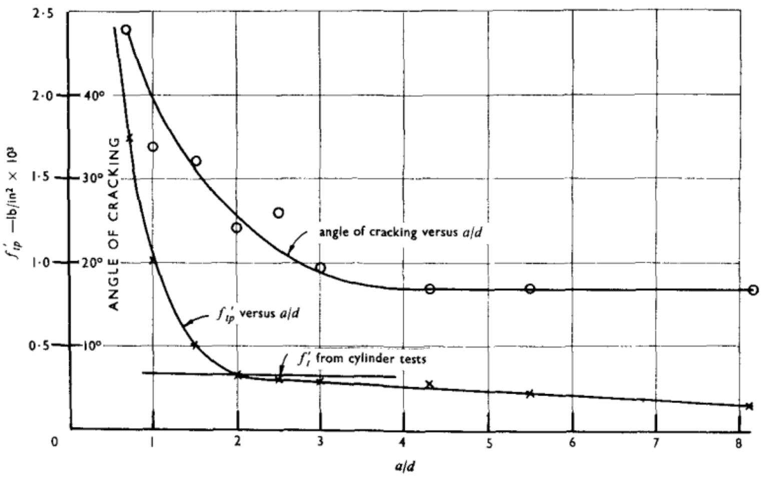

Figure 15 Relation between angle of cracking and f_{tp}' (principal tensile stresses at failure) and the shear span-to-depth ratio (Hicks, 1958)

3.1.3 RBK

The RBK (Richtlijnen Beoordeling Kunstwerken), is a Dutch code to assess and verify structures such as bridges. The inclination angle according to RBK is only dependant on the compressive stress due to prestressing σ_{cp}. The code assumes an angle of 45 degrees for elements where no prestressing is present and a 30-degree angle for elements where the concrete stress due to prestressing σ_{cp} >5 N/mm^2. This concrete stress should be determined at the location where the stresses due to prestressing are completely transferred to the concrete. (Rijkswaterstaat, 2022b)

Between $0 < \sigma_{cp} < 5$ N/mm^2 a linear interpolation should be done from 45 to 30 degrees. The RBK states that these values were used because angles smaller than 45 degrees were found in experimental data when prestressed elements were investigated, whilst observing values of 45 degrees when no prestressing is present. No detailed information is provided on how the 30 degrees or linear interpolation are achieved, and the angle is assumed to be a crude estimate.

3.1.4 Mohr circle

In (Dolan & Hamilton, 2019), the principal angle prior to cracking is discussed based on the Mohr circle. In this theory the element with shear stresses is rotated by the crack angle θ, so that it will be loaded only in principal directions f_1 and f_2. This theory is widely used to analyse stresses in concrete but has in this case been used to estimate the shear crack angle θ. In Figure 16 two Mohr-circles are shown, (a) in case of no prestressing, and (b) in case of prestressing.

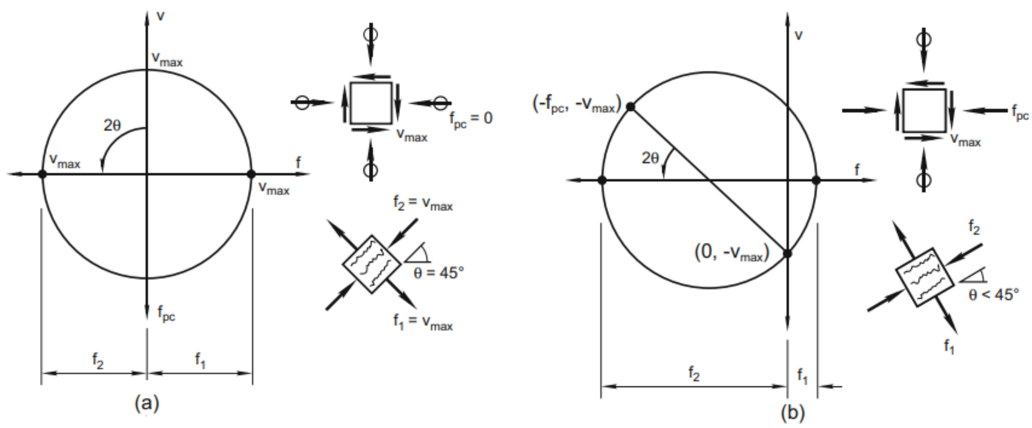

Figure 16 Principal stresses at neutral axis in beam with (a) No prestressing and (b) prestressing (Dolan & Hamilton, 2019)

The shear stress denoted as V_{max}, when prestressing is applied, can be expressed in the following formulae, based on the figure (b) above, Pythagoras theorem and trigonometry:

$$V^2 = \left(\frac{\sigma_{cp}}{2} + f_1\right)^2 - \left(\frac{\sigma_{cp}}{2}\right)^2$$
$$V = \left(\frac{\sigma_{cp}}{2} + f_1\right) * \sin(2\theta)$$
Combining these two formulae an expression is for θ can be obtained:
$$\left(\frac{\sigma_{cp}}{2} + f_1\right)^2 - \left(\frac{\sigma_{cp}}{2}\right)^2 = \left(\frac{\sigma_{cp}}{2} + f_1\right)^2 * \sin^2(2\theta)$$
$$1 - \frac{\left(\frac{\sigma_{cp}}{2}\right)^2}{\left(\frac{\sigma_{cp}}{2} + f_1\right)^2} = \sin^2(2\theta)$$
$$\cos^2(2\theta) = \left(\frac{\frac{\sigma_{cp}}{2}}{\frac{\sigma_{cp}}{2} + f_1}\right)^2$$
$$\theta = \frac{1}{2}\cos^{-1}\left(\frac{\frac{\sigma_{cp}}{f_1}}{\frac{\sigma_{cp}}{f_1} + 2}\right)$$
In this formula f_1 can be replaced by the tensile strength of the concrete as this will be the critical stress in f_1 direction. This results in the graph shown in Figure 17, where the angle is plotted against the ratio σ_{cp}/f_{ct}, where σ_{cp} is the stress due to prestressing and f_{ct} the concrete tensile strength.

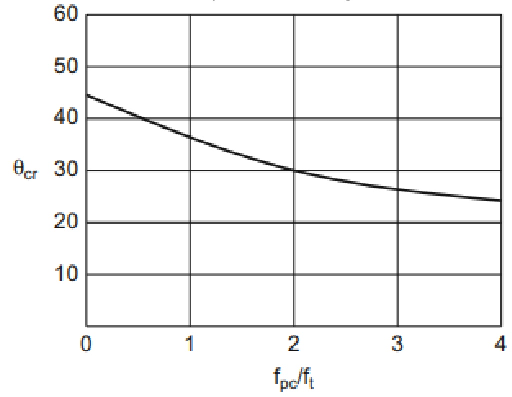

Figure 17 Principal angle based on applied prestressing (Dolan & Hamilton, 2019)

From Figure 17 it can be seen that without prestressing the angle is 45 degrees as is expected. For high prestressing, where prestressing stress is 4 times larger than the tensile strength, the critical angle is roughly 24 degrees. Although related, it should be noted that the angle is not the crack angle but the rotation of the principal directions before cracking. After cracking this method is said to be no longer applicable as the concrete no longer behaves linear and isotropic. Nevertheless, it may give an indication of the crack angle.

3.1.5 Görtz

In (Görtz, 2004) a linearized estimation of the crack angle is given by:
$$cot\theta = 1 - 0.18\frac{\sigma_{cp}}{f_{ctm}} \leq 2.15$$
When the effect of the shear reinforcement ratio is also considered, the following formula can be used instead:
$$cot\theta = 1 + \frac{0.15}{\omega_{w,ct}} - 0.18\frac{\sigma_{cp}}{f_{ctm}} \leq 2.15$$
$$\omega_{w,ct} = \rho_w * \frac{f_y}{f_{ctm}}$$
The latter formula gives low angles when a low amount of shear reinforcement is used. When the minimum shear reinforcement of $\rho_{w,min} = 0.08\sqrt{f_{ck}}/f_{yk}$ (Eurocode2, 2015) is used for C40/50 concrete, a $cot\theta > 2$ is found even without prestressing.

3.1.6 Kuchma, Hawkins, Kim, Sun & Kim

In (Kuchma, Hawkins, Kim, Sun, & Kim, 2008) simplifications to AASHTO LRFD are discussed. In this discussion two formulas are presented for the diagonal compression angle, which is assumed to be equal to the crack angle. AASHTO LRFD uses the angle to estimate the shear capacity, but the angle itself may be inaccurate. Nevertheless, the formulas are given (MPa is used).

SIMP method: $\cot(\theta) = 1 + 1.143 * \frac{f_{pc}}{\sqrt{f_{c'}}} \leq 1.8$

CSA: $\theta = 29 + 3500\varepsilon_S$; where $\varepsilon_s = \frac{\frac{M_u}{d_v} + 0.5N_u + V_u - v_p - A_p f_{po}}{E_s A_{sl} + E_p A_p}$

The formula from the CSA method, which can also be found in (Holt, et al., 2022), requires iteration and assumes a critical cross section. Because the critical cross-section is the desired output and not a known input, additional effort would be required when using this method. This method, which already consists of iteration is therefore not deemed suited to find the crack angle and the critical cross section for continuous beams,

3.1.7 Blesa

In the thesis of (Blesa, 2019) twelve tests have been performed on simply supported, partially prestressed, I-beams. Although these tests are not done on continuous beams, valuable insight is obtained. In (Blesa, 2019), (multi)linear regression analyses are used to estimate the crack angle based on the stress ratio (SR = $\frac{\sigma_{cp}}{f_{ct}}$) and/or the shear reinforcement ratio ρ_w. For cracks in failure, the angle estimated using SR is:

$$cot\theta = 2.0844 + 0.1939 * \frac{\sigma_{cp}}{f_{ct}}$$

For cracks in failure, the angle estimated using ρ_w is:

$$cot\theta = 2.5767 - 126.68 * \rho_w$$

The angle can also be estimated using both SR and ρ_w:

$$cot\theta = 2.42 - 134.90 * \rho_w + 0.23 * \frac{\sigma_{cp}}{f_{ct}}$$

The same has been done for cracks in service rather than in failure. For cracks in service, the angle estimated using the stress ratio is:

$$cot\theta = 1.5813 + 0.4467 * \frac{\sigma_{cp}}{f_{ct}}$$

For cracks in service, the angle estimated using the shear reinforcement ratio is:

$$cot\theta = 2.2754 - 126.9 * \rho_w$$

For cracks in service, the angle estimated using both SR and ρ_w is:

$$cot\theta = 1.94 - 144.38 * \rho_w + 0.48 * \frac{\sigma_{cp}}{f_{ct}}$$

Multiple observations are made on these linear relationships:

- It is visible that for low ρ_w, cotθ will remain above 1.5, even when little or no prestressing is applied. This gives angles of θ < 33.7° even when angles of ~45° may be expected.
- It can be observed that cotθ increases when SR increases but decreases when ρ_w increases. This behaviour is expected and means the crack angle decreases with increasing SR and increases with increasing ρ_w.
- When the crack angles at service and failure load are compared two differences can be identified; cotθ is higher at failure in all cases, and the effect of SR and ρ_w on cotθ is lower at failure compared to the effect under service load.

3.1.8 Zheng (RC)

In (Zheng, et al., 2023) and (Zheng, et al., 2023b) estimations of the strut angle are discussed based on the minimum Energy Principle. This is done to estimate shear stiffness in RC cracked beams. The Formula obtained results in solutions which are too complex to express accurately. Figure 18 however, gives a clear overview of the effects of the shear span-to-depth ratio $\lambda_{MV} = \frac{M}{Vd_v}$, shear reinforcement ratio ρ_v, and longitudinal reinforcement ratio ρ_l.

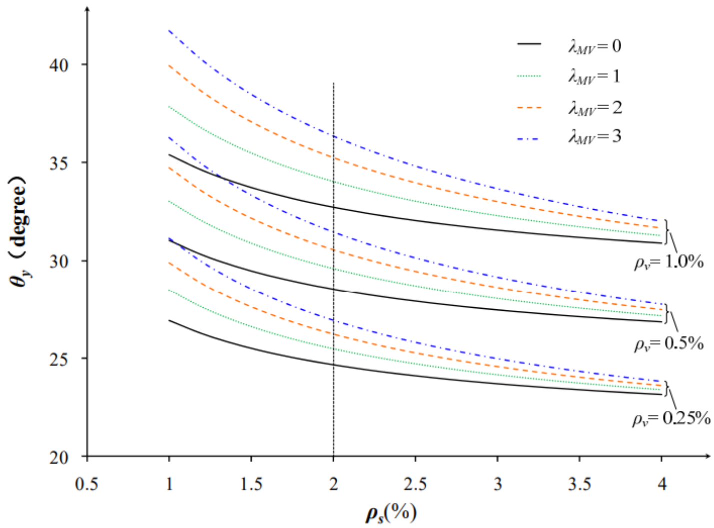

Figure 18 The influence of λ_{MV} on the angle (Zheng, et al., 2023)

An increase in longitudinal reinforcement decreases the strut angle, while an increase in shear reinforcement decreases the strut angle. It can also be observed that λ_{MV}, especially for low longitudinal reinforcement ratios, can have a significant effect on the strut angle, increasing the angle for larger λ_{MV}. This indicates that for larger spans the crack angles will increase.

In (Zheng, et al., 2023b) it is also mentioned that the concrete strength influences the strut angle, but this effect seems to be significantly less than that of λ_{MV}, ρ_v, and ρ_l.

3.1.9 Overview of models

In (Cavagnis F. , 2017) critical shear cracks are considered for reinforced simply supported, cantilever and continuous beams. Prestressed beams are not discussed in detail, but it is mentioned that the same method using a reduced effective shear span can be used. It is observed that the (shear) span to effective depth ratio (a/d) has a clear influence on the location of the critical cross section; for increasing a/d or l/d the distance to the governing control section from the support r_f also increases. When the cantilever beams are investigated, it is shown that the longitudinal reinforcement ratio also affects the location where the crack meets the reinforcement r_a; with increasing amounts of reinforcement r_a becomes larger. Although the governing cross section locations are not constant, it is shown that the capacity at 1d generally is very close to the capacity at the governing cross section. Therefore, in (Cavagnis F. , 2017) it has been concluded that the governing cross section can be assumed to be located at a fixed 1d from static or geometric discontinuities (e.g. supports).

In (Hicks, 1958) a relationship is shown between the shear span-to-depth ratio and the crack angle. Crack angles are close to 45° for very small a/d ratios and reduces for increasing a/d. From the moment a/d = 3.5 is reached the crack angle seems to remain constant around 18° for increasing a/d ratios.

The models that do not require iteration (RBK, Mohr, Görtz, SIMP, Blesa) and consider prestressed concrete (simply supported) have been combined in a graph. The graph shows the relationship between the ratio σ_{cp}/f_{ct} and estimated crack angle θ for simply supported beams. Some models require the concrete compressive strength and/or shear reinforcement ratio, for this reason C40/50 concrete and a minimum shear reinforcement ratio has been assumed while creating the graph. This assumption also makes it possible to express models such as RBK, where the angle is not inherently related to the tensile strength. To prevent the graph from becoming too crowded, the formulas found in (Blesa, 2019) for service loads, and the formulas neglecting the influence of shear reinforcement found in (Blesa, 2019) and (Görtz, 2004) are found in the Appendix A. instead.

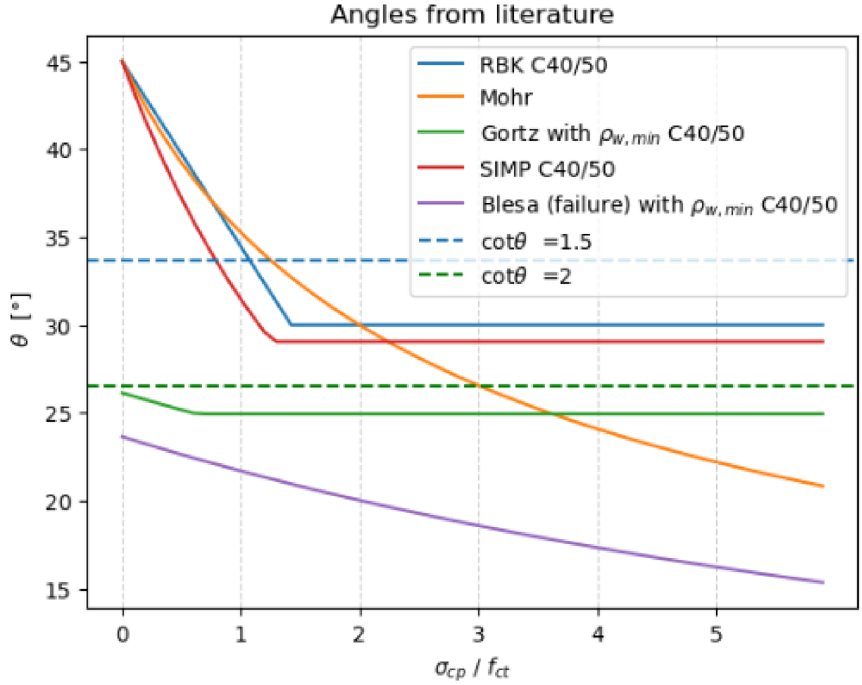

Figure 19 Relationship between the crack angle and σcp/fct for models found in literature for simply supported beams

From Figure 19 it is observed that if the compressive stresses are equal to the tensile strength of concrete, the crack angles of all models are close to or below 33.7° (cotθ =1.5). Because in prestressed concrete the compressive forces are generally larger than the tensile strength, it is assumed for simply supported prestressed beams that the crack angle will be thus likely be lower than 33.7°.

(Zheng, et al., 2023) does not consider prestressing, however it is shown in Figure 18 that for low amounts of shear reinforcement (0.5%) the strut angle will be below 33.7°. If it can be assumed that the crack angle is roughly equal to the strut angle this would further indicate that the angle of 33.7° may be an accurate crack angle. It can also be observed that the shear span-to-depth ratio plays an important role and will increase the strut angle for larger values.

3.2 Experiments

Only a small number of experiments have been found in literature that consider prestressed continuous beams failing in shear. Due to the absence of more relevant experiments, experiments with external prestressing or without identification of the critical shear cracks have also been considered. The small number of experiments meant that no detailed analysis was possible.

3.2.1 Huber, Huber, Kolleger

In (Huber, Huber, & Kollegger, 2018) tests have been done on prestressed cantilever T-beams. The paper also includes tests on simply supported setups and a test on a beam with slightly different loading conditions, but these are not considered in this thesis. Three experiments have been conducted in a similar setup and are considered: The first contained no shear reinforcement, the second contained ρ_w=0.074%, and the third ρ_w=0.168%. All beams have been prestressed to σ_{cp}=4.5

MPa and have a mean splitting tensile strength of roughly 4.5 MPa. Multiple concentrated loads were introduced with piston jacks to simulate a distributed loads in the span, and a single load is introduced at the end of the cantilever.

The experiment without transverse reinforcement shows a critical shear crack that does not originate from a flexural crack and has a crack angle of roughly 12°. Beams with shear reinforcement show critical flexural shear cracks. The crack angles of these beams are around 21° on average (between 18-25°).

3.2.2 Li, Zhang, Niue

In (Li, Zhang, & Niu, 2011) an experimental study has been conducted on shear behaviour of segmental and externally prestressed continuous T-beams. The beams are loaded with concentrated loads. The study contains three monolithic experiments that may be relevant to this thesis. These experiments contain a longitudinal reinforcement ratio of 3% to guarantee shear failure, and a shear reinforcement ratio of 0.34%. The critical crack inclinations found in these experiments are in the range of 25-30°, in the case of a concrete compressive stress of 3 MPa due to prestress. The expected tensile strength is 4.07 MPa (based on C50/60 concrete).

It should be noted that these experiments contain external prestressing and are likely behave differently from internally prestressed beams due to the different load transfer mechanisms. As internally prestressed beams are expected to have higher capacities and different crack patterns, these externally prestressed experiments may not be representative of other prestressed continuous beams, which are more often internally prestressed. Nonetheless, they offer insights into externally prestressed beams and may also provide indications about the behaviour of internally prestressed beams.

3.2.3 Herbrand & Classen

In (Herbrand & Classen, 2015) externally prestressed continuous I-beams have also been investigated. Six tests have been conducted on three continuous beams with concentrated loads, where one span of the beams has a shear reinforcement ratio of 0.067% and the other span a shear reinforcement ratio of 0.133%. The concrete compression due to the internal prestressing was 2.0 MPa in all three beams. In the second and third beam, additional compressive stresses equal to 1.5 and 2.5 MPa respectively were present from external prestressing. The splitting and tensile strength of the concrete are close to 3 MPa. No critical shear cracks have been identified in the paper, however from the crack patterns in Figure 20 angles of 20-30° are identified around the intermediate support.

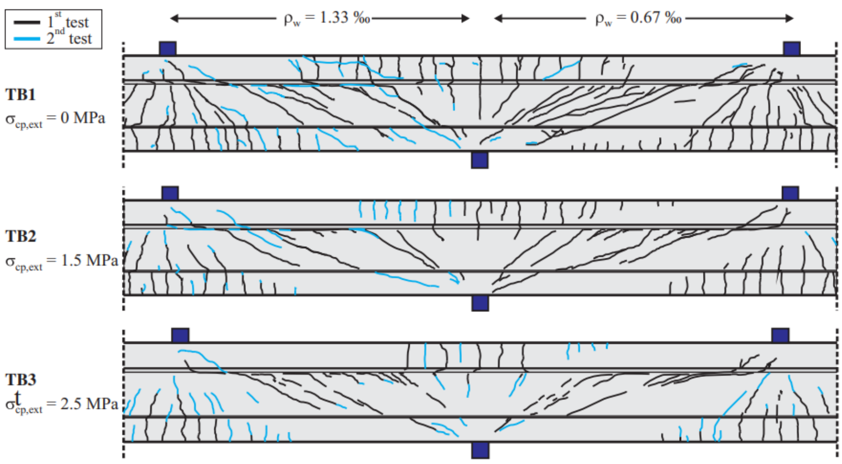

Figure 20 Crack patterns of test beams at shear failure (Herbrand & Classen, 2015)

From the experiments in (Herbrand & Classen, 2015) it is concluded that external prestressing mostly contributes to the initial shear cracking load, whilst only slightly increasing the ultimate shear capacity. When increasing amounts of external prestressing are applied the beam becomes more brittle.

3.2.4 Herbrand, Kueres, Classen, & Hegger

In (Herbrand, Kueres, Classen, & Hegger, 2018) two experiments on continuous prestressed beams with concentrated loads are shown, both with an average concrete compressive stress of 2.5 MPa due to prestressing. The splitting strength is roughly 3.65 MPa on average. The first experiment is done on a rectangular cross-section, the second experiment is done on an I-beam. Both experiments contain two tests, one on a section with 50% of the required shear reinforcement and the other on a section with 200% the required shear reinforcement. After the first section fails, it is strengthened so that the second section may be investigated.

From the crack patterns it can be observed that the smallest crack angles around the intermediate supports vary between 25-32° for all four tests. However, the cracks around the intermediate support did not become critical, instead the cracks found near the point loads became critical shear cracks.

3.2.5 Maurer, Gleich, Zilch & Dunkelberg

In (Maurer, Gleich, Zilch, & Dunkelberg, 2014) a prestressed continuous T-beam with concentrated loads has been tested twice. The first span of the beam contained d8/200 shear reinforcement, and the second span d12/200. This brings the shear reinforcement ratios to roughly 0.08% and 0.19% respectively. The average concrete stress due to prestressing is 4.72 MPa. The expected tensile strength lies between 3.21 and 4.21 MPa (based on C35/35 and C55/67 concrete)

Flexural shear cracks found in the experiment had crack inclinations between 25-40° while shear cracks had an inclination of around 20°. Failure did not occur near the intermediate support, but near the point load, where a flexural shear crack of 30° failed. The failure was caused by the yielding of the shear reinforcement and the subsequent crushing of concrete.

3.2.6 Overview of experiments

Even though some of the experiments are done on externally prestressed beams and the results may differ from internally prestressed beams, the effect of axial compression can still be investigated. For each of the papers σ_{cp}, σ_{cp}/f_{ct}, and θ are given below. For some papers the ratio σ_{cp}/f_{ct} is given as an estimated range. This is because not all papers determined the concrete properties accurately or considered varying prestressing levels.

- In (Huber, Huber, & Kollegger, 2018), the compressive stresses due to prestressing are σ_{cp}=4.5 MPa, $\sigma_{cp}/f_{ct} \approx 1$, and the critical crack angles are θ =18-25° for flexural shear failure. In the beam without transverse reinforcement the critical shear crack did not originate as a flexural crack, this crack has a crack angle of are θ =12°.
- In (Li, Zhang, & Niu, 2011) the compressive stresses due to prestressing are σ_{cp} =3 MPa, $\sigma_{cp}/f_{ct} \approx 0.75$, and the critical crack angles are θ =25-30°.
- In (Herbrand & Classen, 2015) the compressive stresses due to prestressing are σ_{cp} =2-4.5 MPa, $\sigma_{cp}/f_{ct} \approx$ 0.66-1.5, and the critical crack angles are θ = 20-30°.
- In (Herbrand, Kueres, Classen, & Hegger, 2018) the compressive stresses due to prestressing are σ_{cp} =2.5 MPa, $\sigma_{cp}/f_{ct} \approx 0.69$, and the critical crack angles are θ = 25-32°.
- In (Maurer, Gleich, Zilch, & Dunkelberg, 2014) the compressive stresses due to prestressing are σ_{cp} =4.72 MPa, $\sigma_{cp}/f_{ct} \approx$ 1.12-1.47, and the critical crack angles was θ = 30°.

In all experiments σ_{cp}/f_{ct} is estimated between 0.66-1.5 and the largest observed crack angle is 32°. From these experiments it is expected that in the general case that σ_{cp}/f_{ct} >1, the crack angles will likely be below 32°.

3.3 Conclusion

In (Cavagnis F. , 2017) critical shear cracks are considered for reinforced concrete beams. Although it was shown that the locations of the governing cross sections were not constant, the control cross section was proposed to be at 1d from supports, which was also adopted in the prEN 1992 proposal. This location was proposed by (Cavagnis F. , 2017) because he found that the capacity at 1d from supports was generally close to the capacity found at the governing cross section. However, this might only hold for reinforced concrete as prestressed concrete has not been discussed in detail. Therefore, other models are considered in this thesis, where the control section is estimated by finding the shear crack angle.

For simply supported beams it is shown using simple models, that the a/d ratio is an important parameter when determining the crack angle. Additionally, the reinforcement ratios ρ_l and ρ_w have a significant impact on the crack angle. When the different models are compared for prestressed concrete, it is observed that angles below 33.7° are likely to occur for σ_{cp}/f_{ct} >1. It is therefore indicated that 33.7° may be a better estimate for the crack angle than 45°.

It should be noted that applying the models from the simply supported beams to continuous beams may give unsafe estimates because of the inherent differences between the two. Additionally, the models are based on empirical data or principal stresses and may not accurately describe cracking behaviour. However, in the absence of better models, the estimate of 33.7° is assumed to be a reasonable estimate of the crack angles of continuous beams.

A small number of experiments on continuous/cantilever beams are discussed. As only a limited number of experiments can be found in literature, externally prestressed beams are included in this discussion. Additionally, two experiments that have been discussed show critical cracks near the point introduction rather than near the intermediate supports. It is found that for all experiments no critical shear crack angles above 32° are present. The compressive stresses due to prestressing in these experiments lies between 2 and 4.72 MPa, and the ratio σ_{cp}/f_{ct} lies between 0.66-1.5. One experiment is done on a cantilever beam without shear reinforcement. This beam shows a critical shear crack that does not originate from a flexural crack, with a crack angle of 12°.

The models and experimental data show that for prestressing levels close to the tensile strength, the crack angles are expected to be below 33.7° and 32° respectively. Based on this it may be possible to adjust the control section for prestressed continuous beams from 1d to 1.5d (cot(33.7°)). However, because the models are not designed to accurately estimate the crack angles for continuous beams, and there is a limited number of experiments, there is no guarantee that this adjustment would be safe.

4. Finite Element Analysis (Smeared)

Due to the lack of experimental data on prestressed continuous beams with low amounts of shear reinforcement, it is investigated if results of Finite Element Models can be used to investigate what influences the critical crack location and angle. If FEA provides accurate estimates, it may be possible to apply a regression analysis to the results. However, before FEA can be used for this purpose, it should be shown that FEA can indeed provide accurate and consistent estimations for different load and boundary conditions. For this reason, three experiments with significant differences are modelled and the results are compared to the experimental data. The first experiment is done on a simply supported reinforced concrete square beam. The second and third experiments are done on a prestressed T-beam, with experiment 2 being simply supported, and experiment 3 containing a cantilever.

4.1 General settings:

Most of the settings used are given in the guideline (Hendriks & Roosen, 2022). However, as the recommended rotating models are physically unrealistic, different fixed models have also been investigated. The structural analysis done in Diana FEA will consist of a 2D model with quadrilateral elements and quadratic interpolation. Longitudinal reinforcement is modelled with simple line elements, and prestressing tendons are modelled with lines. Interface elements have been added between the (support) plates and the beam to prevent stress localisation.

The external loads are applied as a distributed load acting on the beam, or as concentrated loads acting on load plates. The prestressing load is added as a post-tensioning load: The anchor retention length =0.006 m, the friction factor $\mu = 0.19$ assumes bonded strands (internal tendons), and the wobble factor is assumed to be $k = 0.01$/m. Post tension scheme according to CEB-FIB Model code 1990 has been used. The friction factor and wobble factor are based on (Eurocode2, 2015), the anchor retention length due to anchorage slip is based on (ETA, 2017). Both rotating and fixed crack models are investigated, with different mesh sizes, aggregate sizes, and stiffnesses. To investigate if bond-slip reinforcement is more accurate, several additional models have been created for the aggregate-size based shear retention models, containing bond-slip behaviour. Properties, including the steel stress limits, of prestressing steel is given in Figure 21 found in (Walraven & Braam, 2019) and are based on the code NEN-EN 10138. Unless specified otherwise Y1860S7 will be used.

steel type	type	tensile strength		fracture strain	0,1% proof-stress	maximum tensile stress: during pre-stressing	maximum tensile stress: during pre-stressing with accurate jack	maximum tensile stress: initial stress	slope discontinuity in the σ-ε diagram (ULS)	modulus of elasticity
		f_{pk}	f_{pk}/γ_s	ε_{pu}	$f_{p0,1k}$	$\sigma_{p,max}$	$\sigma_{p,max}$	σ_{pm0}	f_{pd}	E_p
		MPa	MPa	‰	MPa	MPa	MPa	MPa	MPa	GPa
Y1030H	bar	1030	936	35	927	773	773	773	843	205 or 170
Y1670C	wire	1670	1518	35	1503	1336	1428	1253	1366	205
Y1770C	wire	1770	1609	35	1593	1416	1513	1328	1448	205
Y1860S7	strand	1860	1691	35	1674	1488	1590	1395	1522	195

Figure 21 Mechanical properties of prestressing steel (Walraven & Braam, 2019)

The analysis is run in two phases. First the prestressing load is added in a single step, after this the external load is incrementally increased using arc-length or displacement control. Regular Newton-Rhapson is used with both a displacement and a force norm of 0.01. The program is set up to iterate up to 15 times if no convergence occurs, after which it continues to the next increment. The mesh size in the models generally lies between 0.025 and 0.1 m and is in some cases varied to investigate the effect of refining the model.

4.2 Experiment 1 modelling simply supported

4.2.1 Geometry and properties

The beam SC51 found in (Cavagnis, Ruiz, & Muttoni, 2015) is modelled in DIANA FEA. This beam is simply supported, has a rectangular cross section (250 mm wide and 600 mm deep) and has a span of 5600 mm. The beam has 2ϕ28 on both the compressive and tensile sides with effective depth d=556 mm. The failure load was q = 60.4 kN/m and caused a crack pattern as shown in Figure 22.

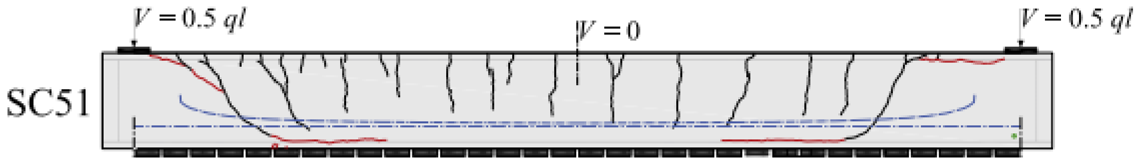

Figure 22 Crack pattern beam SC51 (Cavagnis, Ruiz, & Muttoni, 2015)

4.2.2 Material properties

The material properties that have been found in or derived from the paper are given here. For tables containing an overview including more detailed settings such as the shear retention and bond-slip parameters (only for some models) the reader is referred to Model properties experiment 1 in the Appendix.

The compressive strength of the concrete during testing has been found to be roughly 33.6 MPa. As the young's modulus of the concrete is not mentioned in the experiment, two options are used to estimate it. The first option is used in the 'base' model and uses a Youngs modulus according to C35/40 concrete, E=34000 MPa. The second option, referenced as 'alt. E', uses a calculation from the Eurocode to determine the Young's modulus based on the concrete strength, the mean Young's modulus according to this option is:

$$E_{cm} = 22000(f_{cm})^{0.3} = 31646\ MPa$$

The Poisson ratio used for concrete is 0.2 and is kept constant. The mass density is kept 0 in most models, the effect is tested in a model with a mass density of 2400 kg/m^3 for concrete.
The tensile strength of concrete is calculated according to the (Eurocode2, 2015) based on the compressive strength:

$$f_{ctm} = 0.3 * f_{ck}^{\frac{2}{3}} = 0.3 * (f_{cm} - 8)^{\frac{2}{3}} = 2.606\ MPa$$

The (tensile) fracture energy is once again calculated based on the compressive strength:

$$G_F = 0.073 * f_{cm}^{0.18} = 0.073 * 33.6^{0.18} = 0.137\ N/mm$$

To model supports, steel plates are used with linear elastic steel and a Young's modulus of 210000 MPa and a Poisson ratio of 0.3. The mass density of the steel is not considered.

The reinforcement steel has an average yield strength of roughly 710 MPa (average strength of 870 MPa after hardening). The Young's modulus of steel is assumed to be 200000 MPa. Embedded reinforcement is used to model the reinforcement bars. A linear strain hardening curve has been used to model plasticity. It is assumed that the ultimate plastic strain is equal to 0.05.

$$f_y = 710\ MPa;\ f_u = 870\ MPa;\ \varepsilon_u \cong 0.05$$

2D line interfaces have been added between the support plates and the concrete, the normal stiffness is assumed to be 2e^{13} N/m^3 and the shear stiffness is assumed to be 2e^8 N/m^3.

4.2.3 FprEN 1992-1-1 calculation

Before the FEA and experiment are compared, the capacity is estimated using the formulas found in the upcoming Eurocode (FprEN 1992-1-1, 2023). 1d from the support is considered as the control section. The factor γ_V has been assumed 1.4 for persistent and transient design, and d_{dg} has been assumed to be 32mm based on the maximum coarse aggregate size of 16mm as mentioned in the paper considering this experiment. A more complete calculation can be found in the Appendix**.**

$$a_{cs} = \left|\frac{M_{Ed}}{V_{Ed}}\right| = 624.9\ mm \geq d = 556\ mm$$

$$a_v = \sqrt{\frac{a_{cs}}{4} * d} = 294.7\ mm \leq d = 556\ mm$$

$$V_{Rd,c} = \frac{0.66}{\gamma_V}\left(100\rho_l * f_{ck} * \frac{d_{dg}}{a_v}\right)^{1/3} * b_w d = 96.9\ kN > \tau_{Rdc,min} * b_w d$$

$$V_{Rdc,min} = \frac{11}{\gamma_V}\sqrt{\frac{f_{ck}}{f_{yd}} * \frac{d_{dg}}{d}} * b_w d = 72.8\ kN$$

The maximum shear capacity is thus 96.9 kN according to the (FprEN 1992-1-1, 2023) calculation. To compare this value with the experimental load of q=60.4 kN/m, the shear capacity is rewritten to a distributed load that would cause this shear.

$$q_{Vrd,c} = \frac{V_{Rd,c}}{\frac{1}{2}L - d} = 43.2\ kN/m$$

As may be expected, the capacity found with (FprEN 1992-1-1, 2023) is conservative and is with $q_{Vrd,c}$ = 43.2 kN/m roughly 70% of the experimental value.

4.2.4 Results experiment 1

Numerous Finite Element Analysis have been done in an attempt to accurately model beam SC51. The crack patterns, and load displacement curves, ultimate load and estimated crack angles of all models can be found in the Appendix**.** Several relevant observations are made and are discussed in this chapter.

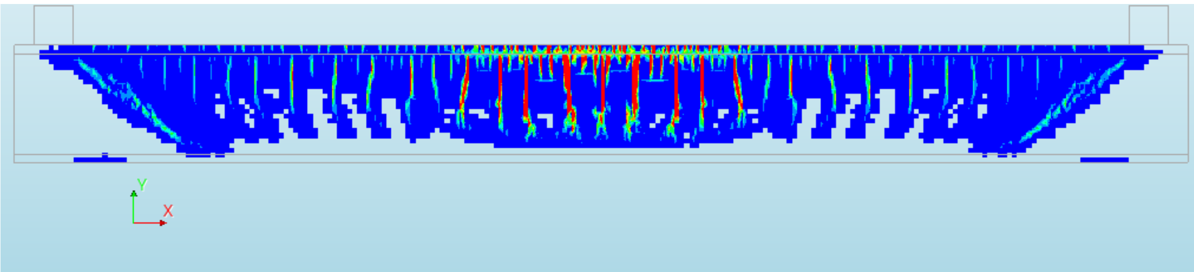

Figure 23 crack pattern experiment 1 fixed model based on mean aggregate size of 8 mm, refined, alt E

The Fixed models severely overestimate the capacity in most cases. For the fixed models with a shear retention based on aggregate size, the FEA was stopped at ~130 kN when still no failure was observed. At this point the longitudinal reinforcement had already become plastic and large flexural cracks are present as can be seen in Figure 23. The crack patterns of the aggregate size-based models were generally not like the experiments, regardless of if bond-slip was modelled.

When a constant shear retention of 0.01, or a damage-based shear retention was used instead of a shear retention based on aggregate size, more realistic capacities and crack patterns were found. The overestimated capacity for the aggregate based shear retention may be explained by how the shear retention decreases with damage. The shear retention is 1 for closed cracks and decreases linearly to 0 when the crack width is equal to the mean aggregate size. This overestimates the capacity, especially for lower crack widths, as in reality the shear retention drops fast for small crack widths. Another possible cause for the high capacity may be that shear locking occurred during the analysis, causing unrealistic results.

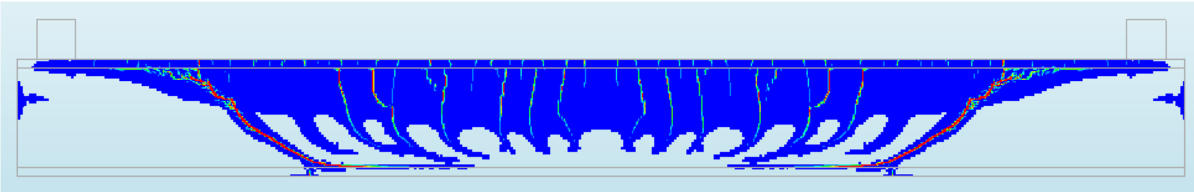

Figure 24 crack pattern experiment 1 rotating model, refined the mesh twice

The crack patterns found for the rotating models were consistent with the experimental crack pattern, and clear shear cracks are observed see Figure 24. The capacities found with the rotating models were also quite reasonable. However, when the mesh is refined, a significant increase in the capacity is observed. This indicates that the mesh size plays a significant role in the estimation and the accuracy is therefore questionable.

The rotating model seems to be the best fit for this rectangular simply supported beam, as the fixed models show unexpectedly high capacities and generally unsatisfactory crack patterns. The capacities found in both the experiment and the models are higher than the estimate using (FprEN 1992-1-1, 2023), this may be expected as this estimate is conservative.

4.3 Experiment 2 modelling simply supported prestressed T-beam

The second experiment, found in (Huber, Huber, & Kollegger, 2018) is done on a simply supported, prestressed T-beam without stirrups PC4.5T000. The beam has a span of 7500 mm, and a load located at 2740 mm from the left support. Square end blocks are assumed to be present to 100mm past the supports to spread the prestressing force. The expected failure load is 709 kN.

4.3.1 Geometry and properties

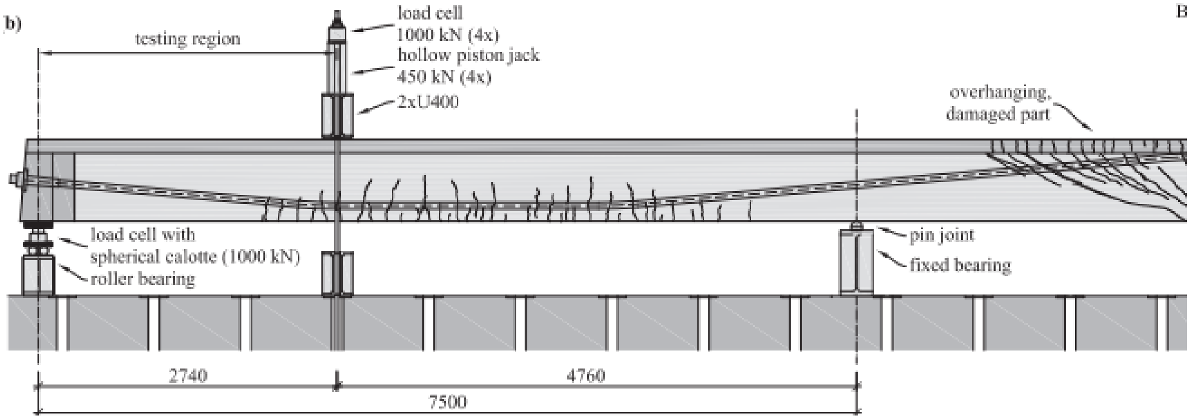

Figure 25 Test setup of a single-span beam subjected to a single point load (Huber, Huber, & Kollegger, 2018)

The test setup that has been modelled is shown in Figure 25. The prestressing tendon is simplified into linear parts in the models, this results in slightly different forces and effective depth throughout the model when compared to the experiment. The prestressing tendons (AP=1050 mm2) have been placed in the model according to the coordinates as shown in the table below. It should be noted that the model has an additional 400 mm (200mm added at both sides) in length, to ensure a 7500 mm span, without introducing high localized stresses.

Table 1 Location of the prestressing tendons experiment 2

X	Y
0	0.367
2.63	0.143
5.27	0.143
7.9	0.367

Other than prestressing tendons, regular longitudinal reinforcement is present. At the bottom, the web contains 6d26 reinforcement located at y=52 mm (from the bottom).
The top flange contains 12d12 reinforcement located at y =687 (from the bottom).
From X>6000 mm, additional reinforcement is present in the top flange; 4d26 +2d20 at y=708 (from the bottom). The dimensions of the top Flange and of the web are 750 x 125 and 225 x 625 mm respectively.

4.3.2 Material properties

The material properties derived from the paper are given here. For tables containing more detailed settings such as the shear retention and bond-slip parameters (only for some models) in addition to the material properties the reader is referred to Model properties experiment 2 in the Appendix.

The Youngs modulus of the concrete is 34351 MPa and the Poisson ratio is assumed to be 0.2. The compressive behaviour of concrete is assumed to be parabolic with a compressive strength of 69.5 MPa and a compressive fracture energy of

$$G_c = 250 * 0.073 * f_{cm}^{0.18} = 39158\ N/m$$

The tensile behaviour is modelled using the Hordijk curve, with a tensile strength of 4.5 MPa and a fracture energy of G_F =154.3 N/m

Steel plates have been used to model the supports and loading plates. These steel plates are linear elastic with a Young's modulus of 200000 MPa and a Poisson ratio of 0.3. The dimensions of the plates are 200 x 200 mm.

The reinforcement steel has a yield strength of 580 MPa and an ultimate strength of 670 MPa at an assumed plastic strain of 0.05. The Young's modulus of reinforcement steel is 200000 MPa.

The prestressing steel has a yield strength of 1750 MPa, and it is assumed that no hardening occurs. In reality the ultimate strength of the prestressing steel is 1908 MPa. The prestressing steel is loaded by a post-tensioning force of 1125 kN. The anchor retention length is assumed to be 0 due to pre-wedging, the coefficient of friction is assumed to be 0.18, and the wobble factor 0.05 m^{-1}.

2D line interfaces have been added between the support plates and the concrete, the normal stiffness is assumed to be $2e^{13}$ N/m^3 and the shear stiffness is assumed to be $2e^8$ N/m^3.

4.3.3 FprEN 1992-1-1 calculation

Before the FEA and experiment are compared, the capacity is estimated using the formulas found in the upcoming Eurocode (FprEN 1992-1-1, 2023). 1d from the concentrated load is considered as the control section. The factor γ_V has been assumed to be 1.4 for persistent and transient design, and d_{dg} has been assumed to be 32mm based on the maximum aggregate size of 16mm as mentioned in the paper considering this experiment. Because the capacity is based on the applied forces (through k_{vp}) it is not possible to find the capacity in a single calculation. For this reason, a simple python script was written, the (rounded) results are given in the formulas below. A more complete calculation can be found in the Appendix.

$$d = \frac{d_s^2 * A_{sl} + d_p * A_p}{d_s * A_{sl} + d_p * A_p} \cong 672\ mm$$

$$a_{cs} = \left|\frac{M_{Ed}}{V_{Ed}}\right| = 2067.9\ mm \geq d = 672\ mm$$

$$a_v = \sqrt{\frac{a_{cs}}{4} * d} = 589.4\ mm \leq d = 672\ mm$$

$$k_{vp} = 1 + \frac{N_{Ed}}{|V_{Ed}|} * \frac{d}{3 * a_{cs}} = 0.42 \geq 0.1$$

$$V_{Rd,c} = \frac{0.66}{\gamma_V}\left(100\rho_l * f_{ck} * \frac{d_{dg}}{k_{vp} * a_v}\right)^{1/3} * b_w d = 209\ kN > \tau_{Rdc,min} * b_w d$$

$$V_{Rdc,min} = \frac{11}{\gamma_V}\sqrt{\frac{f_{ck}}{f_{yd}} * \frac{d_{dg}}{d}} * b_w d = 104.4\ kN$$

The maximum shear capacity is thus 209 kN at the critical control section. To compare this with the experimental load of F=709 kN, the shear capacity is rewritten so that it is expressed as concentrated load located at the same location as in the experiment. The reaction force at the left support was 0.635*F.

$$F_{VRd,c} = \frac{V_{Rd,c} + V_p}{0.635} = 483.6\ kN$$

Thus, the capacity found with (FprEN 1992-1-1, 2023) for this experiment is 483.6 kN. This value is conservative and only 68% of the experimental value.

If the capacity is checked at a control section 1d from the left support, the shear capacity would be 390.4 kN which is equivalent to a concentrated load would of 769.2 kN instead, which is closer to the experiment where the critical crack starts near the left support and reaches a capacity of 709 kN.

The shear capacity using the formula from (FprEN 1992-1-1, 2023) is shown to be highly sensitive to the moment acting on a control section.

4.3.4 Results experiment 2

Several models have been made of beam PC4.5T000. The crack patterns, load displacement curves, ultimate loads and estimated crack angles can be found in the Appendix. The relevant observations are discussed in this chapter.

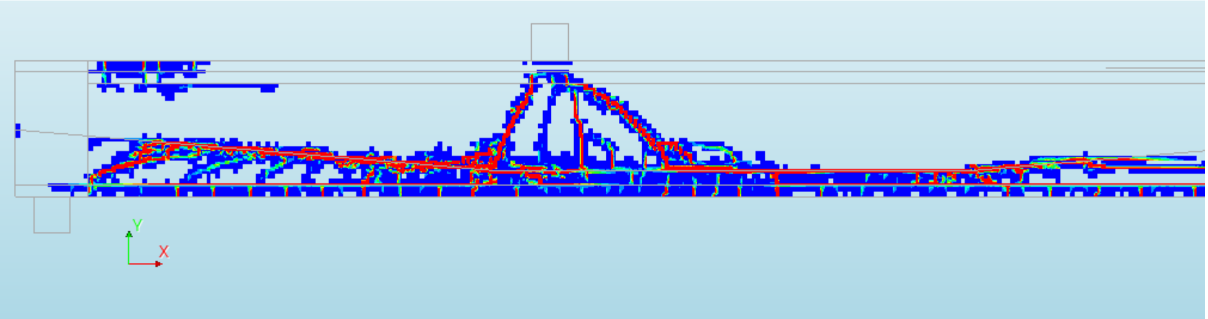

Figure 26 crack pattern experiment 2 rotating model

The crack patterns for the rotating models are quite poor as shown in Figure 26. A small number of flexural cracks are present in addition to large cracks following the reinforcement of steel. The critical shear crack found in the experiment is not observed. The capacity found with the rotating models is 12% higher than the capacity found with the experiment and is therefore quite accurate.

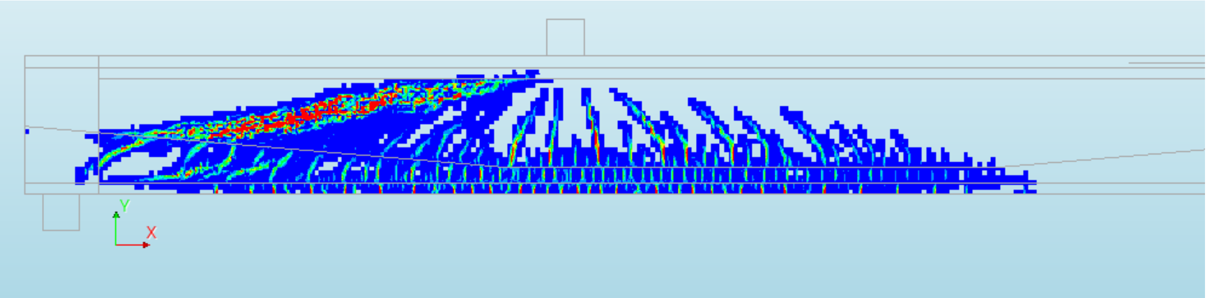

Figure 27 crack pattern experiment 2 fixed model based on mean aggregate size of 12 mm

The crack patterns found with the fixed models based on aggregate size are more in line with the experiments. And a large shear crack can be observed in Figure 27. For some bond-slip models similar results could be found, while in others the crack patterns highly deviate. The capacity is overestimated by 20% in the fixed models, using an aggregate size-based shear retention, which is reasonably accurate. However, when the prestressing load is decreased or removed, a large increase in capacity is observed in the models using an aggregate size-based shear retention, while a decrease is expected. When a damage based or constant shear retention factor of 0.01 is used this unexpected behaviour is not observed but these models are unable to capture the crack patterns for this experiment. Possible causes for the increased capacity for the models using aggregate size-based shear retention are the fact that this shear retention is quite unrealistic, and shear locking.

If displacement control is used for the analysis instead of arc-length control, the capacity is increased by approximately 200 kN, for both rotating and fixed models, which is an unexpected increase of more than 20%. After a rigorous investigation of the settings, the only difference found between arc-length and displacement-controlled models, was the load step size (arc-length control required smaller load steps due to poorer convergence behaviour). For this reason, it is believed that the differences between the arc-length and displacement-controlled variants is caused by convergence behaviour and numerical errors. It is also possible that displacement control overestimates the capacity, as it cannot deal with snap-back behaviour, and tries to solve for displacements that could not be found with arc-length control.

From these results it seems that the fixed model (arc-length control) was able to best describe the shear failure of this simply supported prestressed T-beam. However, it seems to be unable to describe the shear failure in the case without prestressing in the case of aggregate size-based shear retention. Furthermore, the large differences between arc-length and displacement-controlled set-ups, put the accuracy of the models in question, as it may be expected that they should provide roughly the same peak loads.

4.4 Experiment 3 modelling continuously supported prestressed T-beam

Experiment 3 is done before experiment 2 on the same beam found in (Huber, Huber, & Kollegger, 2018). The setup contains a cantilever with a concentrated load to imitate a continuous beam. After failure occurs in the continuous part of the beam, it was possible to test the beam again resulting in experiment 2.

4.4.1 Geometry and properties

Experiment 3 has a span of 10.72 m, and a cantilever of 2.94 m and a total length of 14m. Between supports a distributed load is applied, at the cantilever a single concentrated point load is applied. The concentrated load is kept at a constant ratio of 5.11:1 to the distributed load. Failure occurs at 100.5 kN/m with the point load then being 513.5 kN.

The geometry and reinforcement layout used in the experiment is shown in Figure 28. A simplification has been made to the reinforcement layout in the models; it is assumed 4d26 on the bottom is applied throughout the entire element. At the bottom, the web contains 6d26 reinforcement located at y=62 mm (from the bottom). The top flange contains 12d12 reinforcement located at y =687 (from the bottom). From X>6000 mm, additional reinforcement is present in the top flange; 4d26 +2d20 y=708 (from the bottom).

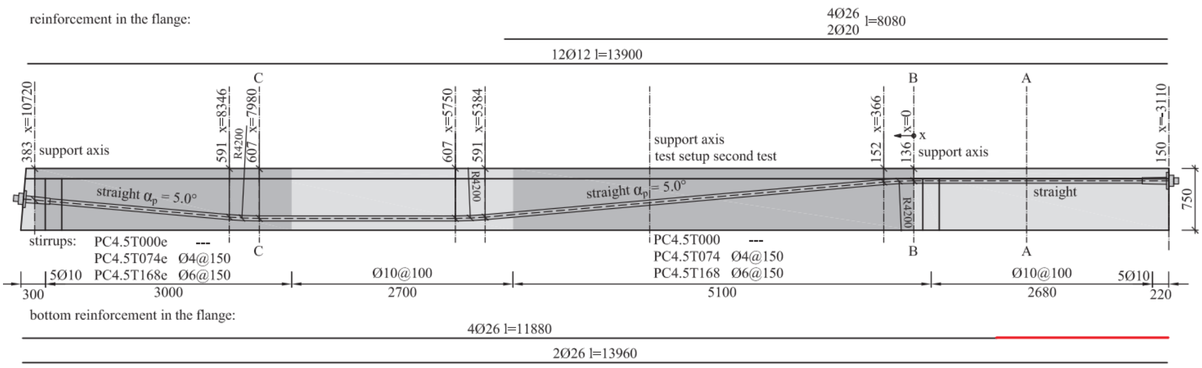

Figure 28 Longitudinal view of the reinforcement layout and tendon profile (Huber, Huber, & Kollegger, 2018)

The prestressing tendons are again modelled as multiple linear segments. The estimated location of the tendons differs slightly from experiment 2 as the estimates are done slightly differently. This small difference should have only a small effect on the results. The tendon profile shown Table 2.

Table 2 Location of the prestressing tendons experiment 3

X	Y
0	0.367
3.03	0.143
5.17	0.143
10.92	0.614
14.06	0.6

4.4.2 DIANA Settings

Because experiment 3 is done with the same beam as experiment 2, all the properties of experiment 2 also apply to this experiment. For the material properties the reader is referred to '4.3 Experiment 2 modelling simply supported prestressed T-beam'. For more detailed model settings, including shear and bond slip behaviour the reader is referred to

Model properties experiment 3 in the Appendix.

4.4.3 FprEN 1992-1-1 calculation

Before the FEA and experiment 3 are compared, the capacity is estimated using the formulas found in the upcoming Eurocode (FprEN 1992-1-1, 2023). 1d from the intermediate support is considered as the control section. The factor γ_V has been assumed to be 1.4 for persistent and transient design, and d_{dg} has been assumed to be 32mm based on the maximum aggregate size of 16mm as mentioned in the paper that considers the experiment. A more complete calculation can be found in the Appendix.

$$d = \frac{d_s^2 * A_{sl} + d_p * A_p}{d_s * A_{sl} + d_p * A_p} \cong 677.8\ mm$$

$$a_{cs} = \left|\frac{M_{Ed}}{V_{Ed}}\right| = 2631\ mm \geq d = 677.8mm$$

$$a_v = \sqrt{\frac{a_{cs}}{4} * d} = 667.8\ mm \leq d = 677.8mm$$

$$k_{vp} = 1 + \frac{N_{Ed}}{|V_{Ed}|} * \frac{d}{3 * a_{cs}} = 0.52 \geq 0.1$$

$$V_{Rd,c} = \frac{0.66}{\gamma_V}\left(100\rho_l * f_{ck} * \frac{d_{dg}}{k_{vp} * a_v}\right)^{1/3} * b_w d = 200.4\ kN > \tau_{Rdc,min} * b_w d$$

$$V_{Rdc,min} = \frac{11}{\gamma_V}\sqrt{\frac{f_{ck}}{f_{yd}} * \frac{d_{dg}}{d}} * b_w d = 103.7\ kN$$

The maximum shear capacity is thus 200.4 kN at the critical control section. To compare this value with the experimental load of q=100.5 kN/m, the shear capacity is rewritten so that it is expressed as distributed load.

$$q_{Vrd,c} = \frac{V_{Rd,c} + V_P}{11.87 - 5.11 - 0.678} = 44.8\ kN/m$$

Where 11.87 comes from the support, 5.11 from the concentrated load at the cantilever and 0.678 from the distributed load. V_P is the shear caused by the prestressing (also present in V_{Ed}) and is equal to 72.26 kN in the tested area.

Thus, the capacity found for this experiment is very conservative and only 45% of the experimental value. In the experiment it is shown that the critical crack is located at ~2800 mm from the intermediate support. According to (FprEN 1992-1-1, 2023) at this location the capacity is ~419 kN or q= 124 kN/m. This value is closer to the experiments but is still very conservative.

4.4.4 Results experiment 3

A small number of models have been created and investigated for the continuous beam PC4.5T000. The crack patterns, load displacement curves, ultimate loads and estimated crack angles of all different models for this experiment can be found in the Appendix. The relevant observations are discussed in this chapter. The rotating model was unable to create a crack pattern like the experiment. Instead, cracks were only observed very close to the support, see Figure 29. The capacity found with the rotating model 11% lower than the experimental value.

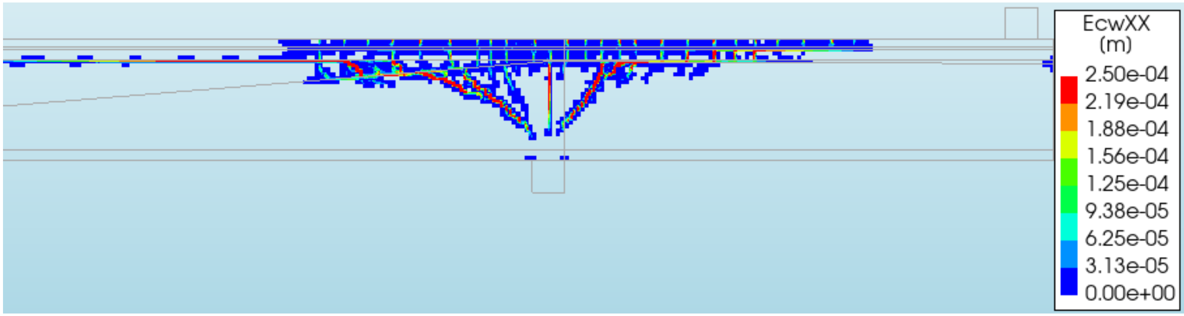

Figure 29 crack pattern experiment 3 rotating model

Of the fixed models, only the models based on a mean aggregate size of 12mm were able to give reasonable crack patterns with a large diagonal crack as is shown in Figure 30**.** The capacity with the fixed model is 16% higher than the experimental value. If no prestressing is present, the capacity is lower as is expected. The crack patterns barely change between the prestressed and non-prestressed variant. Of the three additional models containing bond slip behaviour two gave similar crack patterns. In the third model completely different crack patterns were observed, which shows that bond-slip properties can have a large influence on the crack patterns.

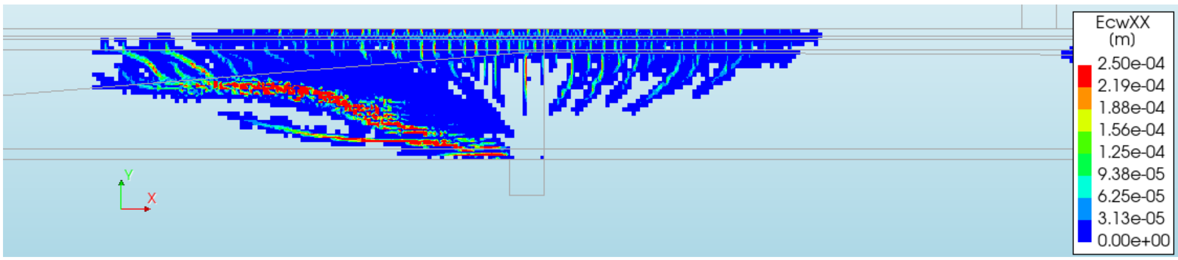

Figure 30 crack pattern experiment 3 fixed crack based on mean aggregate size of 12 mm

The fixed model based on a mean aggregate of 12 mm seems to best estimate the shear behaviour of the continuously supported prestressed T-beam If both the capacity and crack pattern are considered. The rotating models were not able to estimate a reasonable crack pattern.

4.5 Overview Smeared FEA

In the Finite Element Analyses three experiments have been modelled using the Diana FEA software. These experiments included: 1. a simply supported R.C. rectangular beam. 2. a simply supported P.C. T-beam 3. a continuously supported P.C. T-beam. Most of the settings adhered to the RWS guidelines for NLFEA, but some settings have been investigated. It was the hope of the author that with the right settings the shear behaviour could be estimated in an accurate and consistent manner so that the models could be expanded to hypothetical scenarios.

The main differences between models are based on shear retention. Aggregate-size based, damage-based and a constant 0.01 shear retention, as well as rotating models are investigated. These models all contain embedded bar reinforcement, except for the aggregate-size based models, where both embedded bar reinforcement and embedded bond-slip reinforcement are investigated. An overview of the results for each model and each experiment is given in Table 3, all the results can also be found in the Appendix. It can be observed that none of the models was able to estimate the crack angles and capacities in a reasonable manner for all three experiments. It is possible that no model is accurate for all loading- and boundary conditions, which could be related to the fact that generally simply supported beams are investigated under concentrated loads.

Table 3 Overview of the crack patterns and capacity found in FEA compared to the experiments

	Aggregate-size based		Constant shear retention 0.01		Damage based with Poisson reduction		Aggregate-size based Including Bond-slip		Rotating	
Experiment	Cracks	V_{FEM}/V_{Exp}	Cracks	V_{FEM}/V_{Exp}	Cracks	V_{FEM}/V_{Exp}	Cracks	V_{FEM}/V_{Exp}	Cracks	V_{FEM}/V_{Exp}
Experiment 1 (R.C.)	poor	2.00+	reasonable	1.31	good	1.04	-	-	reasonable	1.10 - 1.5
Experiment 2 (P.C.)	reasonable	1.20*	poor	1.08	poor	0.94	reasonable poor	1.18 - 1.33	poor	1.12 - 1.44
Experiment 3 (P.C.)	reasonable	1.16	poor	0.91	poor	0.90	reasonable poor	0.81 - 0.90	poor	0.89

The rotating models, although not perfect, managed to estimate capacities relatively close to the experimental values, depending on mesh size, and required less input parameters. However, the crack angles and critical cross-sections found in the models varied immensely from those found in the experiments. For the purpose of this thesis, the crack angles, or rather the location of the critical cross section must be estimated accurately. This means that the rotating models are not suitable for this thesis.

Three different types of shear retention functions have been investigated for fixed cracks. The aggregate based shear retention overestimated the capacity in all cases but showed reasonable crack patterns when prestressing was present. However, with lower amounts or no prestressing the results indicate shear locking and become untrustworthy. A constant shear retention of 0.01 showed better estimates of the capacity but the crack patterns did not agree with the experiments. Finally, a damage-based shear retention was investigated. In most cases the crack patterns were very different than those found in the experiment. However, the capacities found with the damage-based retention were very accurate, within 10% of the experimental value for all three experiments.

Several bond-slip models have also been investigated for the aggregate-size based shear retention. When determining the bond-slip parameters, multiple different estimates were found in literature. Based on the used bond-slip parameters, significant differences of crack patterns were observed in FEA. It was concluded that without accurate information of the bond it would be difficult to get more accurate results using bond-slip reinforcement compared to embedded bar reinforcement.

In some cases, significant differences in capacity were observed between arc-length and displacement control. This is likely caused by bad convergence behaviour and the fact that displacement control cannot deal with snap-back behaviour. In the case of arc-length control, premature unloading has also been observed in several cases. This indicates that some of these models could have higher capacities.

The experimental capacities and the capacities found with the smeared FEM models have also been compared to the capacities found using the upcoming Eurocode calculations. It is found that in all cases, the calculated capacities according to (FprEN 1992-1-1, 2023), are lower than the experimental and obtained values from the models. The largest difference between experiment and FprEN was found for the prestressed continuous beam where the Eurocode only estimated 45% of the experimental value. This is a further indication that the formulas in the upcoming Eurocode are too conservative for cross-sections where high moments are present.

Additionally, calculations have been done using (FprEN 1992-1-1, 2023) near the critical cross sections found in experiments 2 and 3, instead of at the locations prescribed in the code. The capacities found at these locations are 9% and 24% higher than the experimental values and are therefore not safe to use.

By analysing the smeared FEM results it was observed that none of the models were able to reproduce the crack patterns of all three experiments. Additionally, only the model with a damage-based shear retention was able to estimate the shear capacity within 10% of the experimental value for all experiments. In the other models, the capacity has been overestimated by more than 30% for at least one of the experiments. The fact that the crack patterns and capacities obtained from the models deviate from the experiments, can in most cases be explained by shear locking, bad convergence behaviour, over estimation of the shear retention or over rotation of the cracks. It is also possible that the models are not accurate for all load/boundary conditions, causing inconsistent results between different experiments. It can be concluded that, based on the investigations, the smeared FEA has been unable to estimate the crack patterns in a consistently accurate manner and is thus unsuited for finding the critical cross section.

5. Finite Element Analysis (Discrete)

Beams SC51 (Cavagnis, Ruiz, & Muttoni, 2015) and PC4.5T000 (Huber, Huber, & Kollegger, 2018), also known as Experiment 1 and Experiment 3 in this thesis, have also been modelled using discrete FEM. Using the discrete models, it is clearly shown that the crack location and angle influence the capacity of the investigated members. The available smeared models could be repurposed into discrete models without much additional effort. If the critical crack governs the shear behaviour, discrete models may provide better results than smeared cracking, as the discrete cracks cause the concrete to separate instead of smearing the damage over elements.

For the material properties and DIANA setup the reader is referred to chapter 4. Finite Element Analysis (Smeared)**.** In this chapter the longitudinal reinforcement and prestressing tendons have been modelled as embedded reinforcement or truss-bond slip reinforcement. The discrete cracks have been modelled using discrete crack models and crack dilatancy models. From a preliminary analysis it was found that a notch was sometimes required for failure to occur for discrete cracks. For this reason, the start of the crack was modelled as a small notch (of roughly 10-15 mm). Slightly different capacities were found between triangular and quadrilateral mesh and meshes with and without notches. Because the results show similar capacities and behaviour, for different meshes, mesh dependency was not investigated further.

5.1 Discrete models experiment 1

For experiment 1, a simply supported RC beam under distributed loading, multiple discrete models have been created with an angle of 45°, based on the experiment. Two reinforcement types are investigated. The first type that has been used is embedded reinforcement, which is commonly used to model reinforcement in FEM. The second type is truss bond-slip reinforcement which may provide more accurate results by considering bond-slip, depending on the accuracy of assumed bond properties. Additionally, to consider models both with and without coupling of the shear and normal behaviour, two crack models are considered. The first model is a discrete crack model, where the normal and shear behaviour is uncoupled. The second model is the crack dilatancy model, where the shear and normal behaviour is coupled. Two crack locations are modelled to investigate the effect of the crack location on the shear capacity.

In the Appendix more detailed settings of the discrete models can be found**.** The expected failure load is 60.4 kN/m. To visualize the model, the discrete crack model with a 45° angle and the crack starting at 0.9m is shown in Figure 31.

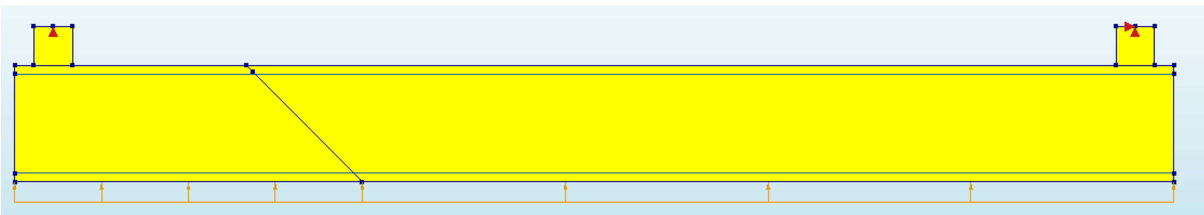

Figure 31 Experiment 1 discrete FEM with the crack located at 0.9m from the left support

The capacities found with the different combinations of crack and reinforcement models are given in Table 4 for the different combinations of reinforcement and crack type**.** From this table it is observed that the crack dilatancy models severely overestimate the capacity while the discrete models underestimate the capacity. Except for the model using a discrete crack with embedded reinforcement, all models show a smaller capacity at 0.9m, where a lower shear, but higher moment is present. This indicates that the discrete cracks may be governed by the cracking load and the acting moment, rather than the shear load.

Table 4 Experiment 1 discrete FEM capacities

Distance to support [m]	Embedded dilatancy (low)	Embedded dilatancy	Bond-slip dilatancy	Embedded Discrete	Bond-slip Discrete
0.2	400+	427	277+	46.5	62.3
0.9	260	255	230+	58	32.5

The models using truss bond-slip reinforcement are modelled according to the CEB-FIB bond-slip function, with its settings based on (CEB-FIP Model code 1990, 1993). For these models, it was not possible to use the bond-slip function according to Doerr as this caused early divergence. All relevant settings for the different models can be found in the Appendix**.**

5.2 Discrete models experiment 3

For experiment 3, multiple discrete models have been created. Differences between models are reinforcement type (embedded or truss bond-slip), and crack type (discrete crack or crack dilatancy; contact density by Li et al.) as before. Additionally, the crack angles are varied to investigate which angle has the lowest capacity. It is expected that the critical shear crack may be found in the model with the smallest shear capacity.

In these models the discrete crack, will propagate from the top of the beam (location depending on the crack angle) to the intermediate support. The crack remains straight (diagonal) and contains a small diagonal notch of roughly 10 mm at the top to prevent the model from diverging before opening the crack. The ultimate load found during the experiment is 100.5 kN/m. Figure 32 shows the model with a 22.6° angle.

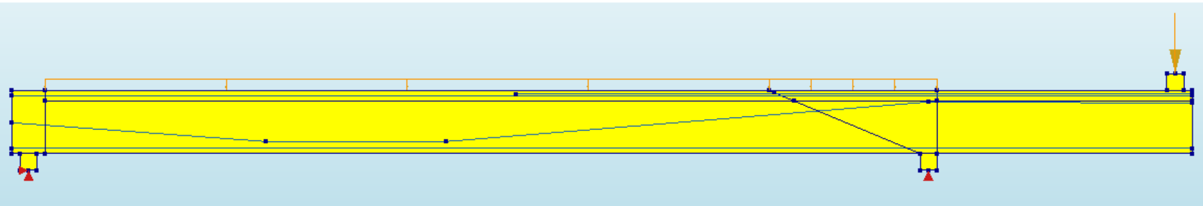

Figure 32 Experiment 3 discrete FEM with the crack angle of 22.6°

In these models, the shear modulus after cracking is assumed to be 10% of the expected pre-cracking stiffness (equivalent to a constant shear retention of 0.1) and therefore 7e10. The constant shear retention factor of 0.1 is found in multiple papers, as well as (Sagaseta, 2008) where the shear retention factors of multiple models are considered. Note that the shear stiffness modulus previously inputted for the discrete crack (dilatancy) interface was a dummy stiffness, which is ~1000 times larger than the actual stiffness.

The capacities for the different models can be found in Table 5**.**

Table 5 Experiment 3 discrete FEM capacities

Crack angle [°]	Embedded dilatancy	Bond-slip dilatancy	Embedded Discrete	Bond-slip Discrete
16.7	200+	200+	200+	200+
22.6	146	147	100	102
30	96	86	53	76
45	73	45	52	32

Initially crack angles of 22.6° and 16.7° were investigated, as these are close to the experimentally found angles. It is observed that the dilatancy models overestimate the capacity for both 16.7 and 22.6 degrees. The discrete models with a 22.6° angle show capacities very close to the experimental values. To ensure that no incorrect conclusions are drawn, angles of 30 and 45 degrees are also investigated. It is found that for increasing crack angles the capacity decreases. Of the investigated angles, the models using 45° shows the smallest capacity and could therefore be considered critical. It is possible that the capacity keeps decreasing for increasing crack angles, but as 45° is already much larger than the expected angle, no additional crack angles are investigated.

5.3 Overview Discrete FEA

Discrete Finite Element Analyses have been done on a simply supported reinforced concrete beam and a continuous prestressed concrete beam in the DIANA software. Because there are different settings available, multiple models have been created and investigated. The main differences between the models are the type of discrete crack (discrete crack type vs crack dilatancy type) and type of reinforcement (embedded reinforcement type vs truss bond-slip type). For the continuous beams different crack angles were considered close to the expected angles (16.7°-22.6°). For the simple supported case two crack locations (0.2 and 0.9 m from the support) were considered but with a constant 45° angle. The expected capacity for the simply supported beam was 60.4 kN/m, for the continuous beam the capacity is expected to be 100.5 kN/m.

For the simply supported experiment with a 45° angle, the crack dilatancy models severely overestimate the capacity for both embedded and truss bond-slip reinforcement. The models showed no signs of failure even when loads three times higher than the expected failure loads were applied, therefore the program was manually interrupted. For the discrete crack models, divergence occurs when loads between 50-105% of the expected failure loads are applied. However, this divergence is sudden and occurs before the crack opens. The different reinforcement types result in different ultimate loads with the embedded reinforcement being relatively constant for different crack locations, while the bond-slip reinforcement shows a larger variation between crack locations.

For the simply supported beams, it is found that the capacity is lower at 0.9m compared to the capacity at 0.2m from the support. This lower failure load further away from the support indicates that the capacity may be more dependent on the moment than on the shear acting on a cross section. Together with the high capacities found using these models near the support, this indicates that the shear behaviour is likely not modelled accurately but may instead focus on mode I failure. In these models it is also required to use zero shear traction or a constant shear stiffness modulus after cracking. It is, however, known that the shear retention in cracked concrete has a nonlinear relationship to the crack width/strain and a constant value is expected to give inaccurate results.

For the continuous beams with dilatancy models, both the embedded and bond-slip reinforcement types gave very similar results. Divergence occurred at loads that are 50 and 100% higher than the expected load for crack angles of 22.6° and 16.7° respectively. For the continuous beams using discrete cracks, the different reinforcement types again gave very similar results. For the angle of 16.7° the program is interrupted as no failure is observed at twice the expected load. When using the angle of 22.6° divergence occurs very close to the expected failure loads. When the additional crack angles of 30° and 45° are investigated as an additional check, divergence was encountered at much lower load values. This would mean that the cracks with high crack angles are critical, which is different from the experiment and smeared FEM. This is another indication that the shear behaviour may not be modelled correctly.

The discrete models indeed show that the capacity is highly dependent on the crack location/angle. However, the discrete cracking approach using FEM could not provide adequate results for the investigated models and properties.

6. Theory of plasticity

This chapter and all following subchapters will discuss the theory of plasticity according to (Nielsen & Hoang, 1984) and the paper of (Zhang J. P., 1997). This method is expected to give reasonable estimates of the critical shear crack angle and location for rectangular prestressed beams. Additionally, this method is able to show a clear effect of the different design parameters on the critical crack angle/location.

In the plastic theory it has been assumed that the concrete is over-reinforced and behaves as a rigid plastic material that follows the modified Mohr-Coulomb failure criterion. When stresses exceed the criterion, a sliding failure occurs along a yield line. The yield line is assumed to be fixed at the outmost fibre of the compression side (near the tip of the crack) while the starting point of the crack is located at an unknown position x from the support.

When two curves in (Zhang J. P., 1997) are considered (see Figure 33), curve 1 representing the cracking load, and curve 2 representing the shear capacity, the location x can be explained. If the crack starts to the left of the intersection point of the curves, the cracking load is higher than the shear capacity. This means that no critical crack is formed.

If the crack starts at the right of the intersection, the cracking load is below the shear capacity of the yield line. This means that the formed cracks do not fail, thus the yield line cannot be located at this position. Only at the intersection where the two curves meet does a critical diagonal crack form and shear failure occur.

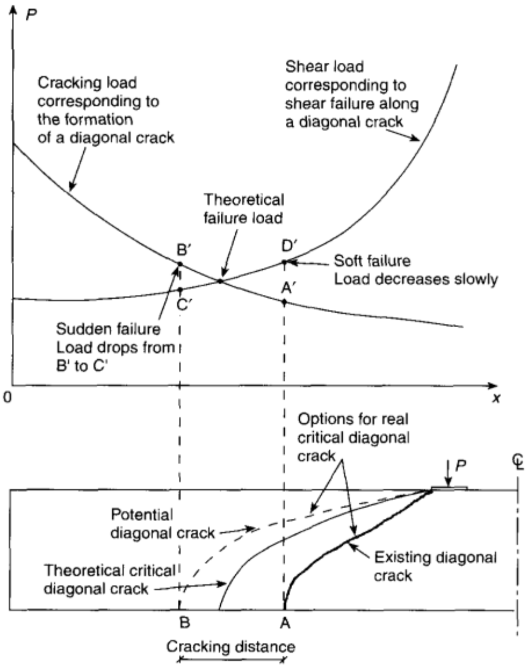

Figure 33 Effect of crack spacing on the position of the critical diagonal crack and on the ultimate load (Zhang J. P., 1997)

According to the explanation given above, x must be at the location where the two curves meet. However, in practice this is not always the case. While a beam is loaded, cracks may occur before the capacity of the beam is reached. These existing cracks can influence the location of the diagonal crack. Due to crack spacing, it is possible that no crack can form at the location of the theoretical crack as is shown in Figure 33.

Imagine a crack formed at location A, at the right of the theoretical location. Because of the crack spacing the first crack left of location A, location B, will be left of the theoretical location. The critical crack can thus be located at either of these two locations. From the figure it is shown that at location A the capacity D’ has not been reached at the cracking load A’, which means that the load can be increased. When the load is increased, either load B’ at location B, or load D’ at location A is reached. If B’ is reached this means that a crack will form at location B. Because the capacity of this crack is lower than the cracking load, the beam will fail immediately, and the load will drop from B’ to C’. If D’ is reached the existing crack A becomes critical and crack B will not be formed. It is important to observe that the critical crack can thus also form to the left or right of the theoretical crack and that in this case the failure load will be higher than the theoretical value.

6.1 Cracking load

In (Zhang J. P., 1997), for a rectangular cross section, the maximum cracking moment for flexural cracks is determined with the expression: $M_{cr} = \frac{1}{6}\gamma bh^2 f_{ct}$

In this expression b and h are the width and height of the beam, f_{ct} is the tensile strength of the concrete and γ is a plasticity factor roughly equal to 1.7 for rectangular cross-sections.

When a fully plastic stress distribution is assumed as shown in Figure 34, the cracking moment can also be expressed as $M_{cr} = \frac{1}{2}bh^2 f_t^*$

It can be seen that $f_t^* = \frac{1}{3}\gamma f_{ct}$

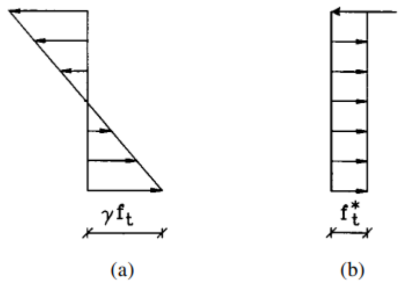

Figure 34 (a) Elastic and (b) plastic equivalent stress distribution in a flexurally cracked section at the maximum cracking moment (Zhang J. P., 1997)

The diagonal cracking moment can be obtained in a fashion similar to flexural cracks. The tensile stresses are perpendicular to the crack. The cracking moment for diagonal cracks thus becomes $M_{cr} = \frac{1}{2}b * L_{AR}^2 * f_t^*$ where $L_{AR} = \sqrt{x_L^2 + h^2}$ and x_L is the horizontal length of the crack equal to a-x.

The tensile strength of concrete can be approximated with the compressive strength and a size effect.

$$f_{ct} = 1.2 * \left(\frac{f_c}{10}\right)^{\frac{2}{3}} * S(h)$$

$$S(h) = \left(\frac{h}{0.1}\right)^{-0.3}$$

Based on experiments the effective tensile strength is:

$$f_t^* \cong 0.6 f_{ct}$$

The diagonal cracking load V=P_{cr} can be found using moment equilibrium around the crack tip (compression side):

$$V * \left(\frac{1}{2}L_0 + a\right) = M_{cr}$$

$$\tau_{cr} = \frac{P_{cr}}{bh} = \frac{1}{2}f_t^* \left(\frac{1 + \left(\frac{a-x}{h}\right)^2}{\frac{a}{h} + \frac{L_0}{2h}}\right)$$

6.2 Ultimate load

The upper bound solution following the modified coulomb failure criterion is:

$$\tau_u = \frac{P_u}{bh} = \frac{1}{2} f_c^* \left(\sqrt{1 + \left(\frac{a-x}{h}\right)^2} - \frac{a-x}{h} \right)$$

Here $f_c^* = \nu f_c$ is the effective compressive strength, ν is a factor for effectiveness and τ_u the average failure shear stress. The solution can be obtained using work equilibrium or a strut and tie model on the beam shown in Figure 35.

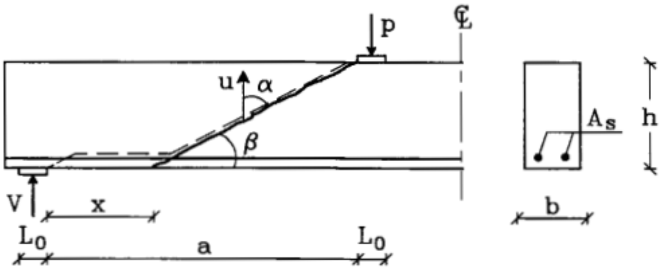

Figure 35 Shear failure mechanism by a yield line following the critical diagonal crack (Zhang J. P., 1997)

6.3 Effective compressive strength and effectiveness factors

To account for plasticity and microcracking, effectiveness factors are introduced for the compressive strength and the tensile strength. These effectiveness factors are found in (Nielsen & Hoang, 1984) and are as follows:

Effective tensile strength $f_t^* \cong 0.6 f_{ct}$

Effective compressive strength uncracked concrete $f_{c0}^* = \nu_0 f_c$

Effective compressive strength cracked concrete $f_c^* = \nu_s f_{c0}^* = \nu_s \nu_0 f_c$

$$\nu_0 = \lambda * f_1(f_c) * f_2(h) * f_3(\rho_l)$$

$$f_1(f_c) = \frac{3.5}{\sqrt{f_c}} \; (5 < f_c < 60\ MPa)$$

$$f_2(h) = 0.27\left(1 + \frac{1}{\sqrt{h}}\right) (0.08 < h < 0.7\ m)$$

$$f_3(\rho_l) = 0.15\rho_l + 0.58\ (\rho_l < 4.5\%)$$

λ is a constant based on the loading type and ν_s is assumed to be a constant 0.5 for shear and bending. λ is roughly 1.6 for concentrated loads and 1.2 for uniform loads. It seems that λ is set equal to 1.2 in case of concentrated loads with prestressing. For limited prestressing stresses this would reduce the capacity. It is suggested in the book (Nielsen & Hoang, 1984) this reduced capacity is because prestressing strands do not have the same ability to develop dowel action. The λ factor for uniform loading with prestressing is not mentioned in the book (Nielsen & Hoang, 1984) or the paper (Zhang J. P., 1997).

As there is little mention of continuous beams in the book, λ is unknown for continuous beams. Therefore, it has been assumed by the author of this thesis that the λ factors of 1.6 and 1.2 can be used for concentrated and uniform loading conditions respectively, regardless of prestressing or boundary conditions. This differs slightly from the theory presented in (Zhang J. P., 1997) but no significant change in behaviour is observed when different λ values are compared.

6.4 Shear capacity of simply supported with concentrated loading

For prestressed beams similar formulae are found in (Zhang J. P., 1997), (Zhang J.-P. , 2001) and (Nielsen & Hoang, 1984). There is a slight difference between the formulae found in (Zhang J.-P. , 2001) and (Zhang J. P., 1997). To ensure that the correct formulae are used, the author of this thesis followed the theory and derived the same formulae as those found in (Zhang J. P., 1997). The formulae for a prestressed, simply supported beam with a concentrated load are as follows:

$$\tau_u = \frac{1}{2} f_c^* \left(\sqrt{1 + \left(\frac{a-x}{h}\right)^2} - \frac{a-x}{h} \right)$$

$$\tau_{cr} = \frac{1}{2} f_t^* \left(\frac{1 + \left(\frac{a-x}{h}\right)^2 + \sigma_{cp} * \frac{d}{h}}{\frac{a}{h} + \frac{L_0}{2h}} \right)$$

$$\nu_0 = 1.2 * f_1(f_c) * f_2(h) * f_3(\rho_l) * f_4\left(\frac{\sigma_{cp}}{f_c}\right)$$

$$f_4\left(\frac{\sigma_{cp}}{f_c}\right) = 1 + 2\frac{\sigma_{cp}}{f_c}$$

6.5 Shear capacity of simply supported with uniform loading

Formulae for simply supported beams with uniform loads but without prestressing, are found in (Zhang J. P., 1997). The beam that has been considered in (Zhang J. P., 1997) is shown in Figure 36. To be able to account for prestressing loads, the same steps are followed, and the formulae are derived with prestressing. They are as follows:

$$\tau_u = \frac{\frac{1}{2} f_c^* \left(\sqrt{1 + \left(\frac{a_0 - x}{h}\right)^2} - \frac{a_0 - x}{h} \right) * \frac{a}{h}}{\frac{a}{h} - \frac{a_0}{h}}$$

$$\tau_{cr} = \left(\frac{\frac{1}{2} f_t^* \left(1 + \left(\frac{a_0 - x}{h}\right)^2\right) + \sigma_{cp} * \frac{d}{h}}{\left(\frac{a}{h} + \frac{L_0}{h}\right) * \left(\frac{a_0}{h} + \frac{L_0}{2h}\right) - \frac{1}{2}\left(\frac{a_0}{h} + \frac{L_0}{h}\right)^2} * \frac{a}{h} \right)$$

$$\nu_0 = \lambda * f_1(f_c) * f_2(h) * f_3(\rho_l)$$

$$\frac{a_0}{h} = \frac{(a/h)^2 - 1}{2(a/h)}$$

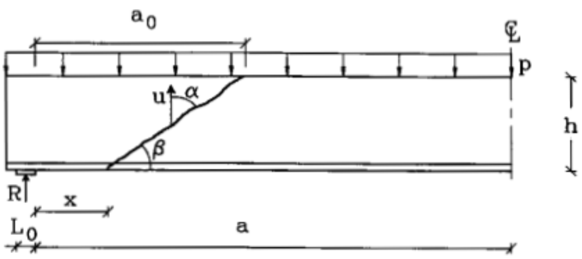

Figure 36 shear span of a beam subjected to a uniform load (Zhang J. P., 1997)

6.6 Shear strength of continuous with concentrated loading

Continuous beams are not touched in the (Zhang J. P., 1997) and only briefly mentioned in the (Nielsen & Hoang, 1984). However, by using the same methods it is possible to obtain formulas for the ultimate and cracking loads. It should be mentioned that without verification/calibration the λ factor cannot be estimated. It has been assumed that lambda equals 1.6.

$$\tau_u = \frac{16}{11} * \frac{1}{2} f_c^* \left(\sqrt{1 + \left(\frac{a-x}{h}\right)^2} - \frac{a-x}{h} \right) = \frac{16}{11} * \frac{1}{2} f_c^* \left(\sqrt{1 + \left(\frac{x_L}{h}\right)^2} - \frac{x_L}{h} \right)$$

$$\tau_{cr} = \frac{\frac{1}{2}f_t^*\left(1+\left(\frac{a-x}{h}\right)^2\right)+\sigma_{cp}*\frac{d}{h}}{\frac{a}{h}-\left(\frac{5}{16}*\frac{L+\frac{1}{2}Lo}{h}\right)} = \frac{\frac{1}{2}f_t^*\left(1+\left(\frac{x_L}{h}\right)^2\right)+\sigma_{cp}*\frac{d}{h}}{\frac{a}{h}-\left(\frac{5}{16}*\frac{L+\frac{1}{2}Lo}{h}\right)}$$

The definition of the variables is shown in Figure 37. Note that $N = \sigma_{cp} * b * h$ for the considered rectangular case.

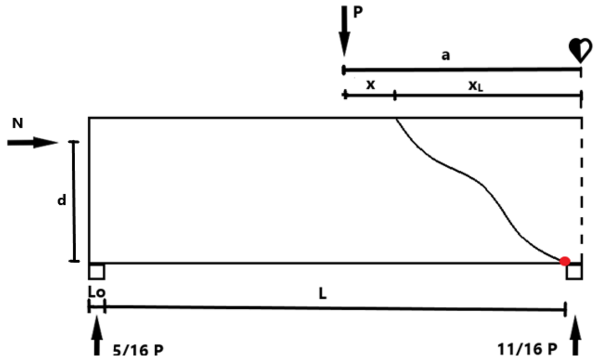

Figure 37 Schematization of the different variables

6.7 Shear strength of continuous with uniform loading

Continuous beams with uniform loading are not touched in (Zhang J. P., 1997) and (Nielsen & Hoang, 1984). Therefore, they have been derived in a similar manner. Because the size of the loading plates is not of relevance to this research, it is assumed the loading plates are infinitely small. This removes the dependency on the loading plate size and increases readability. The resulting formulas are as follows:

$$\tau_u = \frac{L}{\frac{5}{8}L - x_L} * \frac{1}{2}f_c^*\left(\sqrt{1+\left(\frac{x_L}{h}\right)^2}-\frac{x_L}{h}\right)$$

$$\tau_{cr} = \frac{\left(\frac{1}{2}f_t^*\left(1+\left(\frac{x_L}{h}\right)^2\right)+\sigma_{cp}*\frac{d}{h}\right)*L*h}{\frac{1}{2}*(L-x_L)(L+x_L)-\frac{3}{8}*L^2}$$

6.8 Beams without over-reinforcement

Previously it has been assumed that the concrete was over-reinforced to prevent flexural failure. When the assumption of over-reinforcement is not applied, the longitudinal reinforcement is expected to yield and the displacement along the yield lines are no longer necessarily vertical. Although yielding of the reinforcement is expected, it is still possible to find the theoretical shear capacity. In the case that an investigated beam is not over-reinforced ($\Phi < 0.5$) the ultimate shear capacity may, according to (Nielsen & Hoang, 1984), be estimated by:

$$\tau_u = \frac{1}{2}f_c^*\left(\sqrt{4\Phi(1-\Phi)+\left(\frac{a-x}{h}\right)^2}-\frac{a-x}{h}\right)$$

In this formula, the longitudinal reinforcement degree is given as: $\Phi = \frac{A_{sl}*f_y}{b_w*h*f_c}$.

The main results obtained in this thesis using the plasticity theory will assume that the concrete is over-reinforced. The formula for beams without over-reinforcement has been used to check whether assuming over-reinforcement has a significant influence on the crack angle or if it may cause issues.

6.9 Results

Models have been created of simply supported and continuous beams for both concentrated and uniform loads. These beams are assumed to be rectangular with straight prestressing tendons located at the effective depth d. Additionally, it has been assumed that the beams are over-reinforced.

By numerically setting the previously defined formulas for the ultimate and cracking load equal to each other, the capacity and crack angles can be determined. The base input variables for the simply supported beam are set to a= 5, h =0.5, Lo = 0.1, d = 0.4, fc=60, ρ_l=2 for both concentrated and uniform loading. For the continuous beam (symmetric 2 span beam), the base values of the variables are set to L=10, h=0.5, fc=60, ρ_l =2, d=0.4. For each of the input variables, three different values have been used to investigate their effect on the crack angles. In Table 6 and Table 7 this effect can be observed, in these tables only a single variable can deviate from the base values at a time.

Using python τ_{cr} and τ_u are plotted with the base values for σ_{cp} =0, σ_{cp} =2 and σ_{cp} =10. When the ultimate load is equal to the cracking load the corresponding crack is critical. From Figure 38 the crack length x_L and the capacity τ can be read at the intersection of two curves of the same prestressing level. For simplicity the crack angles have been calculated for the intersection points and are added to the legend.

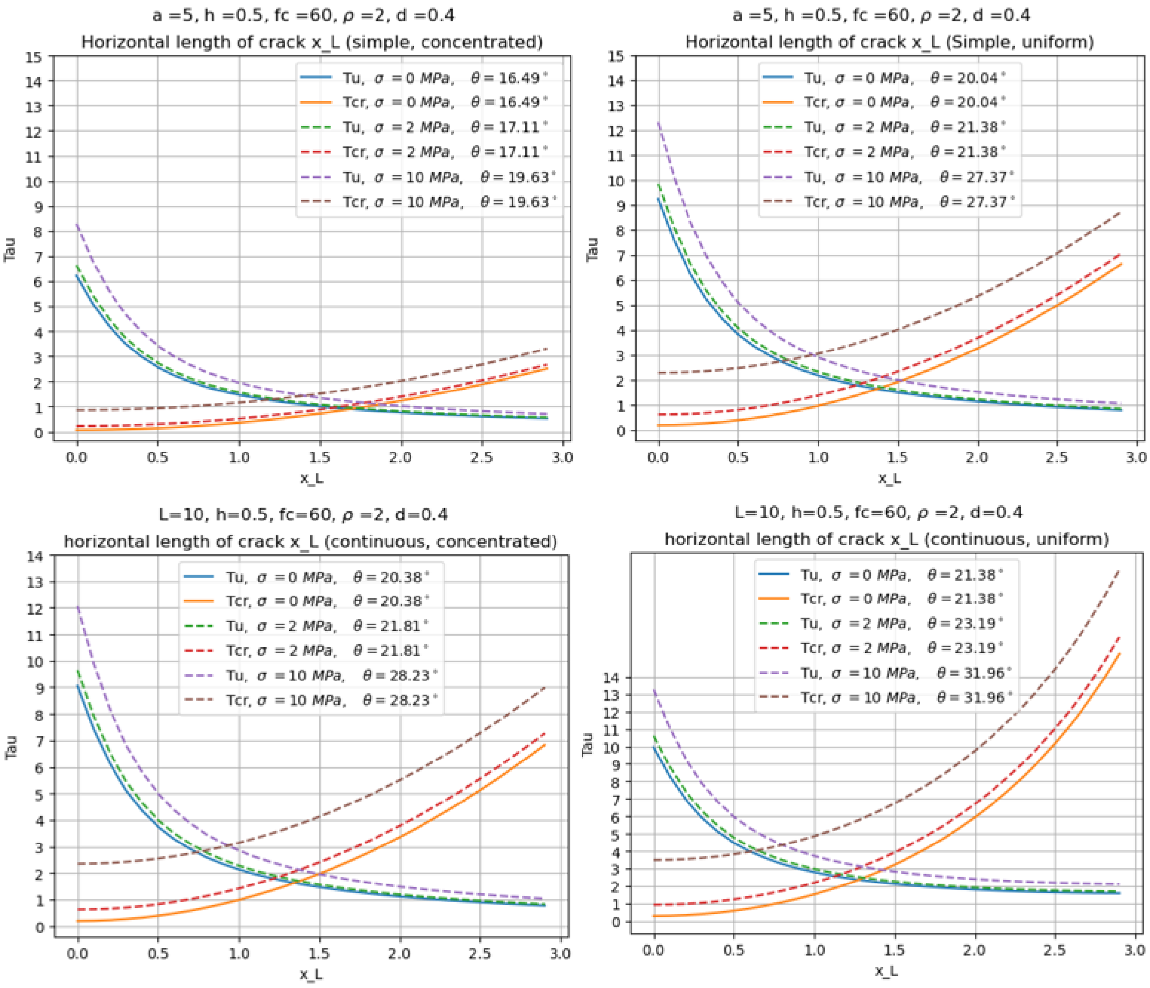

Figure 38 The capacity, crack angles and horizontal crack lengths of simply supported and continuous beams

For each of the variables, two alternative values are also investigated. Only a single variable is changed at a time while all other variables keep their base values. The results are given in tables found in the appendix, where it is shown how the variables affect the crack angle for the models, in the case σ_{cp} = 0 (no prestressing) and in the case σ_{cp} =10 (high prestressing). A third case, σ_{cp} =2 has also been investigated but gave no additional insight. For this reason, only σ_{cp} = 0 and σ_{cp} = 10 are given in this thesis. In the tables, option 2 contains the base values, this explains why θ2 is constant in each table. The tables for all setups can be found in the Appendix**.** Tables for the continuous beam under uniform loading is also shown below.

The angles found in the graphs and tables are calculated as follows:

$$\theta = \text{atan}\left(\frac{h}{x_L}\right) = \text{atan}\left(\frac{h}{a-x}\right)$$

Table 6 the effect of changing a single variable on the crack angle of a continuous beam (uniform load), in case where σ_{cp} = 0 MPa

Changed variable	Option 1	Option 2 (base values)	Option 3	θ1 [°]	θ2 [°]	θ3 [°]
L [m]	4	10	20	28.7	21.4	17.2
h [m]	0.2	0.5	1.0	15.9	21.4	25.6
d [m]	0.135	0.4	0.3	21.4	21.4	21.4
f_c [MPa]	30	60	80	20.5	21.4	20.7
ρ [%]	1	2	5	22.9	21.4	18.8

Table 7 the effect of changing a single variable on the crack angle of a continuous beam (uniform load), in case where σ_{cp} = 10 MPa

Changed variable	Option 1	Option 2 (base values)	Option 3	θ1 [°]	θ2 [°]	θ3 [°]
L [m]	4	10	20	63.1	32.0	21.2
h [m]	0.2	0.5	1.0	24.4	32.0	35.6
d [m]	0.135	0.4	0.3	22.5	32.0	27.9
f_c [MPa]	30	60	80	32.7	32.0	28.5
ρ [%]	1	2	5	36.7	32.0	25.0

All the investigated variables (a, h, d, f_c, ρ, σ_{cp}) affect the crack angle according to the plasticity method. From the tables it seems that the concrete strength f_c, has the least influence on the angle. In the case that the concrete strength is below 60 MPa this effect is especially small and could be ignored without a significant error gain. All other variables seem to be relevant and should be considered.

The results from the graphs and tables show rather small crack angles, between 12-29 degrees (without prestress), that increase with increasing prestressing levels. These results are unexpected as shear cracks without prestressing are expected to have angles between 30-45° that decrease with increased prestressing.

The low crack angles are likely caused by some of the assumptions in this method. Cracks in reality, are not straight, and concrete does not behave as a fully plastic material. These unrealistic assumptions affect mainly the ultimate load P_u of the cracks, where already an uncertain λ factor is present. By changing P_u, the cross-section where $P_u = P_{cr}$ changes. This is also visible when the λ factor is changed, for lower λ P_u decreases, causing the crack angle to increase. Increasing crack angles for increasing prestressing can be explained in a similar manner. When prestressing is increased P_{cr} is increased significantly more than P_u. This causes the angle to increase as the cracks that would otherwise be critical have not been formed yet.

Beams with $\Phi \leq 0.5$ have also been investigated to guarantee that the degree of reinforcement is not the cause of these unexpected crack angles. Instead of assuming that $\Phi = 0.5$ it is now calculated as $\Phi = \frac{A_{sl} * f_y}{b * h * f_c} = \rho_l * \frac{f_y}{f_c}$. The problem is solved numerically using python again, with an additional assumption that the yield strength of the steel is equal to 500 MPa. The resulting tables can be found in the Appendix**.** The resulting angles are larger than those found for over-reinforced beams and the effects of the different parameters is larger. Overall, the crack angles without prestressing are still lower than expected with angles between 15-35°. Like with the over reinforced beams, the angles also increase when prestressing is added.

As a final check, another estimation is done: In (Zhang J. P., 1997) an additional approximation of x is given in the case of simple supports with a concentrated load. This crude approximation is used to check for possible mistakes made while setting up the numerical model. The approximation is as follows:

$$x \cong 0.74 * \left(\frac{a}{h} - 2\right) * h$$

The approximation is compared to the values obtained for the simply supported case with concentrated loading in Table 8. For high a/h ratios the approximation seems to differ from the tabled values by up to 5°, whilst for lower a/h ratios the approximation is quite close to the values found in the tables. Because the previously obtained values are similar to the crude approximation from Zhang, it is assumed no mistakes were made in deriving the values found in the tables.

Table 8 Comparison of angles obtained using plasticity approach vs those obtained from the crude approximation of Zhang

Case number	a	h	a/h ratio	Estimated θ	Obtained θ	Difference
Case 1	2	0.5	4	21.6°	22.4°	0.8°
Case 2	5	0.5	10	13.8°	16.5°	1.7°
Case 3	10	0.5	20	8.5°	13.1°	4.6°
Case 4	5	0.2	25	7.1°	12.0°	4.9°
Case 5	5	1.0	5	19.8°	20.1°	0.3°

6.10 Conclusion

For a small variety of variables, the location of the crack, and the crack angles are obtained with the use of the plasticity method found in (Nielsen & Hoang, 1984) and by extending the theory to continuous and prestressed beams. It is shown that the crack angles found with this method are generally below 25 degrees for non-prestressed beams and increase when prestressing is applied. This is inconsistent with the knowledge that shear failure most often occurs under an angle of 30-45 degrees, and under smaller angles in case of prestressing.

A crude estimation, found in (Zhang J. P., 1997), has been used to confirm no mistakes were made while setting up the numerical model for the simply supported case, and no obvious errors were found. Additionally, a model without over-reinforcement was investigated. This model showed slightly larger crack angles overall, but the unexpected behaviour remained. It is determined that the low crack angles are likely caused by the assumptions and simplifications made within this approach. The increased crack angle for prestressed beams can be explained by the relatively large increase in P_{cr} compared to P_u. The cracks with smaller angles, that were critical without prestressing, have not formed yet when the prestressed beam fails.

Even though this method may not accurately estimate the crack angles and critical cross section, some observations may hold true and should therefore be mentioned: The concrete strength f_c has the smallest influence on the crack angle and could in most cases be neglected in the over-reinforced beams. The lever arm d of the prestressing force influences the angle; however, this is only significant if prestressing levels are not too low. The prestressing stress σ, shear span a, the height of the beam h and the reinforcement ratio ρ show a clear influence on the crack angle. Extra attention should be given to these variables when a detailed model is developed for the crack angle or location of the critical cross section.

7. Discussion

This thesis aimed to investigate the location of the critical shear crack for prestressed continuous concrete beams without shear reinforcement. If the location of the critical cross section is known, it may be possible to move the control sections in the upcoming Eurocode from 1d from the support to the critical location. If the control section moves away from the intermediate support, a higher design capacity would be found. This could solve the problem of overly conservative designs for prestressed continuous beams without shear reinforcement.

In literature, several models estimate the location of the critical crack, or the critical crack angle, based on one or more of the following variables: σ_{cp}, ρ_l, ρ_w, a, d, and f_{ck}. A consistent behaviour is observed for the models; for increasing prestressing levels, the crack angle decreases. Most models agree that for $\sigma_{cp} > f_{ct}$, the crack angles are likely below 33.7°, which is equivalent to a horizontal crack length of more than 1.5d. From these results it may seem obvious that the control section may be moved from 1d to 1.5d, but this would be a premature conclusion. The models that were considered, are based on principal stresses or experiments on simply supported beams, and there is no guarantee these models can accurately estimate the crack angles of continuous beams. The model used in (Cavagnis F. , 2017) considered effects of different variables and loading conditions on the location of the critical cross section of reinforced concrete. Cavagnis did not go into much detail about prestressed concrete, but did mention that prestressing causes a reduction of the effective shear span. Although Cavagnis opted to use a constant control section located at 1d for all load conditions, it is observed that depending on the beam properties, the critical cross section could be located between 1d and 1.5d for a cantilever beam, even if no prestressing was present. It may be quite possible that if prestressing would have been considered by Cavagnis, values of larger than 1.5d would have been found like in the other models. Unfortunately, none of the models are designed to estimate the crack angles of prestressed continuous beams. For this reason, the results obtained from the models are only indicative and cannot be used as a conservative estimate.

In the absence of accurate models for prestressed continuous beams, experiments found in literature are investigated. Given enough experimental data, it may be possible to create and validate a model by means of a regression analysis or machine learning model, or by identifying the minimum and maximum crack angles. However, only a small number of experiments on prestressed continuous beams have been documented in literature. Of the experiments found on prestressed continuous beams, only 12 beams are relevant to this study and have been investigated. As there is such a small number of experiments no model can be developed. Therefore, the data is instead compared to the models discussed previously. In the experiments σ_{cp}/f_{ct} is roughly between 0.66-1.5, with σ_{cp} being between 2-4.72 MPa. The largest observed crack angle in these experiments is 32°. For these experiments it holds that the crack angles are smaller than 33.7° for $\sigma_{cp} > f_{ct}$, as was indicated by the different models. There is thus a strong indication, from models and experiments, that the critical cross section will be farther than 1.5d from the intermediate support. However, as there is a limited sample size, and some of these experiments contain external prestressing, no definitive conclusions can be drawn from these experiments.

Because it was not possible to determine the critical cross section using literature alone, smeared FEA (Finite Element Analysis) has been considered. For the smeared FEA, three different experiments have been modelled using a variety of settings. Quite accurate capacities could be obtained using certain shear retention settings, but the crack patterns found in the experiments could not be recreated in a consistently accurate manner. There are several possible reasons why the crack patterns obtained with FEA differ from the experiment. One reason is that FEA suffers from (small) numerical errors. As the simulation continues, these errors can stack and lead to results that are different from what may be expected. Differences can also be caused by many model assumptions such as (but not limited to) mesh size, homogeneity and element types, which can influence the results. Although much care has been taken while setting up the models, it is also possible that human errors are present. Finally, it is also possible that the results found in the three experiments are not representative and could be outliers. In an attempt to get better crack patterns, several model settings have been varied. The resulting crack patterns were not considered accurate and consistent enough to find the critical crack location and study the effect of different beam properties on the critical location.

The three experiments that were considered for smeared FEA, have also been compared to the shear capacity found in the upcoming Eurocode (FprEN 1992-1-1, 2023). It was found that the Eurocode capacities were conservative, especially for the prestressed continuous beam, where the estimated capacity was less than half the experimental value. This further illustrates that for prestressed continuous beams without shear reinforcement, the new Eurocode is too conservative. Estimates have also been made for the critical locations that had been found in experiments 2 and 3. It is shown that at these critical locations (FprEN 1992-1-1, 2023) overestimates the capacity by 9% and 24% respectively. It is therefore not safe to simply move the control section from 1d to the critical cross section. If the location of the critical cross section were to be used in upcoming Eurocode, changes will have to be made to the formulas for them to remain safe.

In addition to smeared FEA, discrete FEA has also been investigated. In discrete FEA, the crack must be defined a priori. However, as the crack location/angle is unknown, multiple models must be investigated to find the critical location/angle. This roundabout way to find the critical crack was ineffective as the critical cracks differed from the cracks found in the experiments. For a prestressed continuous beam, of the four investigated angles (16.7°, 22.6°, 30°, 45°), the lowest capacity was observed for models containing 45° angles, while the crack angle in the experiment was found to be below 20°. The capacities of the finite element models were also quite different from the experimental capacity. The models with small angles severely overestimate the capacity while the models with a 45° angle underestimated the capacity. Several possible causes have been identified that may explain the difference between the discrete models and the experiments. In these models, concrete is assumed to be linear elastic, with the exception of a single discrete crack. The flexural cracks are not considered even though they influence the load transfer and stiffness, and thus the capacity of the critical crack. It may also be possible that sub-optimal properties have been used for the different reinforcement types (embedded vs truss-bond slip) or discrete crack types (discrete crack vs crack dilatancy), and that better results may be obtained with different properties. Finally, it should be noted that only a small number of cracks are considered in the investigations and that the 'critical crack' may have been skipped. If more cracks are considered it may be possible to get a better estimate of the critical crack angle and location. However, considering many different cracks with this method is unrealistic as it would take a large amount of time.

Finally, a plasticity approach has been considered. Using this approach, crack angles for different beam properties and loading conditions have been determined. It was found that σ_{cp}, ρ, a, d, h, and f_{ck} influence the critical crack. The crack angles are determined by finding the location of the minimum capacity, which is found by setting the cracking and ultimate load, equal to each other. The angles found using this method are significantly smaller than expected. This is likely caused by the assumptions and simplifications that have been used within this method. Assumptions such as fully plastic concrete and straight yields lines influence the capacities of a crack, which in turn influence the critical crack location. It may be possible to obtain better crack angles if more realistic assumptions are made. However, it is likely that a large increase in complexity is required before any significant improvements are obtained. In this method prestressing was also shown to increase the crack angles, which contradicts the models and experiments found in literature. The reason why the crack angles increase with prestressing in this plasticity method can be explained in a simple manner: Prestressing increases the cracking capacity significantly more than the ultimate capacity of a crack. This means that cracks with smaller angles, which would have been critical without prestressing, have not yet formed due to the increased cracking capacity when another crack reaches its capacity in the prestressed case.

When investigating Finite Element Models, it was found that in some cases the (critical) crack was formed before failure occurred and could thus carry additional loads before failing. In cases where the critical crack formed at failure, the cracking load was likely higher than the ultimate capacity of the crack, causing immediate failure when the cracking load is reached. This is similar to what is found in the plasticity approach, where both the cracking and ultimate load of a crack must be exceeded. The combination of the ultimate and cracking load is therefore expected to determine the shape and location of the critical cross section.

Although no definitive model could be developed to estimate the critical cross section, it was observed by several models and experiments from literature, as well as the plasticity approach, that the critical crack is influenced by σ_{cp}, ρ, a, d, and f_{ck} or f_{ct}. While not investigated, it is expected that this influence will also be present in FEA. Thus, it is important to consider all these variables when developing a model that identifies the critical cross-section. However, developing and validating such a model without a larger number of experiments will be difficult, as may be observed from this thesis.

8. Conclusion

The aim of this thesis was to investigate the location of the critical shear crack, near intermediate supports, for prestressed concrete beams without shear reinforcement. The research questions of this thesis are:

1. “How can the location of the first control section, around intermediate supports, be determined and implemented to improve the proposed Eurocode, for prestressed concrete elements with less than the minimum required shear reinforcement?”
    a. What are the differences between the old formula, and the proposed formulae? and why should the new formulae be improved?
    b. What methods can be used to estimate the shear crack angle or critical cross section?
    c. What is the expected location of the shear critical cross-section near intermediate supports for prestressed beams with less than the required amount of shear reinforcement.
    d. What are the limitations of the models/estimates of the critical shear crack location?
    e. Can the models/estimates be implemented in the proposed Eurocode without any other changes to the proposal in a safe manner?

The answers to these questions are summarised below.

The formula found in the current Eurocode is based on a regression analysis. This formula will be replaced in the upcoming Eurocode by a formula based on the Critical Shear Crack Theory. A clear difference is that the shear capacity in the proposed formula will be influenced by the aggregate size and acting moment and will require iteration to solve. It was found that the capacity of prestressed continuous beams without shear reinforcement was severely underestimated using the proposed formula. If no changes are made to the proposal, this may have large consequences for both new and existing structures, as more material or different designs would be needed to meet the code requirements. Moving the control section further away from intermediate supports to a critical cross section, would provide a higher capacity and could solve this problem.

The critical cross section can be estimated by $\cot(\theta)*d$, where θ is the crack angle and d is the effective depth. In literature, multiple models, experiments and modelling methods can be found to estimate the crack angle. In this thesis the plasticity theory, Finite Element Analyses and models/crack patterns from literature are used to estimate the location of the critical cross section.

The location of the critical control section could not be definitively estimated but it was observed that the critical location is influenced by the cracking and ultimate loads of different cracks. The parameters σ_{cp}, ρ, a, and d are shown to influence the crack angle, and the models and experiments indicate that the critical location for $\sigma_{cp} > f_{ct}$ is farther than 1.5d from the intermediate supports.

The models in literature were based on simply supported beams and/or principal stress directions. Additionally, only a limited number of relevant experiments were available in literature, which made it impossible to arrive at a conclusive answer. The plasticity theory and the FEA were also not deemed accurate and consistent enough to estimate the critical cross section, likely due to the assumptions and simplifications that have been made in these methods.

Using the FprEN1992-1-1, the shear capacity has been estimated at the critical cross sections found in two experiments. It was found that the capacity for these experiments is overestimated if the critical cross section is used. It is therefore not safe to only check the capacity at the critical cross section, unless changes are made to the FprEN1992-1-1 or the definition of the critical cross section.

Considering the results, it is expected that the critical cross section can be moved farther away from the intermediate support for prestressed beams without shear reinforcement. While multiple models and experiments show that the critical cross section is likely located at a distance larger than 1.5d from the intermediate support, this was not proven. It is therefore important that further research and experiments are done on prestressed continuous beams without shear reinforcement, to determine the critical cross section. It should be noted that the critical cross section could not be used to estimate the shear capacity in a safe manner. Therefore, additional research should be considered on how to safely implement the critical control section in the FprEN1992-1-1.

References

AASHTO LRFD. (2007). Bridge Design Specifications, SI Units, 4th Edition.

Adviesbureau ir. J.G Hageman B.V. (2021). Shear resistance of prestressed members without shear reinforcement according to prEN 1992-1-1/D7. *file 10308*.

Adviesbureau ir.J.G. Hageman B.V. (2023). Impact van de nieuwe EC2 op de dwarskrachtbeoordeling van bestaande brugdekken. *Dossier 10943*.

Aydin, B. B., Tuncay, K., & Binici, B. (2019). Simulation of Reinforced Concrete MemberResponse Using Lattice Model. *Journal of Structural Engineering, 145(9)*. doi:https://doi.org/10.1061/(asce)st.1943-541x.0002381

Blesa, U. C. (2019). *Theoretical and experimental study of the behaviour at service and failure of partially prestressed concrete beams under flexure and shear.* PhD Thesis, Universitat Politècnica de Catalunya, Barcelona Tech, Barcelona. Retrieved from http://hdl.handle.net/10803/668253

Cavagnis, F. (2017). Shear in reinforced concrete without transverse reinforcement: from refined experimental measurements to mechanical models. doi:10.5075/epfl-thesis-8216

Cavagnis, F., Ruiz, M. F., & Muttoni, A. (2015). *Shear failures in reinforced concrete members without transverse reinforcement: An analysis of the critical shear crack development on the basis of test results.*

Cavagnis, F., Ruiz, M. F., & Muttoni, A. (2018). A mechanical model for failures in shear of members without transverse reinforcement based on development of a critical shear crack. *Engineering Structures 157*, 300-315.

CEB-FIP Model code 1990. (1993).

Collins, M. P., Bentz, E., Sherwood, E. G., & Xie, L. (2008). An adequate theory for the shear strength of reinforced concrete structures. *Magazine of Concrete Research 60(9)*, 635-650.

DIANA FEA. (n.d.). *Bond-Slip of Post-Tensioned Reinforcement in Two-Dimensional Elements.* Retrieved from dianafea: https://dianafea.com/tutorial/bond-slip-of-post-tensioned-reinforcement-in-2d-elements/

Dolan, C. W., & Hamilton, H. R. (2019). *Prestressed Concrete, Building, Desing, and Construction.* Springer International Publishing. doi:https://doi.org/10.1007/978-3-319-97882-6

ETA. (2017). *European Technical Approval ETA-08/0012 Tensacciai Post-Tensioning System.*

Eurocode2. (2015). Design of concrete structures- part 1-1:general rules and rules for buildings (NEN-EN 1992-1-1+C2+A1) (nl).

FprEN 1992-1-1. (2023). *Eurocode 2 - Design of concrete structures - Part 1-1: General rules and rules for buildings, bridges and civil engineering structures.*

Görtz, S. (2004). *Zum Schubrissverhalten von Stahlbeton- und Spannbetonbalken aus Normal- und Hochleistungsbeton.* RWTH AACHEN.

Hendriks, M. A., & Roosen, M. A. (2022). Guidelines for Nonlinear Finite Element Analysis of Concrete Structures. *Rijkswaterstaat Centre for Infrastructure, RTD 1016-1:2022*.

Herbrand, M., & Classen, M. (2015). Shear tests on continuous prestressedconcrete beams with external prestressing. *Structural Concrete, 16*, 428-437. doi:https://doi-org.tudelft.idm.oclc.org/10.1002/suco.201400082

Herbrand, M., Kueres, D., Classen, M., & Hegger, J. (2018). Experimental Investigations on the Shear Capacity of Prestressed Concrete Continuous Beams with Rectangular and I-Shaped Cross-Sections. *High Tech Concrete: Where Technology and Engineering Meet*, 658-666. Retrieved from https://link.springer.com/chapter/10.1007/978-3-319-59471-2_78

Hicks, A. B. (1958). *The influence of shear span and concrete strength upon the shear resistance of a pre-tensioned prestressed concrete beam.*

Holt, J., Bayrak, O., Okumus, P., Stavridis, A., Murphy, T., Panchal, D., . . . Randiwe, A. (2022). Concrete Bridge Shear Load Rating Guide and Examples: Using the Modified Compression Field Theory. *FHWA-HIF-22-025*. Retrieved from https://rosap.ntl.bts.gov/view/dot/62795

Huber, P., Huber, T., & Kollegger, J. (2018). Influence of loading conditions on the shear capacity of post-tensioned beams with low shear reinforcement ratios. *Engineering Structures 170*, 91-102.

Kaschube, J., & Dieter, D. (2021). A discrete element model for reinforced concrete. *PAMM, 20(1)*. doi:https://doi.org/10.1002/pamm.202000258

Kuchma, D. A., Hawkins, N. M., Kim, S.-H., Sun, S., & Kim, K. S. (2008). Simplified shear provisions of the AASHTO LRFD Bridge Design Specifications. *PCI Journal 53(3)*, 53-73. doi:https://doi.org/10.15554/pcij.05012008.53.73

Li, G., Zhang, C., & Niu, C. (2011). Experimental Study on Shear Behavior in Negative Moment Regions of Segmental Externally Prestressed Concrete Continuous Beams. *Journal of Bridge Engineering, 18(4)*, 328-338. doi:https://doi.org/10.1061/(asce)be.1943-5592.0000351

Maurer, R., Gleich, P., Zilch, K., & Dunkelberg, D. (2014). Querkraftversuch an einem Durchlaufträgeraus Spannbeton. *Beton- und Stahlbetonbau 109 (10)*, 654-665. doi:https://doi-org.tudelft.idm.oclc.org/10.1002/best.201400054

Muttoni, A., & Ruiz, M. F. (2008). Shear Strength of Members without Transverse Reinforcement as Function of Critical Shear Crack Width. *ACI structural journal 105*, 163-172.

Muttoni, A., & Ruiz, M. F. (2019). From experimental evidence to mechanical modeling and design expressions: The Critical Shear Crack Theory for shear design. *Structural Concrete 20 (4)*, 1464-1480.

Nielsen, M. P., & Hoang, L. C. (1984). *Limit Analysis and Concrete Plasticity.* CRC Press.

Pinto, G., & Cantero, D. (2022). *Modelling post-tensioned structures with DIANA FEM software.*

Rijkswaterstaat. (2022b). RTD 1006. *Richtlijnen Beordeling Kunstwerken*.

Rombach, G., & Faron, A. (2019). Numerical analysis of shear crack propagation in a concrete beam without transverse reinforcement. *Procedia Structural Integrity, 17*, 766-773. doi:https://doi.org/10.1016/j.prostr.2019.08.102

Roosen, M., Yang, Y., & Dieteren, G. (2023). De invloed van normaalkracht op de dwarskracht. *Cement 8*, 30-37.

Ruiz, G., Elices, M., & Planas, J. (1998). Experimental study of fracture of lightly reinforced concrete beams. *Materials and Structures 31*, 683-691. Retrieved from https://doi-org.tudelft.idm.oclc.org/10.1007/BF02480445

Sabbagh-Yazdi, S., & Amiri, T. (2021). An efficient automatic adaptive algorithm for cohesive crack propagation modeling of concrete structures using matrix-free unstructured Galerkin Finite Volume Method. *Computers &Amp; Mathematics With Applications, 97*, 237-250. doi:https://doi.org/10.1016/j.camwa.2021.06.004

Sadeghian, V., & Vecchio, F. (2018). The MODIFIED COMPRESSION FIELD THEORY: THEN AND NOW . *ACI Structural Journal SP-328*, 3.1-3.20.

Sagaseta, J. (2008). *The influence of aggregate fracture on the shear strength of reinforced concrete beams.* London.

Schlangen, E., & Mier, J. G. (1992). Simple lattice model for numerical simulation of fracture of concrete materials and structures. *Materials and Structures, 25(9)*, 534-542. doi:https://doi.org/10.1007/bf02472449

Shirzehhagh, M., & Fakhimi, A. (2021). Insights on crack initiation and propagation in reinforced concrete beams, a bonded-particle approach. *Engineering Structures, 244*. doi:https://doi.org/10.1016/j.engstruct.2021.112783

Silva, S. D., Mutsuyoshi, H., & Witchukrangkrai, E. (2008). Evaluation of Shear Crack Width in I-Shaped Prestressed Reinforced Concrete Beams. *Journal of Advanced Concrete Technology Vol. 6, No.3*, 443-458.

Slobbe, A., Hendriks, M., & Rots, J. (2012). Sequentially linear analysis of shear critical reinforced concrete beams without shear reinforcement. *Finite Elements in Analysis and Design 50*, 108-124. doi:https://doi.org/10.1016/j.finel.2011.09.002

Soparat, P., & Nanakorn, P. (2008). Analysis of Cohesive Crack Growth by the Element-Free Galerkin Method. *Journal of Mechanics, 24(1)*, 45-54. doi:https://doi.org/10.1017/s1727719100001544

Tejchman, J., & Bobiński, J. (2013). *Continuous and Discontinuous Modelling of Fracture in Concrete Using FEM.* Springer.
Vecchio, F. J., & Collins, M. P. (1986). The Modified Compression-Field Theory for Reinforced Concrete Elements Subjected to Shear. *ACI Journal 83*, 219-231.
Vellwock, A. E., & Libonati, F. (2024). XFEM for composites, biological, and bioinspired materials: a review. *Materials, 17(3), 745*. doi:https://doi.org/10.3390/ma17030745
Walraven, J. (1981). Fundamental Analysis of Aggregate Interlock. *Journal of the Structural Division, ASCE, Vol. 107, No. ST11*, 2245-2270.
Walraven, J., & Braam, C. (2019). *CIE3150/4160 Prestressed concrete.* Delft: Faculty of Civil Engineering and Geoscience.
Yang, Y., & Roosen, M. (2023). Dwarskrachtweerstand gebaseerd op scheurwijdte. *cement 1*, 42-50.
Zhang, J. P. (1997). *Diagonal cracking and shear strength of reinforced concrete beams.*
Zhang, J.-P. (2001). *Shear strength of reinforced concrete beams with critical diagonal cracks.*
Zheng, K., Ni, S., Zhang, Y., Gu, J., Gao, M., & Wei, Y. (2023). Post-Cracking Shear Stiffness Model of Reinforced Concrete Beams. *Buildings, 13(11), 2814*. doi:https://doi.org/10.3390/buildings13112814
Zheng, K., Zhou, S., Zhang, Y., Wei, Y., Wang, J., Wang, Y., & Qin, X. (2023b). Simplified Evaluation of Shear Stiffness Degradation of Diagonally Cracked Reinforced Concrete Beams. *Materials, 16(13), 4752*. doi:https://doi.org/10.3390/ma16134752
ZSUTTY, T. (1971). Shear Strength Prediction for Separate Catagories of Simple Beam Tests. *ACI journal 68*, 138-143.

Appendix

Appendix A. Additional crack angle estimations in literature

To prevent Figure 19, shown in chapter 3. Inclination of shear cracks in literature**,** to become cluttered**,** less important relationships are shown in Figure 39. Cracks under service loads are deemed less important as these may not become critical cracks and may therefore not be relevant. In (Görtz, 2004) and (Blesa, 2019) there are expressions that consider the shear reinforcement ratios and allow investigation of beams with low amounts of shear reinforcement, which are of interest in this thesis. Excluding this effect would likely reduce the accuracy, because a significant variable is removed from the estimation, and remove the ability to investigate beams with low amounts of shear reinforcement. For this reason, the expressions which exclude the shear reinforcement from these models are also deemed less relevant.

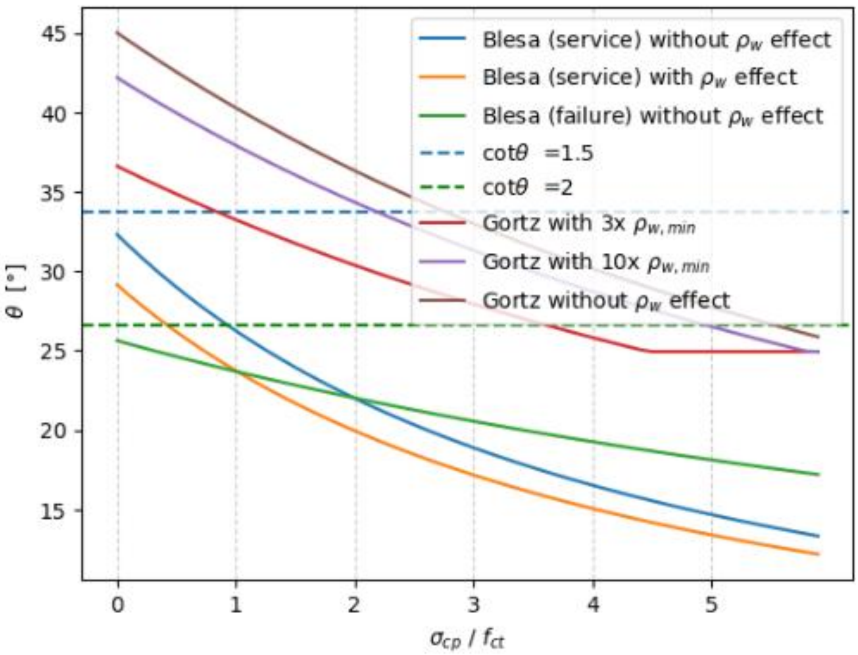

Figure 39 Additional relationship between the crack angle and σ_{cp}/f_{ct} for models found in literature for simply supported beams

The (Blesa, 2019) models give reasonably similar results, and remain below 33.7°, for this reason no more attention is given to these models.

It has been observed however, that the angles found with the model from (Görtz, 2004), without the shear reinforcement ratio, are higher and significantly larger than 33.7° at σ_{cp}/f_{ct} =1. For this reason, it is compared to variations where the shear reinforcement ratio is considered and three or ten times the minimum reinforcement ratio. With increasing amounts of shear reinforcement, the results become closer to those found in the model that does not consider shear reinforcement effects. Even with ten times the minimum reinforcement ratio, there is still roughly a 3° difference between the models that do and do not consider the shear reinforcement effect. Because there is a significant difference between the models that do and do not consider the shear reinforcement effect, and because the shear reinforcement ratio is known to be small, the model from (Görtz, 2004) without the shear reinforcement effect is not considered in the main report.

Appendix B. Finite Element Analysis (Smeared)

Model properties experiment 1

The material properties used in the different models are given in Table 9 and Table 10. For some properties multiple settings are given, this is because multiple variations have been investigated. In the caption of the crack patterns, the legend of load-displacement curves and the model names in the overview the used settings are provided.

Table 9 concrete model properties used in experiment 1

Young's modulus	E=34000 MPa / E_{alt}=31646 MPa
Poisson ratio	0.2
Crack orientation	Fixed / rotating
Tensile curve	Hordijk
Tensile strength	2.606 MPa
Mode I tensile fracture energy	137 N/m
Shear retention function (applicable to fixed crack orientation)	Constant (0.01) / damage based / aggregate size based (4 / 6 / 8 / 12 mm)

Table 10 steel model properties used in experiment 1

Young's modulus	E=200000 MPa
Yield strength	710 MPa
Ultimate strength	870 MPa
Ultimate strain	ε_u= 0.05

Multiple bond-slip models with a cubic bond slip function by Doerr have also been investigated as an alternative to embedded reinforcement. In (Tejchman & Bobiński, 2013) it is mentioned that the Parameter c should be roughly 1.9f_t and the shear slip plateau 0.06 mm. Due to convergence issues the shear slip plateau had to be changed to 0.6 mm for some cases; In two extreme cases, running a model with 0.06 mm did not only cause early divergence but also caused the file to become corrupted and unreadable. In all cases divergence at low load levels could not be prevented.

As can be seen in (Pinto & Cantero, 2022) there are multiple methods to approximate the normal and shear stiffness modulus. The resulting stiffness moduli can differ significantly, and divergence may occur when they are too large or too small. The moduli used in the FEA models are based on the methods found in (Pinto & Cantero, 2022) as to not be too unrealistic, but are varied within ranges that do not cause numerical issues. This has been done to investigate if certain combinations would provide a more accurate response in the FEA models as is suggested in (Pinto & Cantero, 2022). If bond-slip is modelled this is mentioned in the name of the model, the properties are in Table 11.

Table 11 Bond-slip settings used for experiment 1 (smeared)

	Agg 12	**Agg 12 increased bond stiffness**	**Agg 6**	**Agg 6 refined**	**Agg 6 v2**	**Agg 6 v3**	**Agg 6 v4**
Normal stiffness modulus [N/m³]	2e13	6e13	2e13	2e13	2.6e11	8.6e11	8.6e14
Shear stiffness modulus [N/m³]	1e11	6e12	1e11	1e11	2.6e10	2.6e11	2.6e11
Parameter c [N/m²]	6.2e6	6.2e6	6.2e6	6.2e6	6.2e6	6.2e6	6.2e6
Shear slip at plateau [m]	6e-4	6e-5	6e-4	6e-4	6e-5	6e-5	6e-5

Crack patterns experiment 1

Rotating

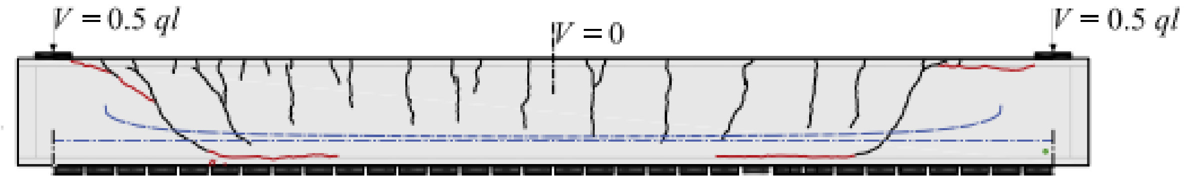

Figure 40 experiment 1 observed crack pattern

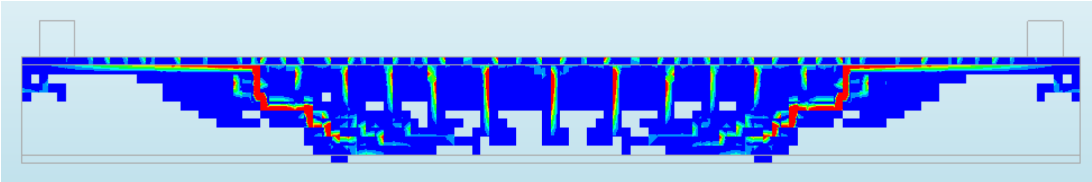

Figure 41 crack pattern experiment 1 rotating model

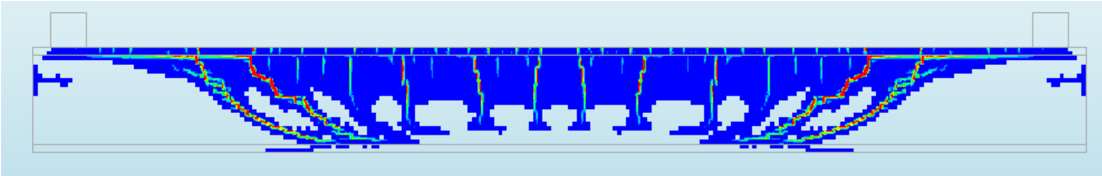

Figure 42 crack pattern experiment 1 rotating model, refined mesh

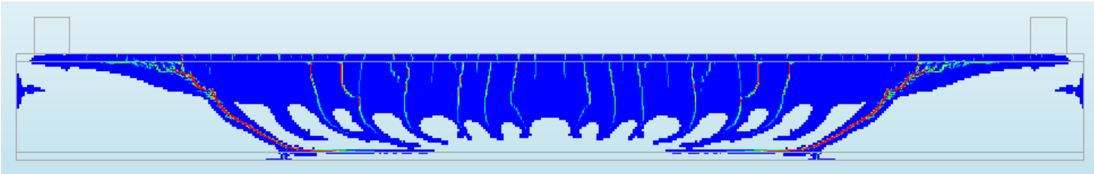

Figure 43 crack pattern experiment 1 rotating model, refined the mesh twice

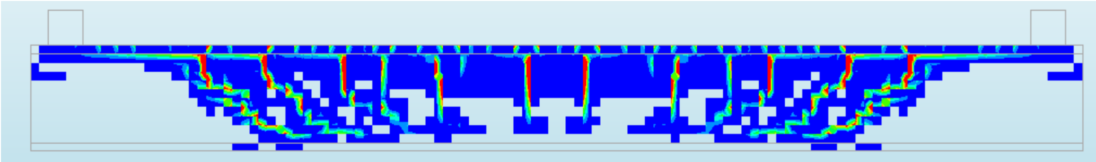

Figure 44 crack pattern experiment 1 rotating model, alternative E

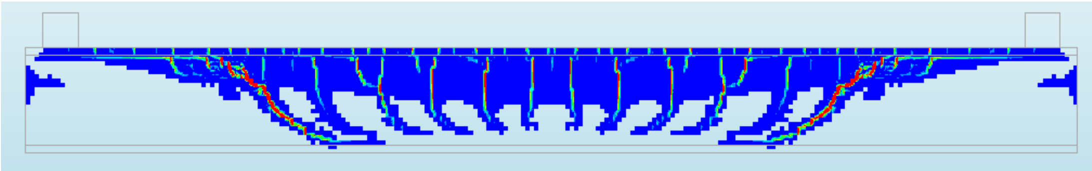

Figure 45 crack pattern experiment 1 rotating model, alternative E, refined

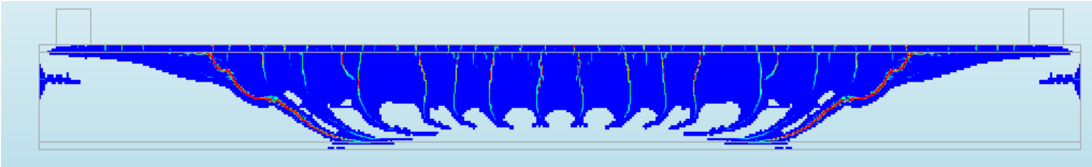

Figure 46 crack pattern experiment 1 rotating model, alternative E, refined twice

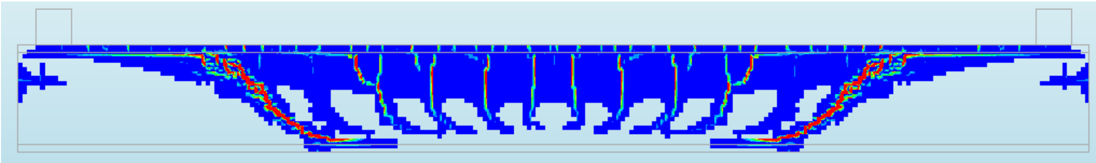

Figure 47 crack pattern experiment 1 rotating model, alternative E, refined (improved interface)

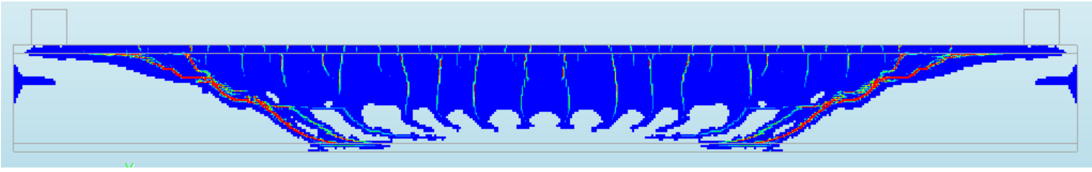

Figure 48 crack pattern experiment 1 rotating model, alternative E, refined twice (improved interface)

Fixed

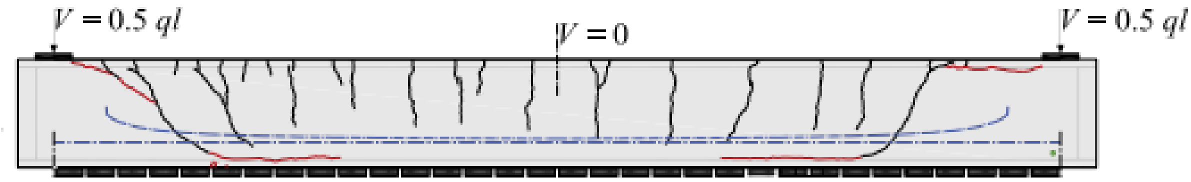

Figure 49 experiment 1 observed crack pattern

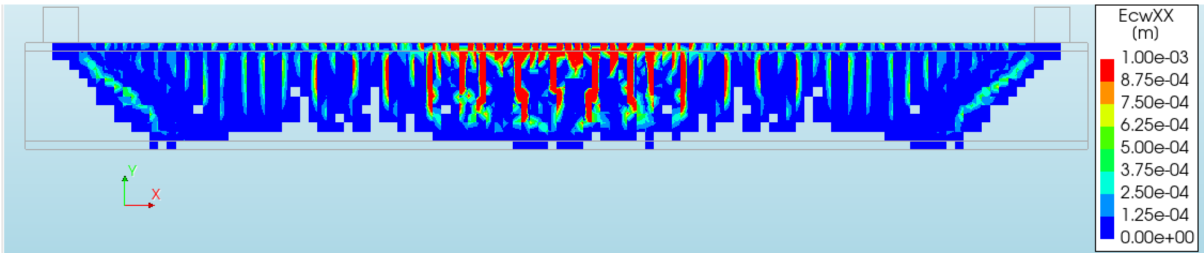

Figure 50 crack pattern experiment 1 fixed model based on mean aggregate size of 12 mm

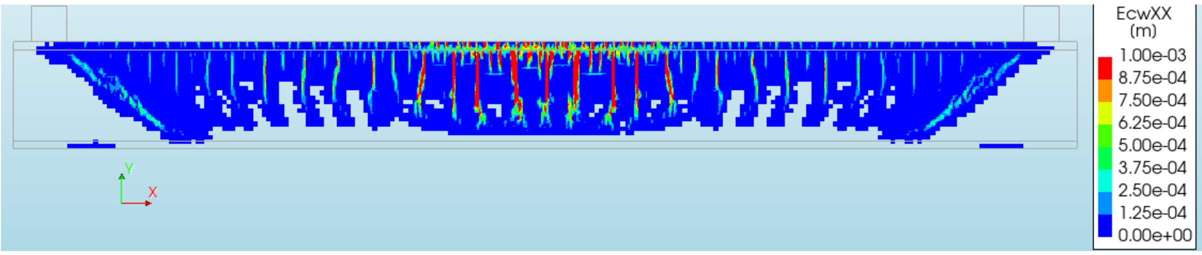

Figure 51 crack pattern experiment 1 fixed model based on mean aggregate size of 8 mm, refined, alt E

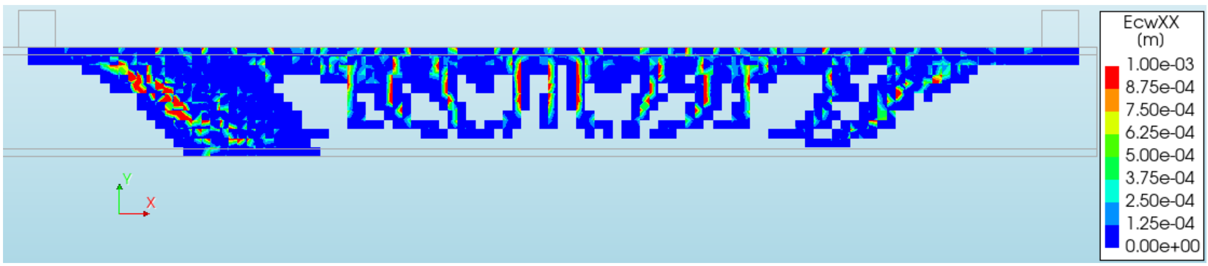

Figure 52 crack pattern experiment 1 fixed model with constant shear retention of 0.01

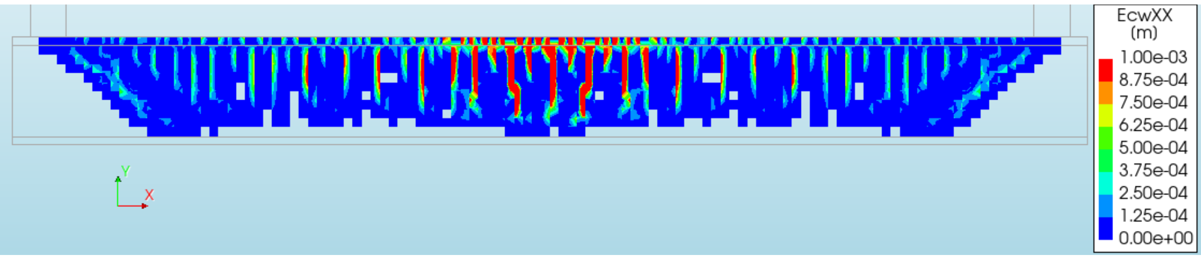

Figure 53 crack pattern experiment 1 fixed model based on mean aggregate size of 4 mm

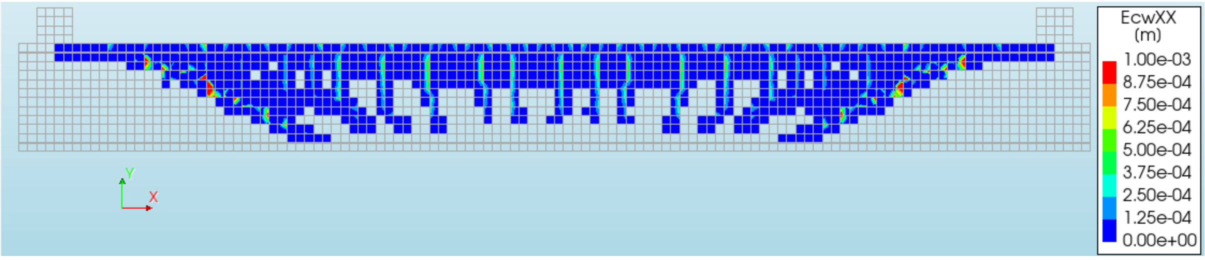

Figure 54 crack pattern experiment 1 fixed model with damage-based retention factor

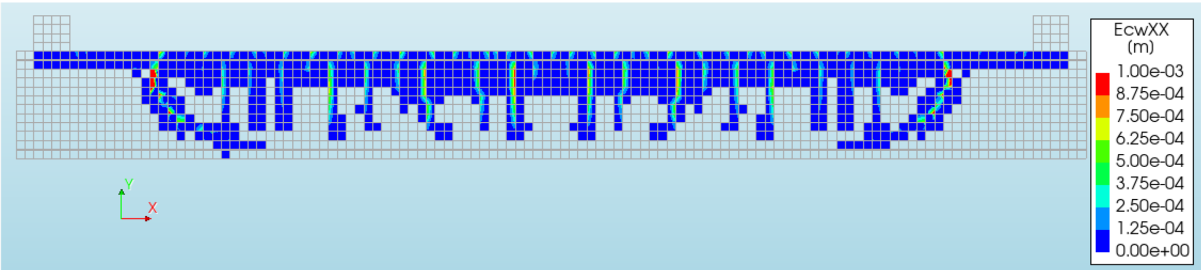

Figure 55 crack pattern experiment 1 fixed model with damage-based retention factor and damage-based Poisson reduction

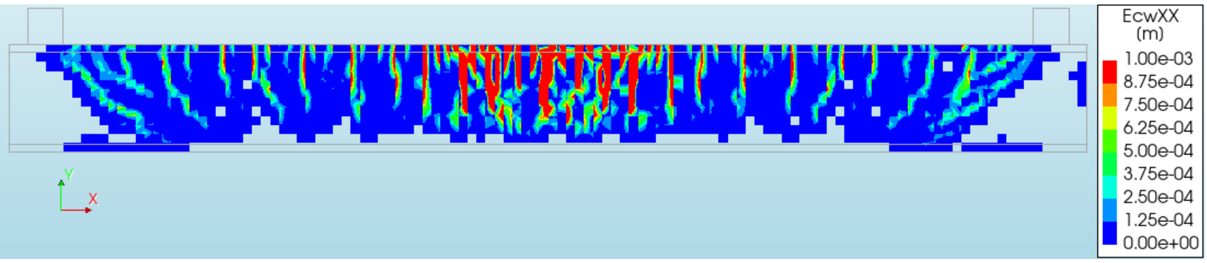

Figure 56 crack pattern experiment 1 fixed and bond-slip model based on mean aggregate size of 12 mm

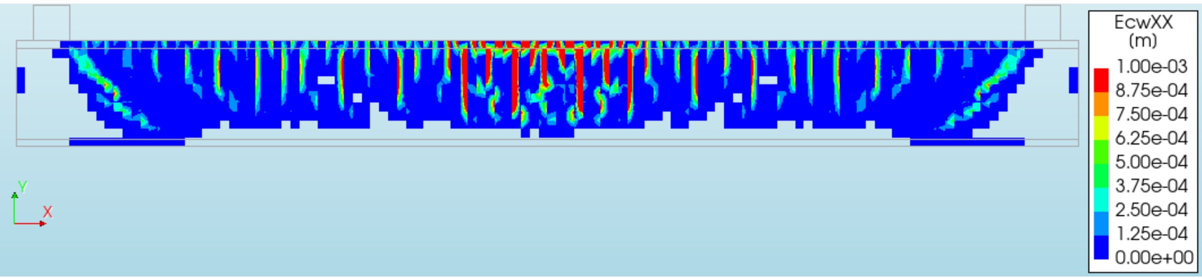

Figure 57 crack pattern experiment 1 fixed and bond-slip model based on mean aggregate size of 12 mm, increased bond stiffness

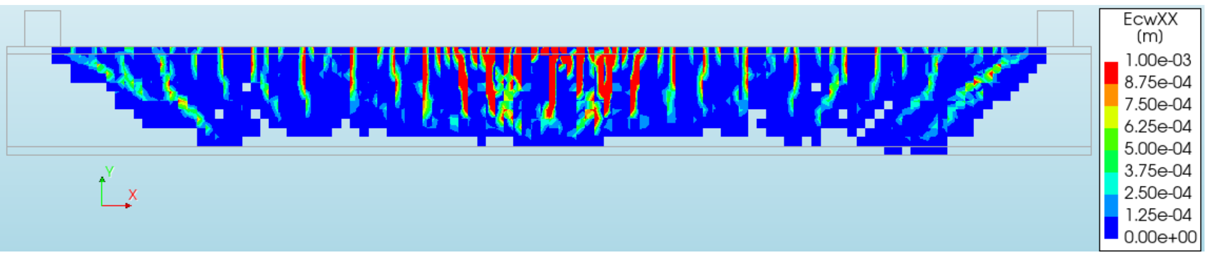

Figure 58 crack pattern experiment 1 fixed and bond-slip model based on mean aggregate size of 6 mm

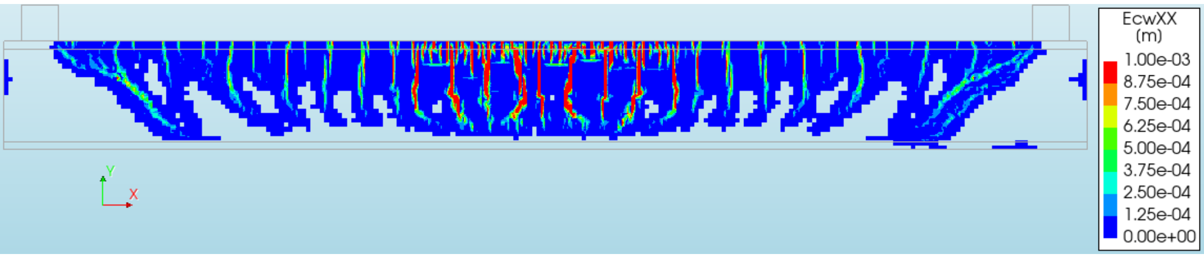

Figure 59 crack pattern experiment 1 fixed and bond-slip model based on mean aggregate size of 6 mm, refined

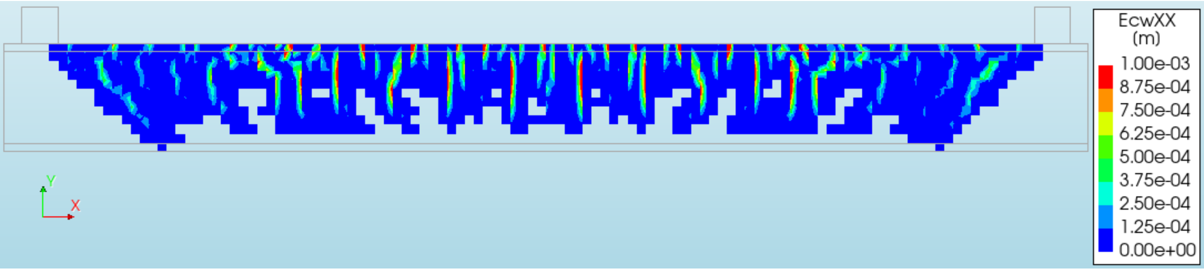

Figure 60 crack pattern experiment 1 fixed and bond-slip model based on mean aggregate size of 6 mm v2

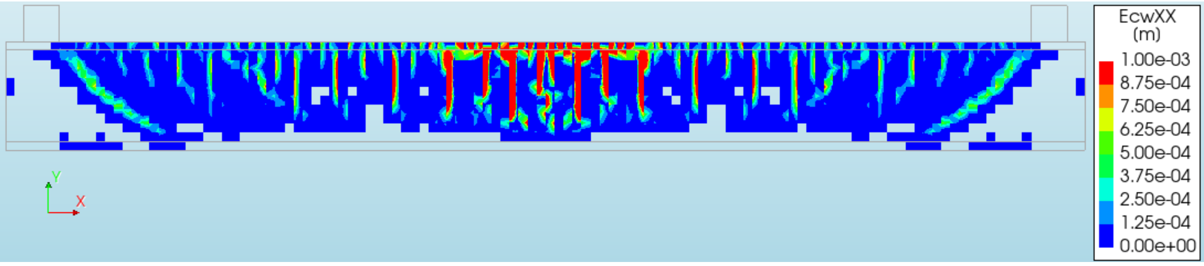

Figure 61 crack pattern experiment 1 fixed and bond-slip model based on mean aggregate size of 6 mm v3

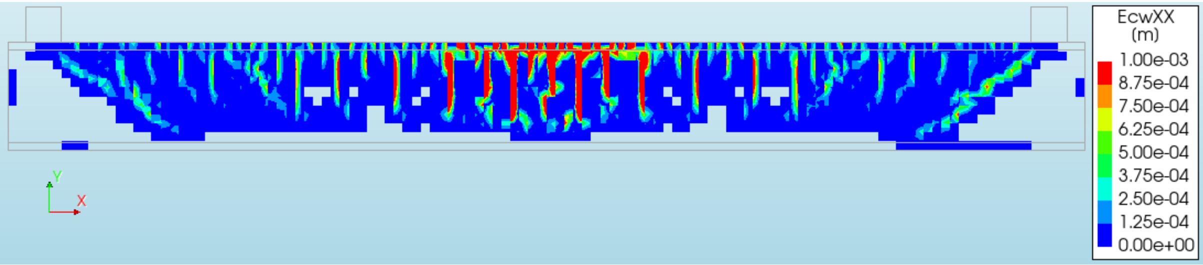

Figure 62 crack pattern experiment 1 fixed and bond-slip model based on mean aggregate size of 6 mm v4

Load-Displacement curves experiment 1

Rotating

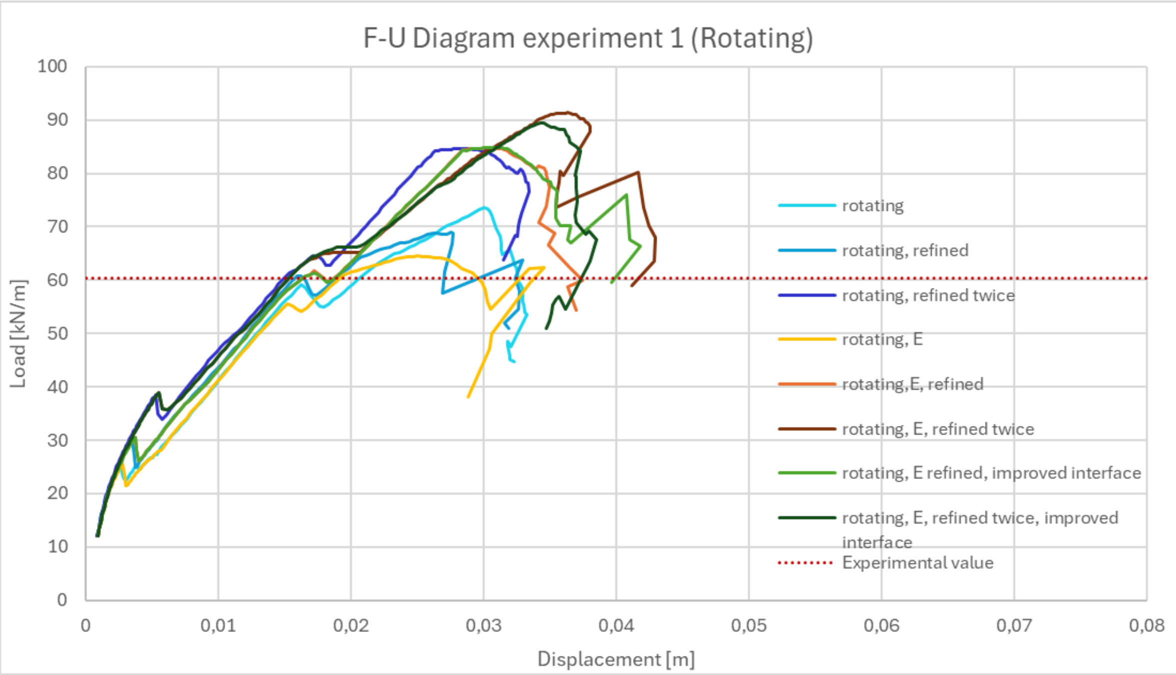

Figure 63 load displacement curves of experiment 1 (rotating) shown in one graph (experimental capacity = 60.4 kN/m)

Fixed

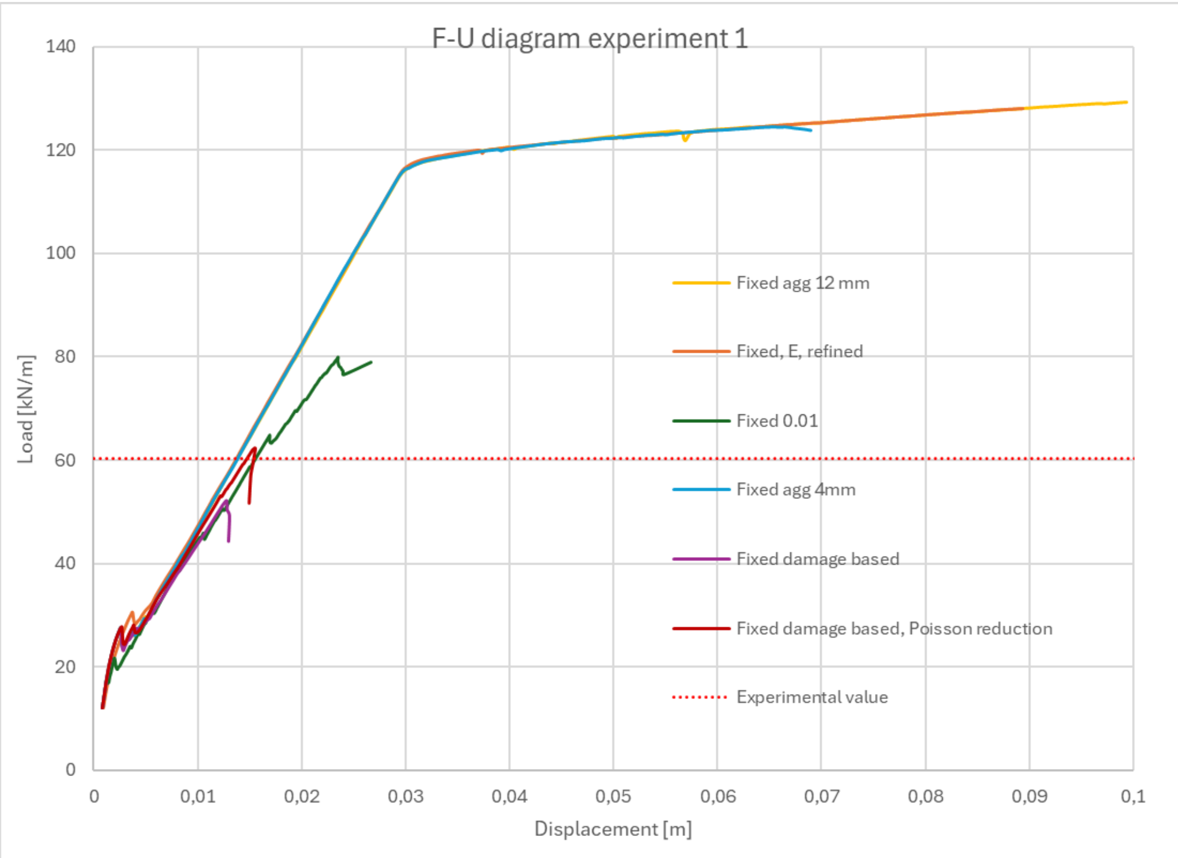

Figure 64 load displacement curves of experiment 1 shown in one graph (experimental capacity = 60.4 kN/m)

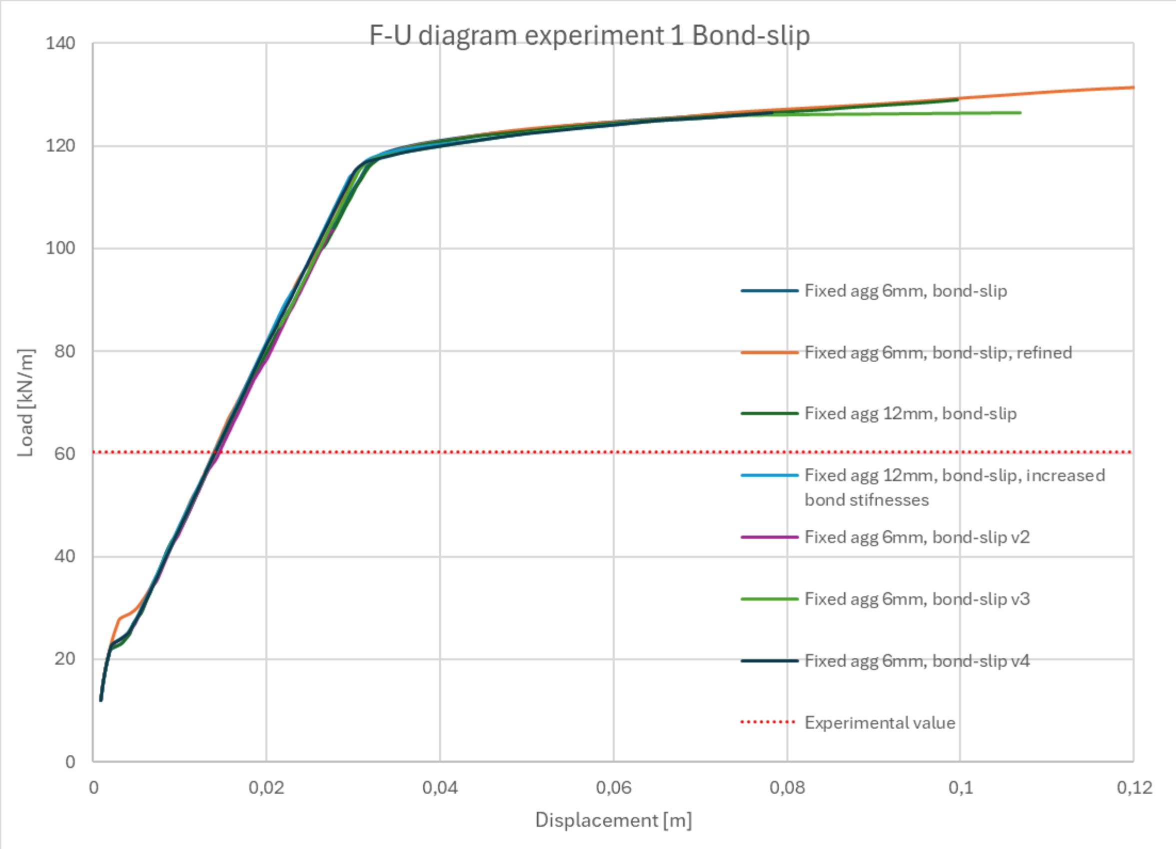

Figure 65 Load displacement curves of experiment 1 bond-slip models shown in one graph (experimental capacity = 60.4 kN/m)

FprEN calculations experiment 1

All calculations are done for the critical cross-section located at 1d from the support and γ_V = 1.4, d_{dg} =32mm, f_{ck} =33.6 and d=556mm.

$$M_{Ed} = \frac{1}{2} L * q * d - \frac{1}{2} d^2 * q$$

$$V_{ed} = \left(\frac{1}{2} * L - d\right) * q$$

$$a_{cs} = \left|\frac{M_{Ed}}{V_{Ed}}\right| = \left|\frac{\left(\frac{1}{2} * 5600 * 556 - \frac{1}{2} * 556^2\right) \cancel{* q}}{\left(\frac{1}{2} * 5600 - 556\right) \cancel{* q}}\right| = 624.9\ mm \geq d = 556\ mm$$

$$a_v = \sqrt{\frac{a_{cs}}{4} * d} = \sqrt{\frac{624.9}{4} * 556} = 294.7\ mm \leq d = 556\ mm$$

$$\rho_l = \frac{A_{sl}}{b_w d} = \frac{2 * \left(\frac{28}{2}\right)^2 * \pi}{250 * 556} = 0.00886\ \%$$

$$V_{Rd,c} = \frac{0.66}{\gamma_V} \left(100 \rho_l * f_{ck} * \frac{d_{dg}}{a_v}\right)^{1/3} * b_w d = \frac{0.66}{1.4} \left(0.886 * 33.6 * \frac{32}{294.7}\right)^{\frac{1}{3}} * 250 * 556 = 96.9\ kN$$

$$V_{Rd,c} \geq \tau_{Rdc,min} * b_w d$$

$$V_{Rdc,min} = \frac{11}{\gamma_V} \sqrt{\frac{f_{ck}}{f_{yd}} * \frac{d_{dg}}{d}} * b_w d = \frac{11}{1.4} \sqrt{\frac{33.6}{435} * \frac{32}{556}} * 250 * 556 = 72.8\ kN$$

$$q_{VRd,c} = \frac{V_{Rd,c}}{\frac{1}{2} L - d} = 43.2\ kN/m$$

Overview experiment 1

Table 12 Overview of experiment 1 results

Model	Failure load q (kN/m)	Estimated angle (°)	Plastic steel?
EXPERIMENT	**60.4**	**40**	
FprEN 1992-1-1 calculation	**43.2**		
Rotating	73.6	30	No
Rotating refined	69.1	26	No
Rotating refined twice	84.7	29	No
Rotating (alt. E)	64.5	34	No
Rotating (alt. E) refined	84.8	31	No
Rotating (alt. E) refined (interface improved)	84.8	34	No
Rotating (alt. E) refined twice	91.4	27	No
Rotating (alt. E) refined twice (interface improved)	89.5	25-32	No
Fixed agg 12mm	129+	-	Yes at 114 kN/m
Fixed agg 8mm (alt. E) refined	128+	-	Yes at 115 kN/m
Fixed shear retention 0.01	79	34	No
Fixed mean agg 4 mm	124 (divergence)	-	Yes at 114 kN/m
fixed damage based	52	26	No
Fixed damage based with Poisson reduction	62.5	42	No
Fixed agg 12mm, bond-slip	129	- Flexural failure	Yes at 115 kN/m
Fixed agg 12mm, bond-slip, increased bond stifnesses	124	- Flexural failure	Yes at 115 kN/m
Fixed agg 6mm bond-slip	126	-	Yes at 115 kN/m
Fixed agg 6mm, bond-slip, refined	132	- Flexural failure	Yes at 115 kN/m
Fixed agg 6mm bond-slip v2	103	- unexpected divergence	No
Fixed agg 6mm bond-slip v3	126	- Flexural failure	Yes at 115 kN/m
Fixed agg 6mm bond-slip v4	126	- Flexural failure	Yes at 115 kN/m

Model properties experiment 2

The material properties used in the different models are given in Table 13 and Table 14Table 10. For some properties multiple settings are given, this is because multiple variations have been investigated. In the caption of the crack patterns, the legend of load-displacement curves and the model names in the overview the used settings are provided. If displacement control has been used instead of arc-length control this has also been mentioned.

Table 13 concrete model properties used in experiment 2

Young's modulus	E=34351 MPa
Poisson ratio	0.2
Crack orientation	Fixed / rotating
Tensile curve	Hordijk
Tensile strength	4.5 MPa
Mode I tensile fracture energy	154.3 N/m
Shear retention function (applicable to fixed crack orientation)	Constant (0.01) / damage based / aggregate size based (12 mm)
Compression curve	Parabolic
Compressive strength	69.5 MPa
Compressive fracture energy	39158 N/m

Table 14 steel model properties used in experiment 2

Young's modulus steel	E=200000 MPa
Yield strength	580 MPa
Ultimate strength	670 MPa
Ultimate strain	ε_u= 0.05
Yield strength prestressing tendon	1750 MPa
Applied post tensioning force	0 / 281 kN ($\frac{1}{4}$ prestressing load) / 1125 kN
The anchor retention length	0 m
Coefficient of friction	0.18
Wobble factor	0.05 m^{-1}

Additional bond-slip models have been investigated. In total four bond slip models are used as is shown in Table 15. One of the models is based on the tutorial (DIANA FEA). Models with increased normal and shear stiffness moduli have also been tested. However, early divergence occurred which could not be prevented, and these results have been omitted. In the case that bond slip is modelled this is mentioned in the name of the models, the legend of graphs or captions of figures. Bond-slip has only been considered for fixed models with a shear retention based on a mean aggregate size of 12 mm.

Table 15 Bond-slip settings used for experiment 2 (smeared)

	No bond failure	**Doerr failure**	**Doerr failure Tutorial values V1**	**Doerr failure Increased stiffness**
Normal stiffness modulus [N/m³]	2e12	2e13	1e12	2e13
Shear stiffness modulus [N/m³]	1e10	1e11	2e10	2e12
Parameter c [N/m²]	- (No failure)	9e6	2e7	9e6
Shear slip at plateau [m]	- (No failure)	6e-4	0.1	6e-5

Crack patterns experiment 2

Rotating

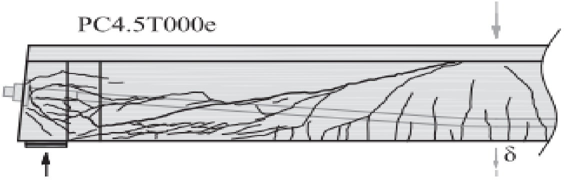

Figure 66 experiment 2 observed crack pattern

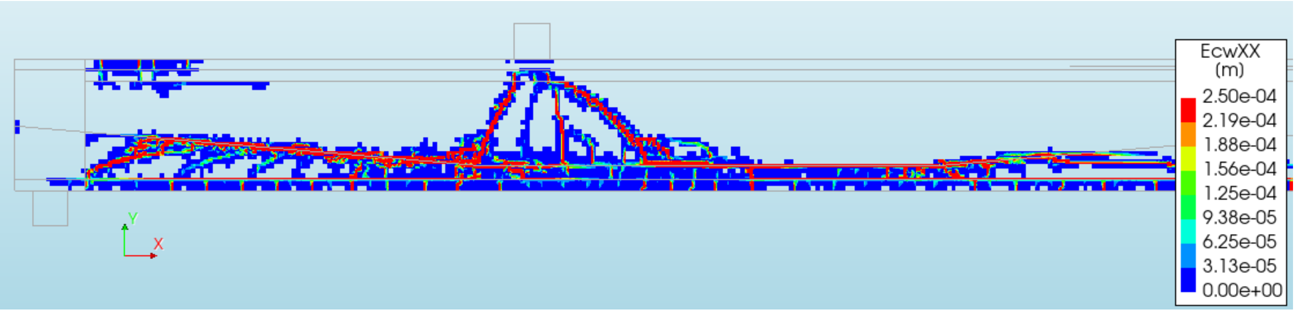

Figure 67 crack pattern experiment 2 rotating model

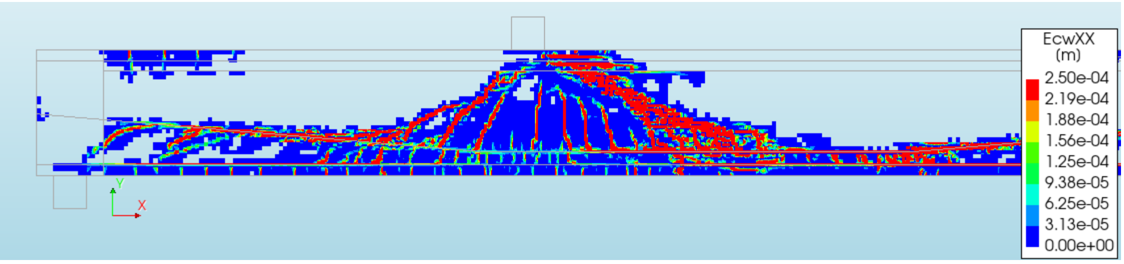

Figure 68 crack pattern experiment 2 rotating model, displacement control

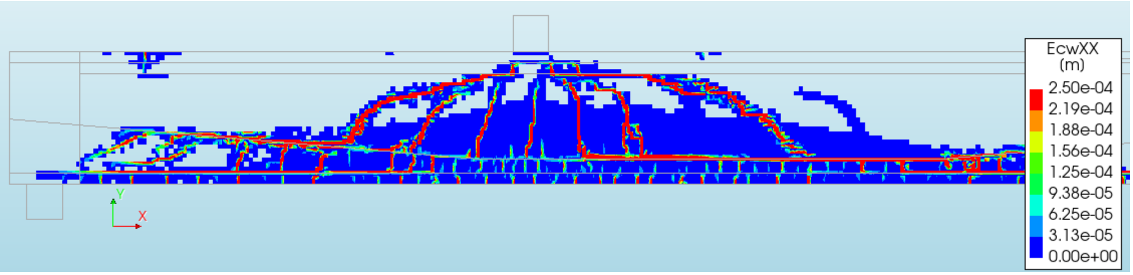

Figure 69 crack pattern experiment 2 without prestressing load

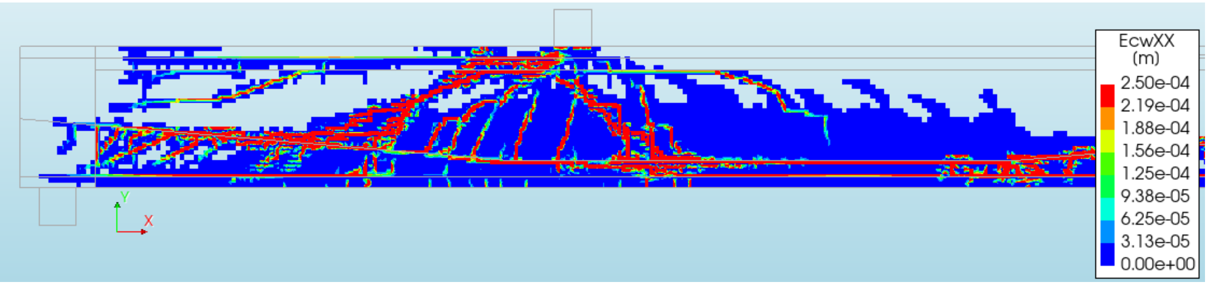

Figure 70 crack pattern experiment 2 without prestressing load, displacement control

Fixed

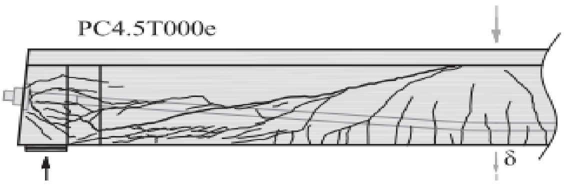

Figure 71 experiment 2 observed crack pattern

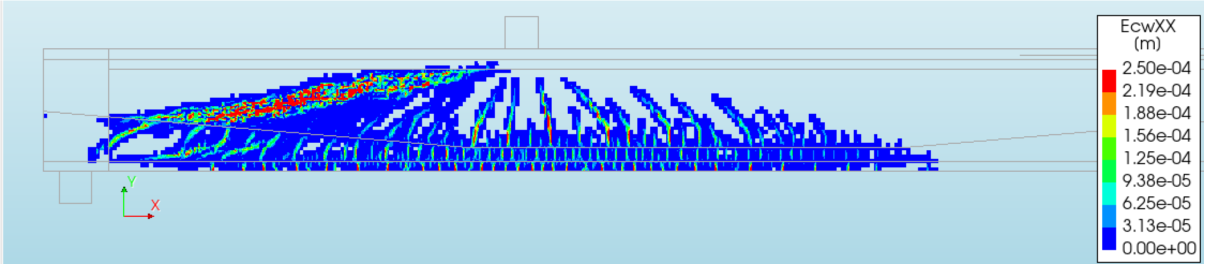

Figure 72 crack pattern experiment 2 fixed model based on mean aggregate size of 12 mm

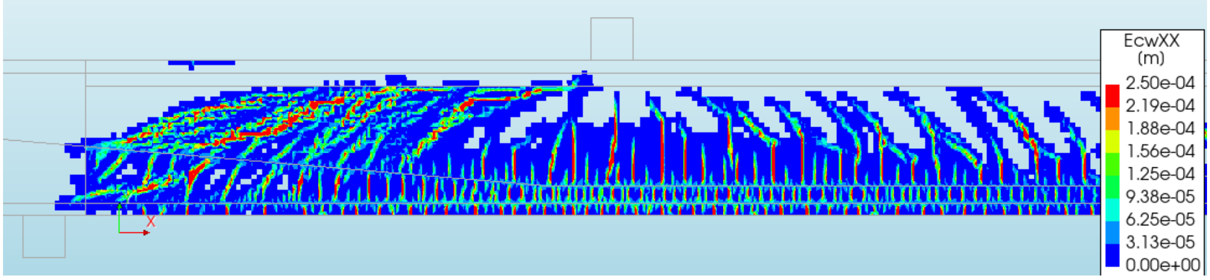

Figure 73 crack pattern experiment 2 fixed model based on mean aggregate size of 12 mm, when only 1/4 prestressing is applied

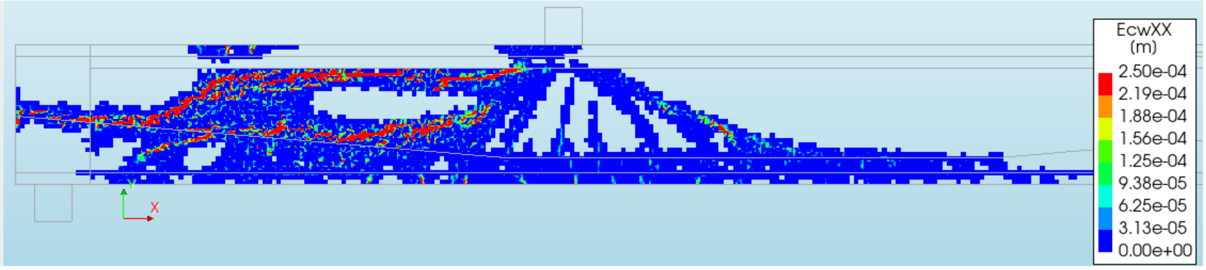

Figure 74 crack pattern experiment 2 fixed model with constant retention factor of 0.01

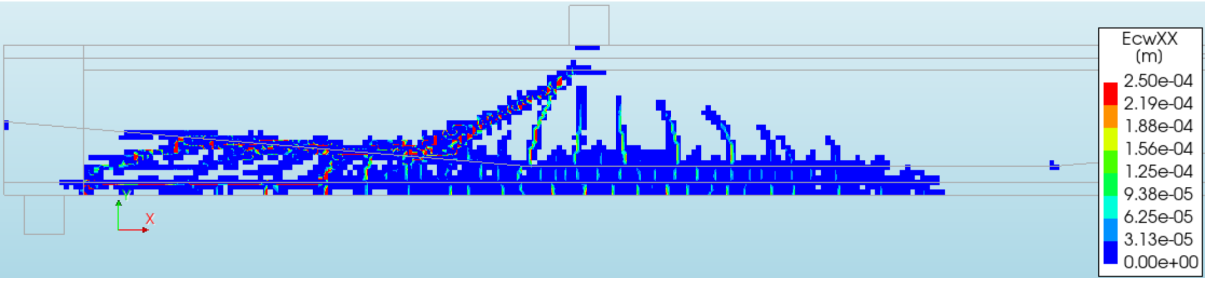

Figure 75 crack pattern experiment 2 fixed, damage based, Poisson reduction

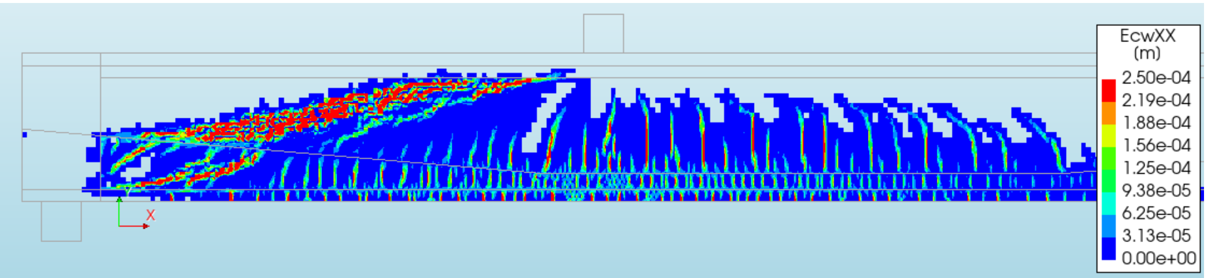

Figure 76 crack pattern experiment 2 fixed model based on mean aggregate size of 12 mm, disp. control

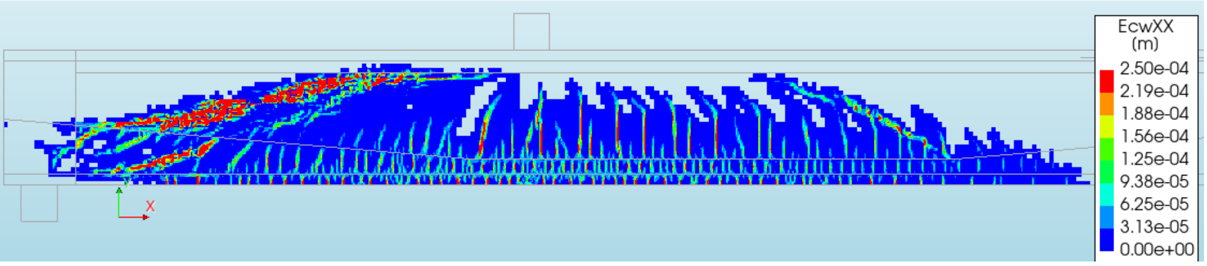

Figure 77 crack pattern experiment 2 fixed model based on mean aggregate size of 12 mm, disp. control, phased support

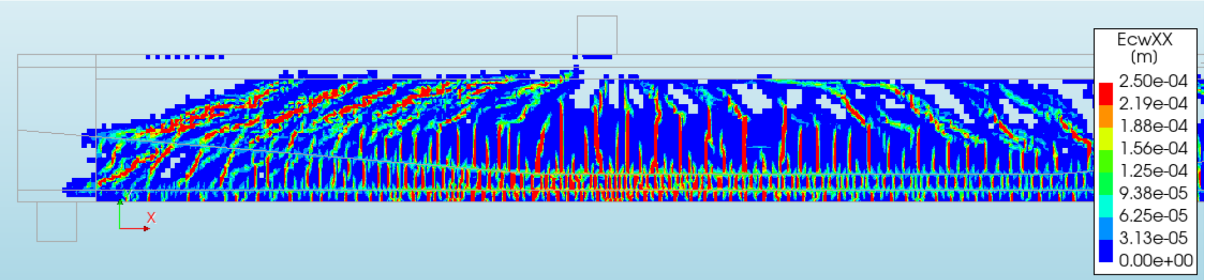

Figure 78 crack pattern experiment 2 fixed model based on mean aggregate size of 12 mm, without prestressing load

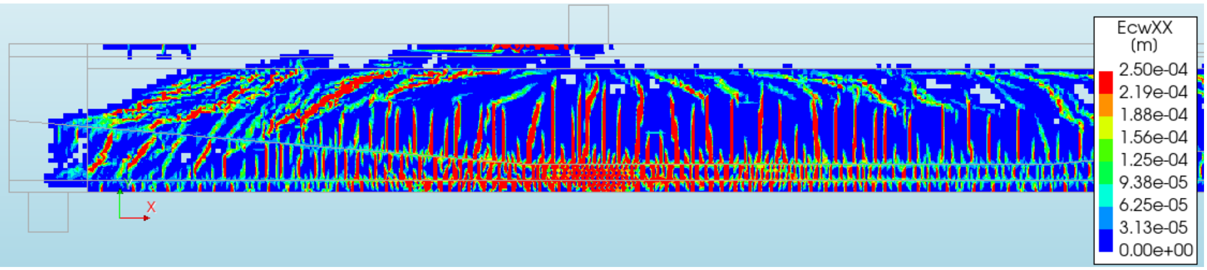

Figure 79 crack pattern experiment 2 fixed model based on mean aggregate size of 12 mm, without prestressing load, disp. control

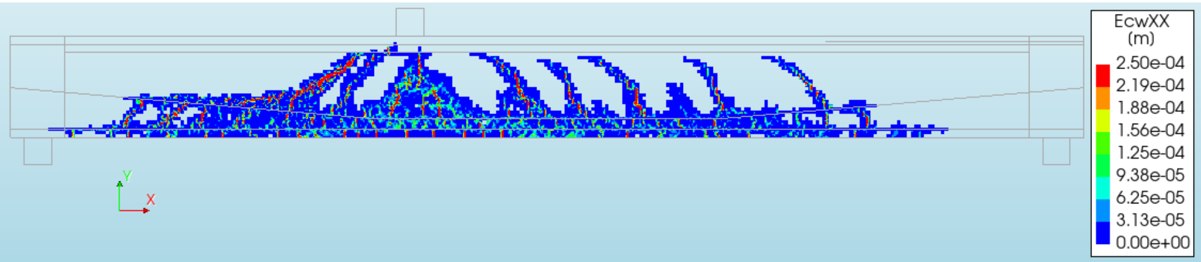

Figure 80 crack pattern experiment 2 fixed model, without prestressing load, retention factor 0.01

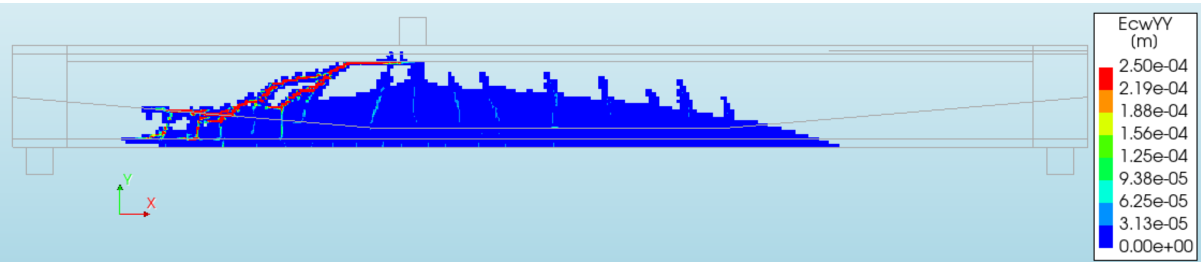

Figure 81 crack pattern experiment 2 fixed model based on mean aggregate size of 12 mm, without prestressing load, damage based

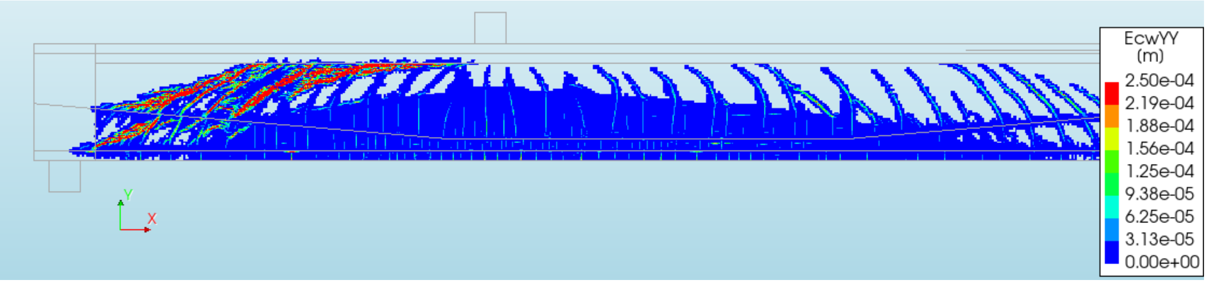

Figure 82 crack pattern experiment 2 fixed model based on mean aggregate size of 12 mm, without prestressing load, refined

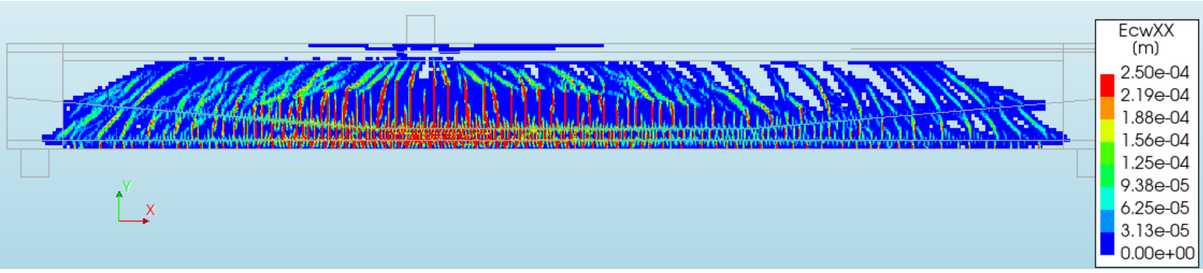

Figure 83 crack pattern experiment 2 fixed model based on mean aggregate size of 12 mm, without prestressing load, included Poisson reduction when damaged

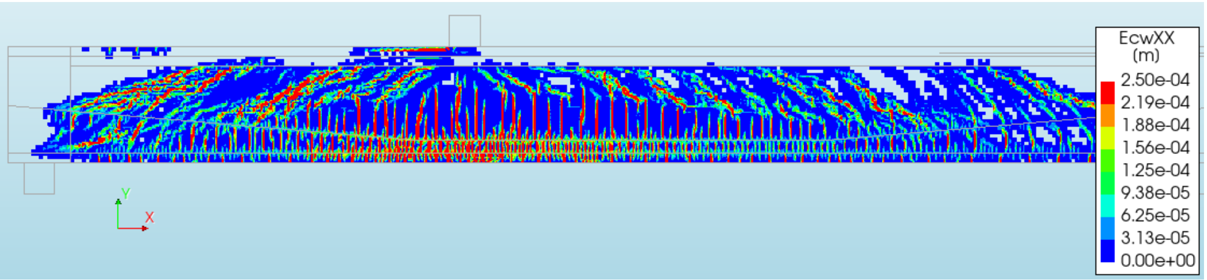

Figure 84 crack pattern experiment 2 fixed model based on mean aggregate size of 12 mm, without prestressing load, with class 3 beam reinforcement instead of embedded.

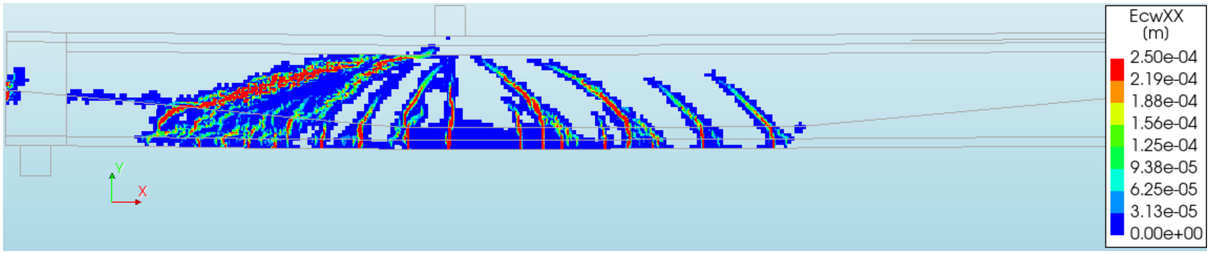

Figure 85 crack pattern experiment 2 fixed bond-slip model based on mean aggregate size of 12mm, no bond failure, at peak load

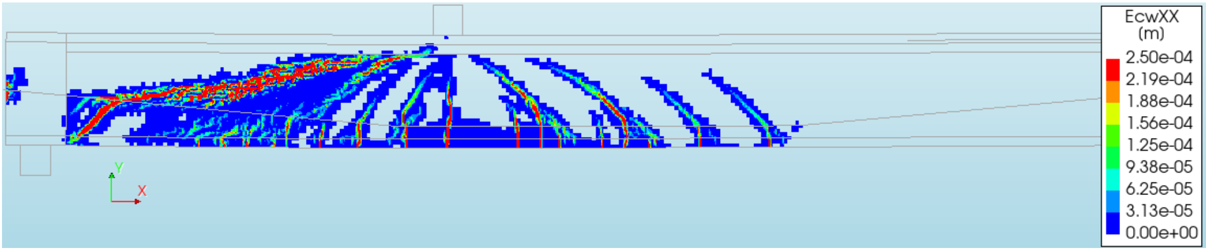

Figure 86 crack pattern experiment 2 fixed bond-slip model based on mean aggregate size of 12mm, no bond failure, AFTER peak load just before divergence

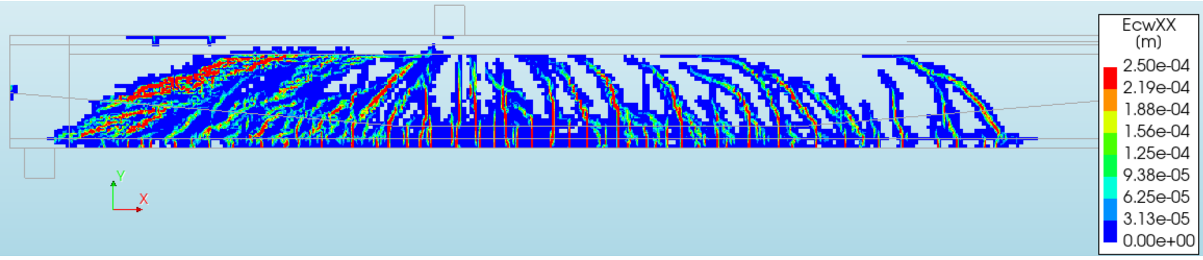

Figure 87 crack pattern experiment 2 fixed bond-slip model based on mean aggregate size of 12mm, Doerr failure

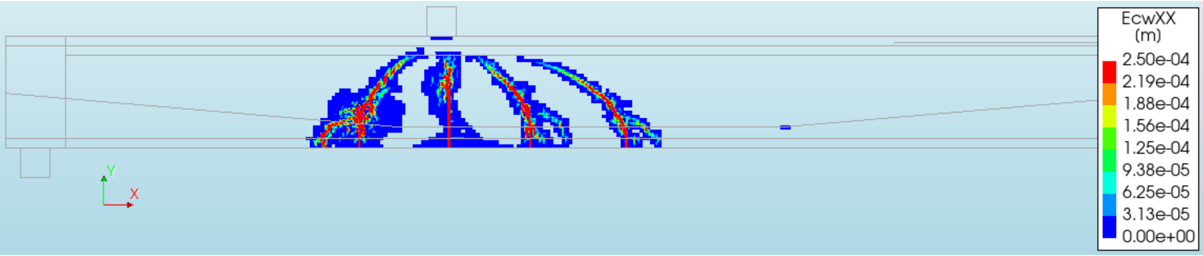

Figure 88 crack pattern experiment 2 fixed bond-slip model based on mean aggregate size of 12mm, Doerr failure, tutorial values

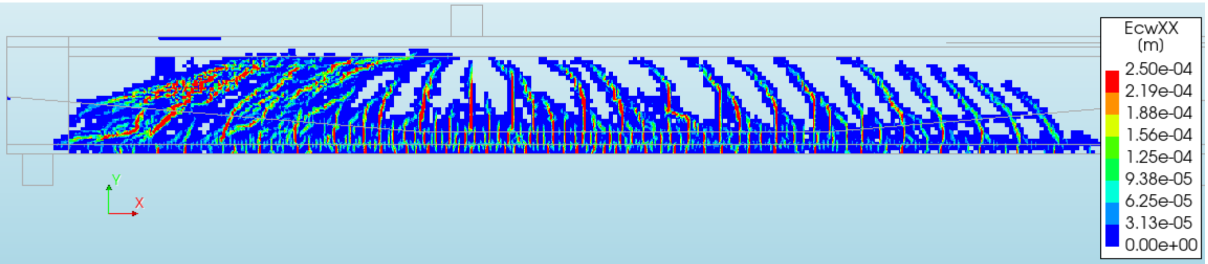

Figure 89 crack pattern experiment 2 fixed bond-slip model based on mean aggregate size of 12 mm, Doerr failure increased stiffnesses

Load-Displacement curves experiment 2

Rotating

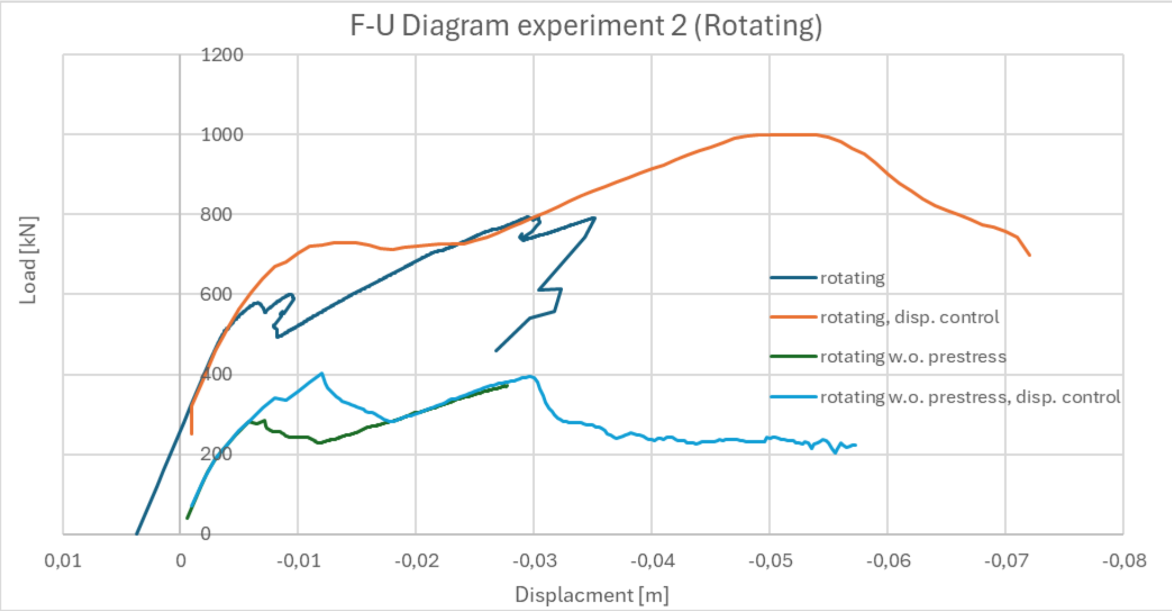

Figure 90 Load displacement curves of experiment 2 (rotating) in one graph (including a load- controlled check) (experimental capacity 709 kN)

Fixed

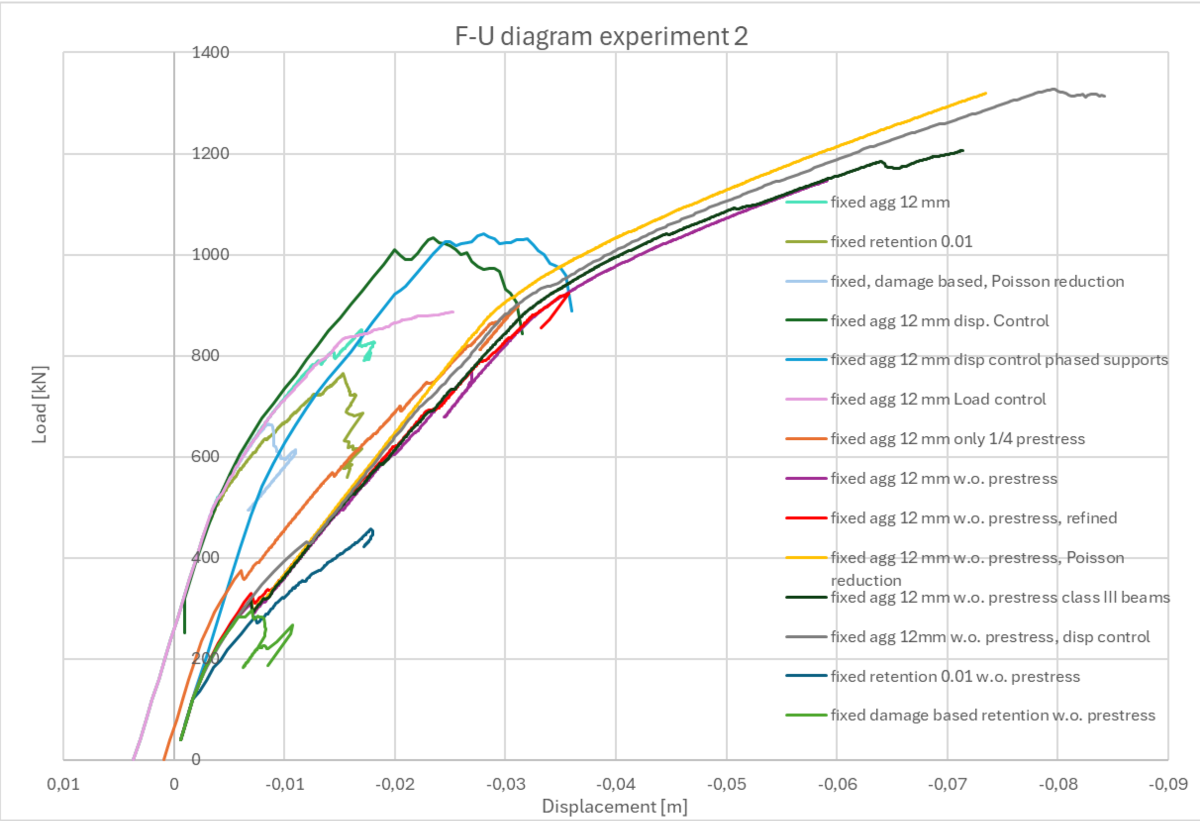

Figure 91 Load displacement curves of experiment 2 in one graph (including a load- controlled check) (experimental capacity 709 kN)

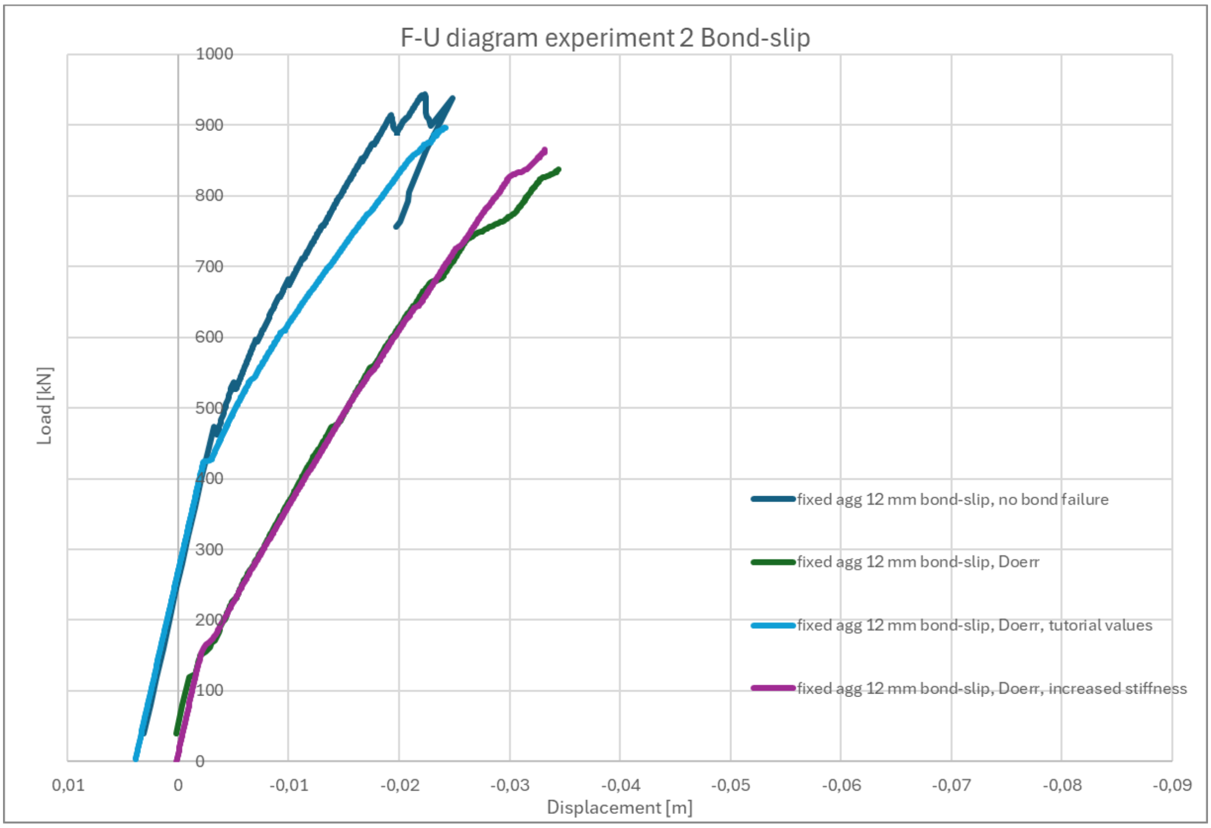

Figure 92 Load displacement curves of experiment 2 bond-slip models in one graph (including a load- controlled check) (experimental capacity 709 kN)

In the F-U Diagrams the prestressed models start off with a displacement (in opposite direction), this is caused by the prestressing load which causes initial displacements. The exception is the model with displacement control and a phased support. This model places the support at the load location after the prestressing has been applied, and only then it will start to record displacements.

When the prestressing load is reduced or removed, an unexpected increase in capacity is observed. The increased capacity cannot be explained; therefore, the reliability of FEA results is questionable. Only when damage based, or a constant shear retention factor of 0.01 is used, does the capacity decrease for the models without prestressing.

Just before the critical shear crack starts to develop, differences start to occur between the arc-length control (turquoise) and the displacement control (dark green and blue) in Figure 91. Eventually the peak loads found by displacement control will also be ~200 kN higher than those found when using arc-length control. When analysing the crack patterns of models using arc-length and displacement control just before the critical crack develops, some differences can be seen. The crack patterns are shown below.

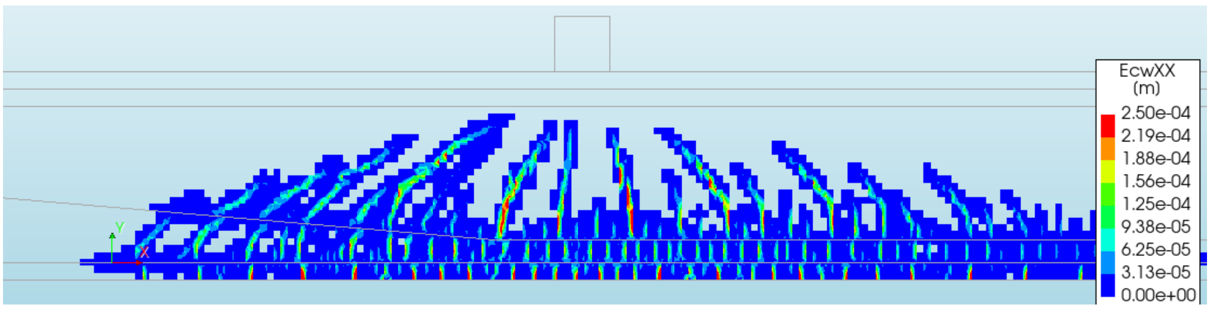

Figure 93 fixed, arc-length control before critical crack develops

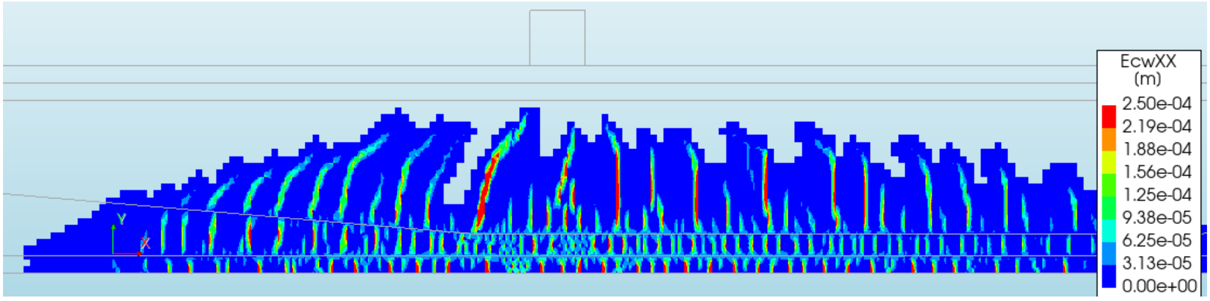

Figure 94 fixed, displacement control before critical crack develops

Two main differences can be observed: 1. The variant with displacement control has slightly more cracks, thus the crack spacing in the arc-length control is bigger. 2. The cracks in the displacement control variant start off almost vertical before they incline toward the load. In the arc-length control variant, the cracks almost immediately incline toward the load.

When the load/displacement is slightly increased multiple cracks connect, causing the critical crack to develop. In the arc-length control this happens at a lower load/displacement. Likely because the displacement controlled variant inclines at a later stage.

The reason why the crack pattern differs may be a worse convergence behaviour of arc-length control. All settings were checked, apart from how the loading is controlled and the load steps (arc-length needs smaller steps to prevent divergence) no differences between the models are present.

FprEN calculations experiment 2

All calculations are done for the critical cross-section located at 1d from the load and γ_V = 1.4, d_{dg} =32mm, f_{ck} =69.5. Values written in the calculations may have been rounded.

$$d_p = 750 - \left(143 + (367 - 143) * \frac{(d - 350)}{2430}\right) = 577.3\ mm$$

$$d = \frac{d_s^2 * A_{sl} + d_p^2 * A_p}{d_s * A_{sl} + d_p * A_p} = 672.1\ mm$$

dp and d are solved iteratively with Ap = 1050 mm^2, Asl = 3285 mm^2 and ds = 698 mm.

$$V_p = \sin(5°) * 1125 = 98.05\ kN$$

$$M_{Ed} = 0.635 * F * (2940 - d) - V_p * (2940 - d)$$

$$V_{Ed} = 0.635 * F - V_p$$

$$\mathrm{a_{cs}} = \left|\frac{\mathrm{M_{Ed}}}{\mathrm{V_{Ed}}}\right| = |2940 - 672.1| = 2067.9\ \mathrm{mm} \geq \mathrm{d} = 672.1\ \mathrm{mm}$$

$$\mathrm{a_v} = \sqrt{\frac{\mathrm{a_{cs}}}{4} * \mathrm{d}} = \sqrt{\frac{2067.9}{4} * 672.1} = 589.5\ \mathrm{mm} \leq \mathrm{d} = 672.1\ \mathrm{mm}$$

$$k_{vp} = 1 - \frac{P}{V_{ed}} * \frac{d}{3 * a_{cs}} = 1 - \frac{1125}{209.1} * \frac{672.1}{3 * 2067.9} = 0.42 \geq 0.1$$

$$\rho_l = \frac{A_{sl} * d_s + A_p * d_p}{bd^2} = \frac{6 * \left(\frac{26}{2}\right)^2 * \pi * 698 + 1050 * 577.3}{225 * 672.1^2} = 0.0278\ \%$$

$$\mathrm{V_{Rd,c}} = \frac{0.66}{\gamma_V}\left(100\rho_l * \mathrm{f_{ck}} * \frac{\mathrm{d_{dg}}}{k_{vp}\mathrm{a_v}}\right)^{1/3} \mathrm{bd} = \frac{0.66}{1.4}\left(2.8 * 69.5 * \frac{32}{0.42 * 672}\right)^{\frac{1}{3}} * 225 * 672 = 209\ \mathrm{kN}$$

$$\mathrm{V_{Rd,c}} \geq \tau_{\mathrm{Rdc,min}} * \mathrm{b_w d}$$

$$\mathrm{V_{Rdc,min}} = \frac{11}{\gamma_V}\sqrt{\frac{\mathrm{f_{ck}}}{\mathrm{f_{yd}}} * \frac{\mathrm{d_{dg}}}{\mathrm{d}}} * \mathrm{b_w d} = \frac{11}{1.4}\sqrt{\frac{69.5}{435} * \frac{32}{672.1}} * 225 * 672.1 = 104.4\ \mathrm{kN}$$

$$\mathrm{F_{VRd,c}} = \frac{\mathrm{V_{Rd,c}} + V_p}{0.635} = 483.57\ \mathrm{kN}$$

Overview experiment 2

Table 16 Overview of experiment 2 results

Model	Failure load F (kN)	Estimated angle (°)	Plastic steel?
EXPERIMENT	**709**	**16 (left crack)**	
FprEN 1992-1-1 calculation	**483.6**		
Lattice models	**510-600**	**30-45**	
Rotating	793.6	58 (left crack), 39 (right crack)	No
Rotating (disp control)	1000	35 and 48 (left cracks), 29 (right crack)	No
Rotating w.o. prestress	372.9	25 (left crack), 28 (right crack)	No
Rotating w.o. prestress (disp control)	402.5	25	No
Fixed agg12	852	13-21	No
Fixed ¼ prestress load	882+	-	No
Fixed retention 0.01	765	-	No
Fixed damage based, Poisson reduction	665	45	no
Fixed (disp control)	1033	13-21	Yes after peak load
Fixed (disp control) phased	1040	13-21	Yes after failure
Fixed w.o. prestress	1146+	-	Yes at 870 kN
Fixed w.o. prestress (disp control)	1327.3	-	Yes at 872 kN
Fixed w.o. prestress (ret 0.01)	456	32	No
Fixed w.o. prestress (damage)	297	22	No
Fixed w.o. prestress refined	900	29	Yes at 874 kN
Fixed w.o. prestress Poisson reduction	1320+	-	Yes at 868 kN
Fixed w.o. prestress class III	1206+	-	Yes at 905 kN
Fixed bond-slip no bond failure	943	22	No
Fixed bond-slip Doerr	838	22	No
Fixed bond-slip Doerr, tutorial values	897	45-52	No
Fixed bond-slip Doerr, increased stiffnesses	866	30	No

Model properties experiment 3

The material properties used are given in Table 17 and Table 18Table 14Table 10. For some properties more than one setting/value is given, this is because multiple variations have been investigated. In the caption of the crack patterns, the legend of load-displacement curves and the model names in the overview the used settings are provided. If displacement control has been used instead of arc-length control this has also been mentioned.

Table 17 concrete model properties used in experiment 3

Young's modulus	E=34351 MPa
Poisson ratio	0.2
Crack orientation	Fixed / rotating
Tensile curve	Hordijk
Tensile strength	4.5 MPa
Mode I tensile fracture energy	154.3 N/m
Shear retention function (applicable to fixed crack orientation)	Constant (0.01) / damage based / aggregate size based (12 mm)
Compression curve	Parabolic
Compressive strength	69.5 MPa
Compressive fracture energy	39158 N/m

Table 18 steel model properties used in experiment 3

Young's modulus steel	E=200000 MPa
Yield strength	580 MPa
Ultimate strength	670 MPa
Ultimate strain	ε_u= 0.05
Yield strength prestressing tendon	1750 MPa
Applied post tensioning force	0 / 1125 kN
The anchor retention length	0 m
Coefficient of friction	0.18
Wobble factor	0.05 m^{-1}

Additional bond-slip models have been created for experiment 3, Table 19 contains the settings used in these models. Models with higher stiffnesses or CEB FIB models instead of cubic Doerr were also considered, however, early divergence occurred and could not be prevented. As not all models considered bond-slip behaviour, it is specifically mentioned in the name of the models when bond-slip is modelled. Bond-slip has only been considered for fixed models with a shear retention based on a mean aggregate size of 12 mm.

Table 19 Bond-slip settings used for experiment 3 (smeared)

	Bond slip	**Bond slip v2**	**Bond slip v3**
Normal stiffness modulus [N/m^3]	2e12	2e13	3.75e12
Shear stiffness modulus [N/m^3]	1e10	1e11	3.75e11
Parameter c [N/m^2]	9e6	9e6	9e6
Shear slip at plateau [m]	6e-4	6e-4	6e-5

Crack patterns experiment 3

Rotating

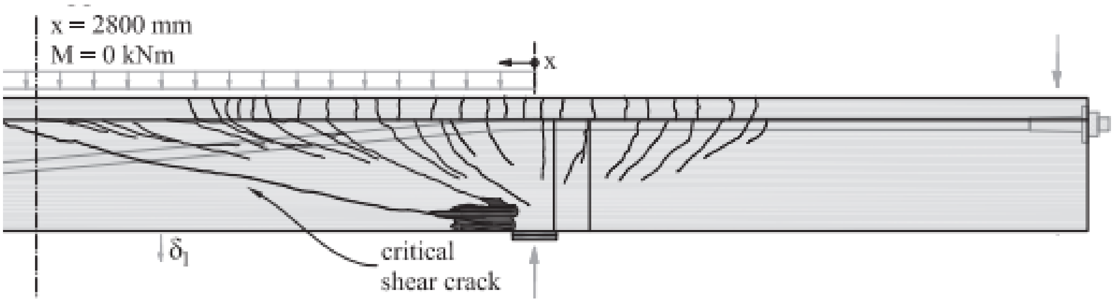

Figure 95 experiment 3 observed crack patterns

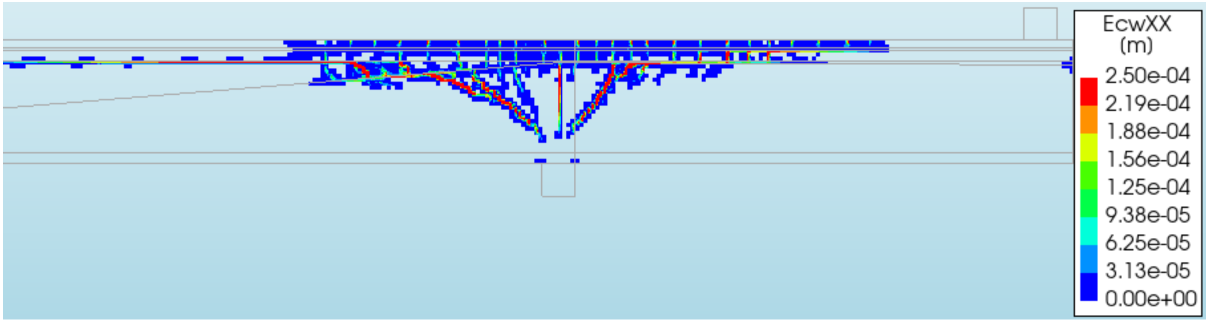

Figure 96 crack pattern experiment 3 rotating model

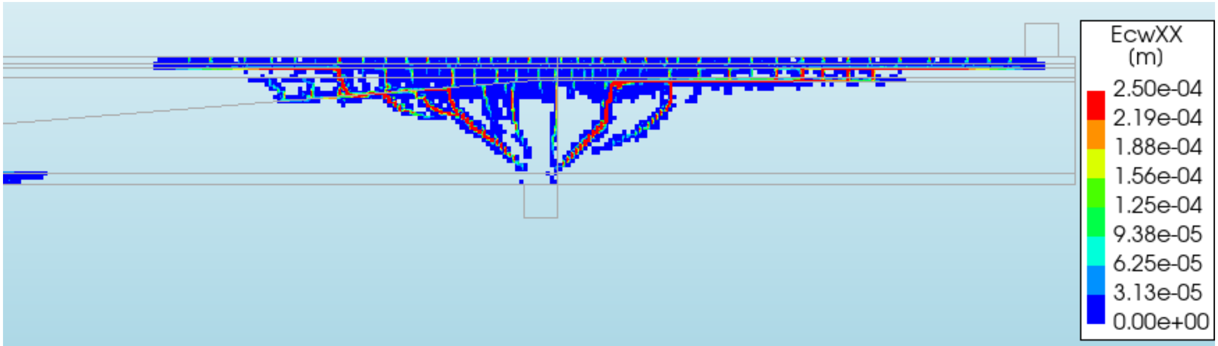

Figure 97 crack pattern experiment 3 rotating model without prestressing load

Fixed

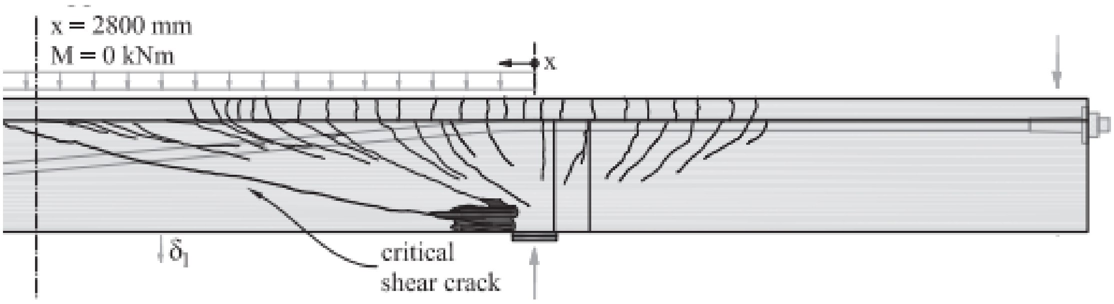

Figure 98 experiment 3 observed crack patterns

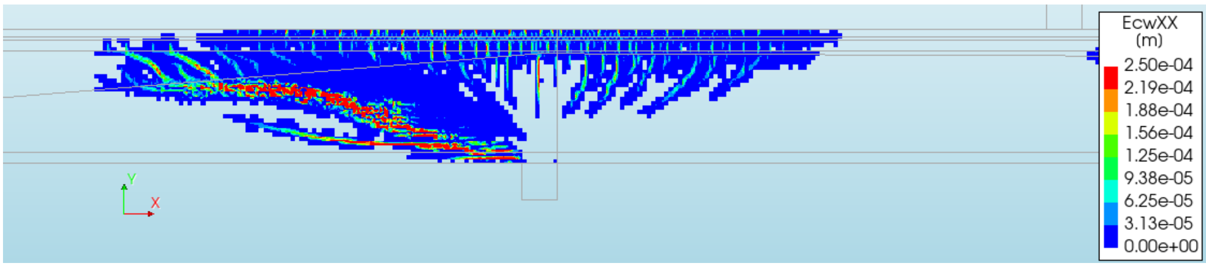

Figure 99 crack pattern experiment 3 fixed crack based on mean aggregate size of 12 mm

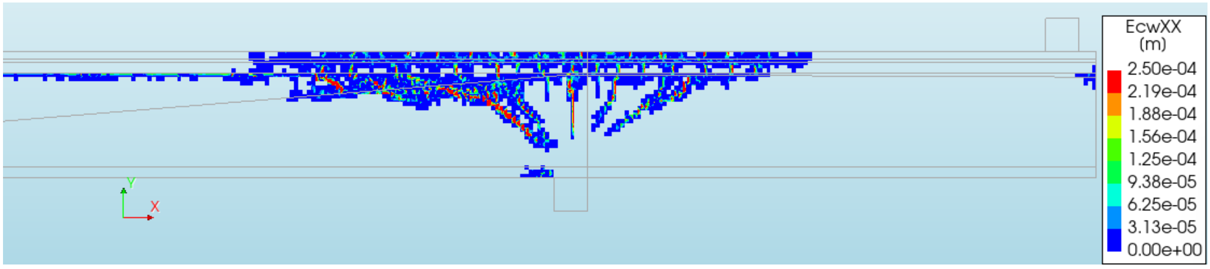

Figure 100 crack pattern experiment 3 fixed crack, constant retention factor 0.01

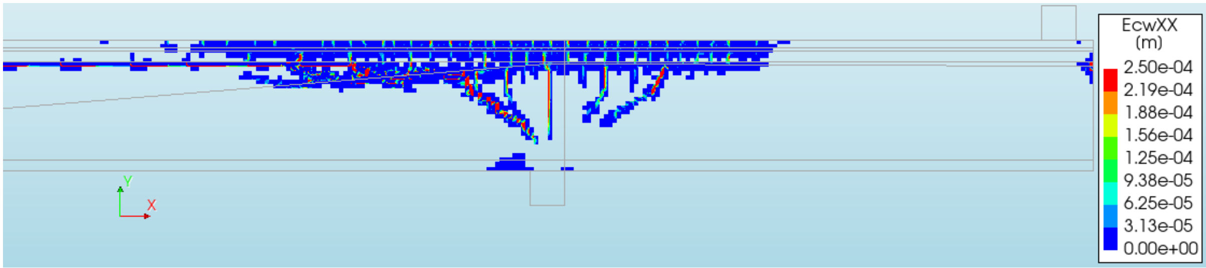

Figure 101 crack pattern experiment 3 fixed crack damage based, with Poisson reduction based on damage

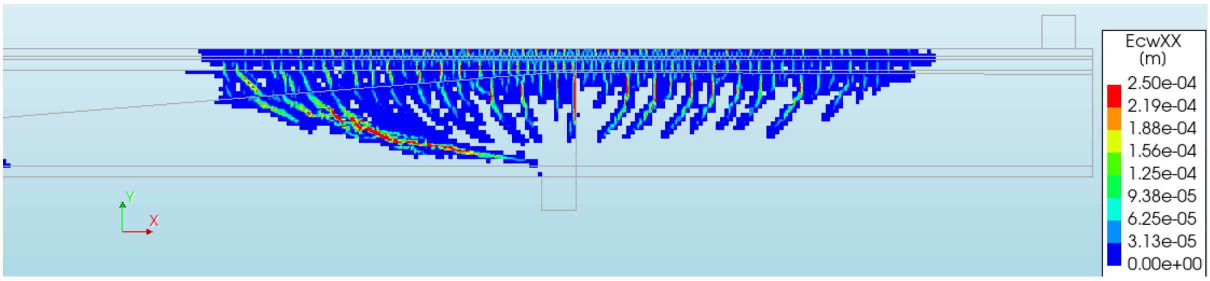

Figure 102 crack pattern experiment 3 fixed crack based on mean aggregate size of 12 mm, without prestressing load

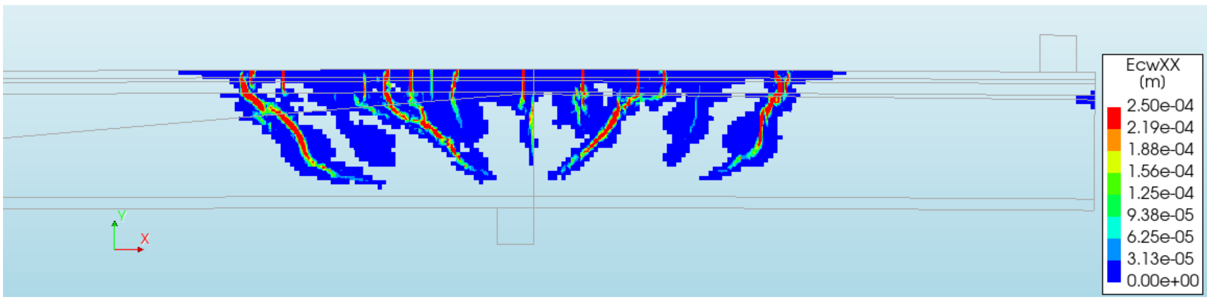

Figure 103 crack pattern experiment 3 fixed bond-slip model based on mean aggregate size of 12 mm

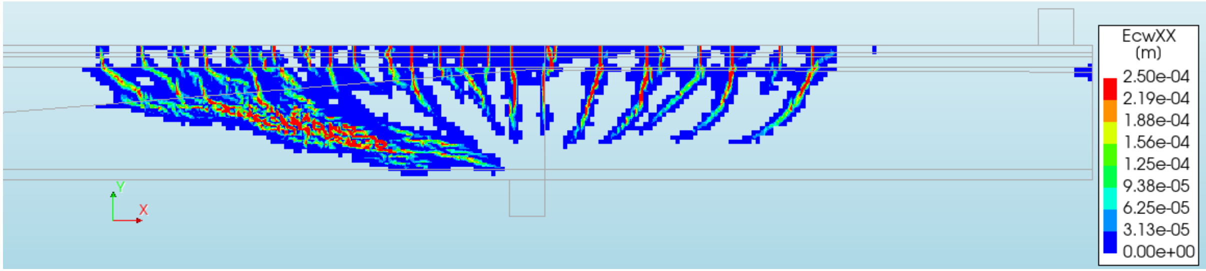

Figure 104 crack pattern experiment 3 fixed bond-slip model based on mean aggregate size of 12 mm v2

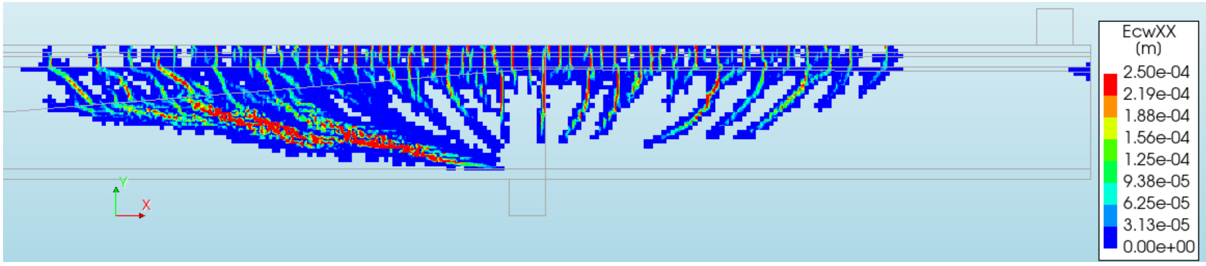

Figure 105 crack pattern experiment 3 fixed bond-slip model based on mean aggregate size of 12 mm v3

Load-Displacement curves experiment 3

Rotating

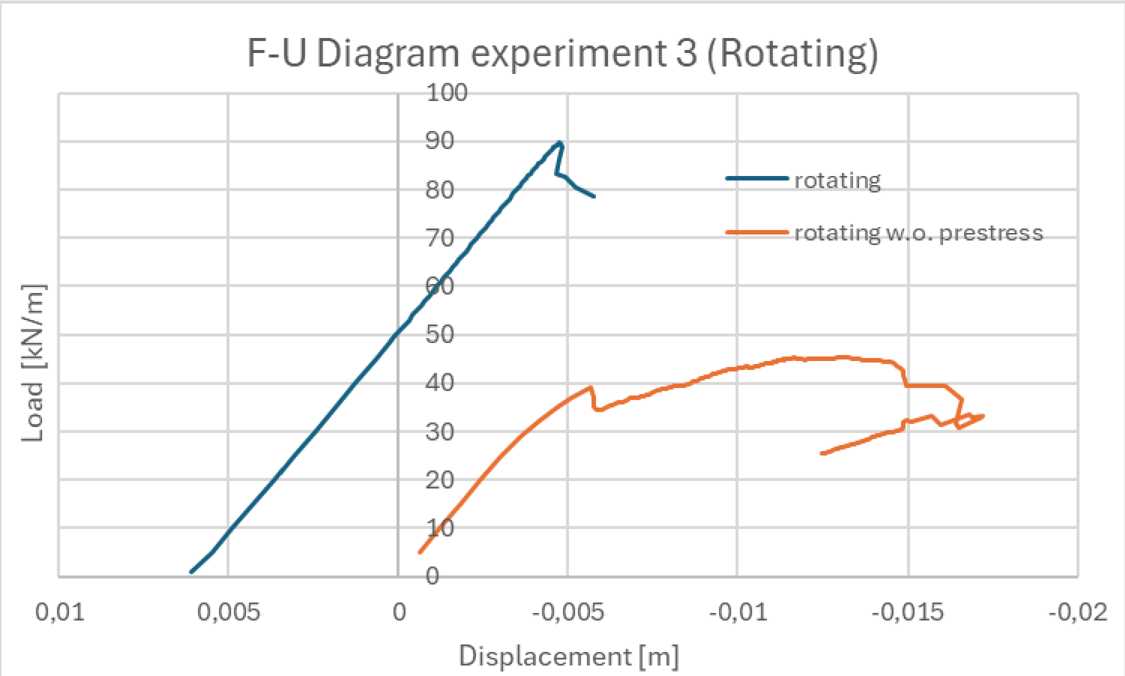

Figure 106 Load displacement curves of experiment 3 (rotating) in one graph (experimental capacity 100.5 kN/m)

Fixed

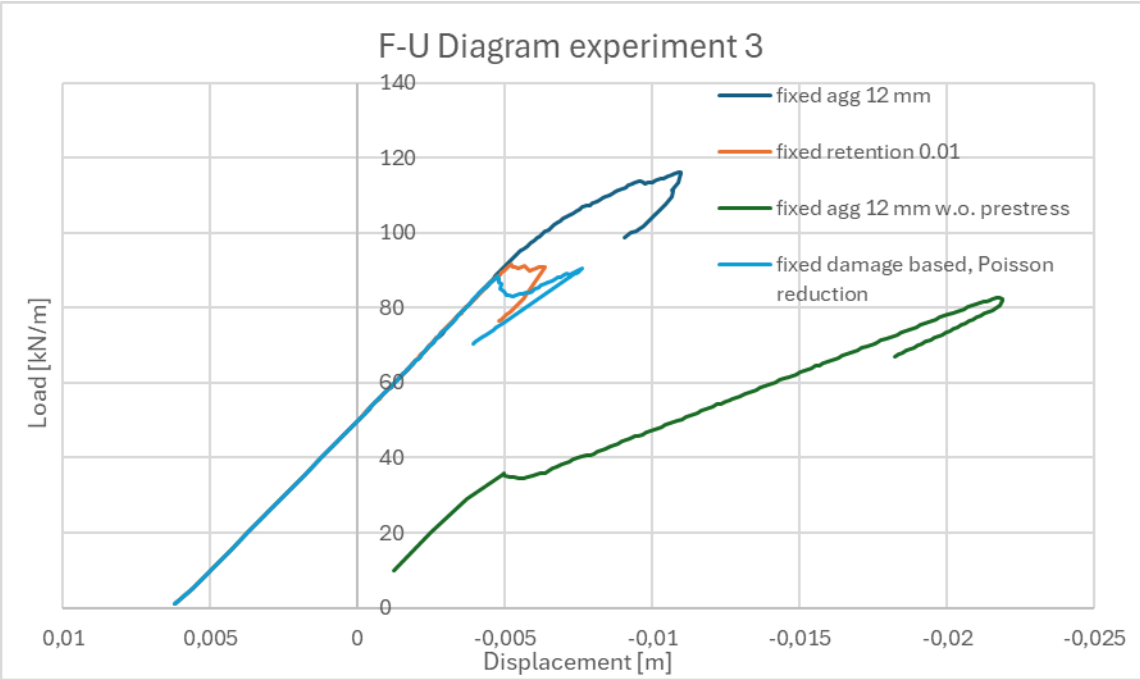

Figure 107 Load displacement curves of experiment 3 in one graph (experimental capacity 100.5 kN/m)

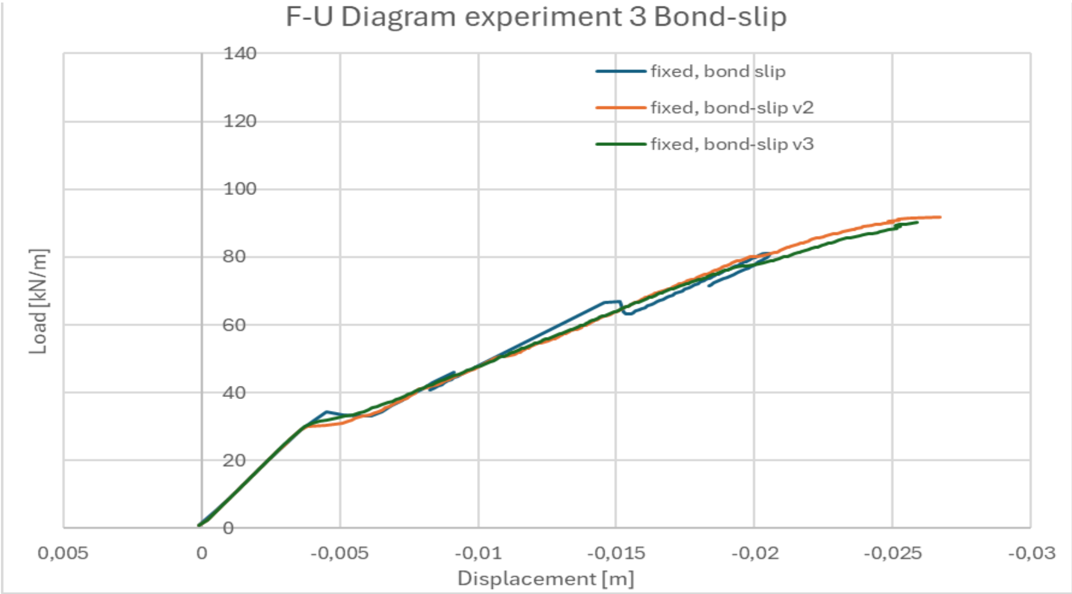

Figure 108 Load displacement curves of experiment 3 Bond-slip models in one graph (experimental capacity 100.5 kN/m)

FprEN calculations experiment 3

All calculations are done using a solver for the critical cross-section located at 1d from the intermediate support and γ_V = 1.4, d_{dg} =32mm, f_{ck} =69.5. Values written in the calculations may have been rounded. The support reaction at intermediate support is R_B (excluding prestressing effects).

$$d_p = 750 - \left(136 + (607-136) * \frac{(d-350)}{5384-350}\right) = 583.3\ mm$$

$$d = \frac{d_s^2 * A_{sl} + d_p^2 * A_p}{d_s * A_{sl} + d_p * A_p} = \frac{698^2 * 4109 + 583.3^2 * 1050}{698 * 4109 + 583.3 * 1050} = 677.8\ mm$$

$$R_B = \frac{\left(\frac{1}{2} * 10.72^2 * q + 5.11 * 13.66 * q\right)}{10.72} = 11.87q$$

$$V_p = \sin(5°) * 1125 * \frac{(2630 + 5270)}{10720} = 72.3\ kN$$

$$M_{Ed} = \left((2940 + d) * 5110 + \frac{1}{2} d^2 - 11870 * d\right) * 1 + V_p * d = 527.3\ kNm$$

$$V_{Ed} = (11870 - 5110 - d) * q - V_p = 200.4\ kN$$

$$a_{cs} = \left|\frac{M_{Ed}}{V_{Ed}}\right| = 2631\ mm \geq d = 677.8mm$$

$$a_v = \sqrt{\frac{a_{cs}}{4}} * d = 667.8\ mm \leq d = 677.8mm$$

$$k_{vp} = 1 + \frac{N_{Ed}}{|V_{Ed}|} * \frac{d}{3 * a_{cs}} = 0.52 \geq 0.1$$

$$\rho_l = \frac{A_{sl} * d_s + A_p * d_p}{bd^2} = \frac{\left(4 * \left(\frac{26}{2}\right)^2 + 2 * \left(\frac{20}{2}\right)^2 + 12 * \left(\frac{12}{2}\right)^2\right)\pi * 698 + 1050 * 583.3}{225 * 677.8^2} = 0.0337\ \%$$

$$V_{Rd,c} = \frac{0.66}{\gamma_V}\left(100\rho_l * f_{ck} * \frac{d_{dg}}{k_{vp} * a_v}\right)^{1/3} * b_w d = \frac{0.66}{1.4}\left(3.37 * 69.5 * \frac{32}{0.52 * 667.8}\right)^{\frac{1}{3}} * 225 * 677.8 = 200.4\ kN > \tau_{Rdc,min} * b_w d$$

$$V_{Rdc,min} = \frac{11}{\gamma_V}\sqrt{\frac{f_{ck}}{f_{yd}} * \frac{d_{dg}}{d}} * b_w d = \frac{11}{1.4}\sqrt{\frac{69.5}{435} * \frac{32}{677.8}} * 225 * 677.8 = 103.7\ kN$$

$$q_{VRd,c} = \frac{V_{Rd,c} + V_P}{11.87 - 5.11 - 0.678} = 44.8\ kN/m$$

Overview experiment 3

Table 20 Overview of experiment 3 results

Model	**Failure load q (kN/m)**	**Estimated angle (°)**	**Plastic steel?**
EXPERIMENT	**100.5**	**12**	
FprEN 1992-1-1 calculation	**44.8**		
Rotating	89.7	29	no
Rotating w.o. prestress	45.4	27	no
Fixed agg12	116.2	16	no
Fixed with retention 0.01	91.5	31	no
Fixed damage based, and Poisson reduction	90.36	40	no
Fixed w.o. prestress	82.5	19	no
Fixed agg12 Bond-slip	81	45 (crack does not go to support, crosses reinforcement at 1.4 m from intermediate support.)	no
Fixed agg12 Bond-slip v2	91	20	no
Fixed agg12 Bond-slip v3	90.25	17	no

Appendix C. Finite Element Analysis (Discrete)

First discrete model

To get comfortable with modelling discrete models, the unreinforced beam with D= 150 found in the article (Ruiz, Elices, & Planas, 1998) has been modelled by using a vertical discrete crack in the middle of the beam. The beam contains a notch and fails in flexure. Using linear softening, a tensile strength of 3.8 MPa and a fracture energy 62.5 N/m in a discrete model, similar results can be found as in the article without any convergence issues. The peak load found in the discrete model is about 30% larger, this increased load can partly be explained by the fact that the splitting tensile strength has been used in the model which is higher than the actual tensile strength.

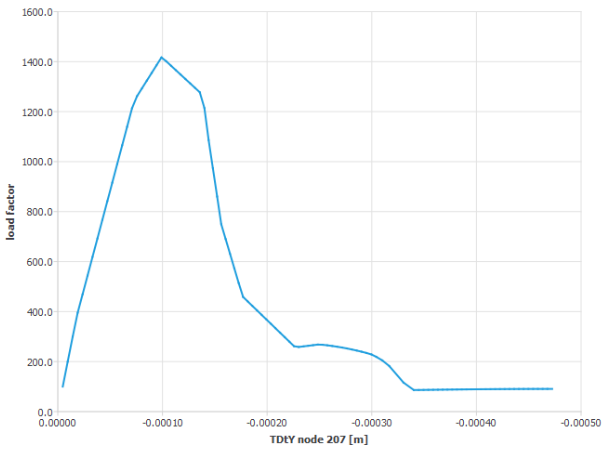

Figure 109 load-displacement curve D=150 for discrete mode

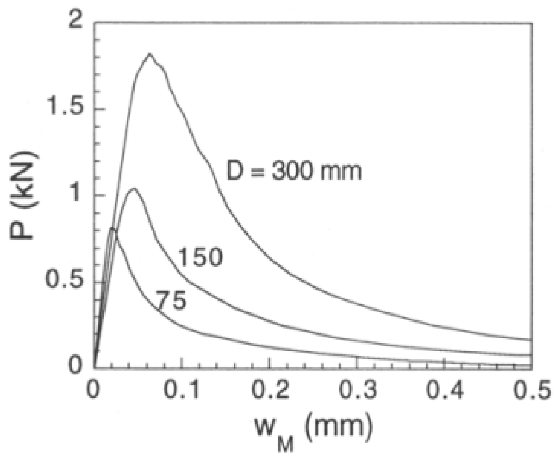

Figure 110 load-crack opening curves. (Ruiz, Elices, & Planas, 1998)

With this, an unreinforced concrete beam failing in flexure has been successfully modelled.

Experiment 1

Beam SC51 (Cavagnis, Ruiz, & Muttoni, 2015), a simply supported beam with distributed loading is modelled using the discrete cracking approach. Two different methods are used: Crack dilatancy and discrete cracking. The settings of both models can be found in this chapter. The additional settings required for the bond slip models are also given.

Crack dilatancy settings

The crack dilatancy settings (low) are shown in Table 21**.**

Table 21 Dilatancy settings used for experiment 1 (low)

Normal stiffness modulus	1e12 N/m^3
Shear stiffness modulus	1e11 N/m^3
Cubic compressive strength	6e7 N/m^2
Tensile strength	3e6 N/m^2
Maximum aggregate size	0.012 m
Fracture energy	137 N/m

It was found that rather low stiffness moduli had been used in the previous table. The stiffnesses are increased to a dummy stiffness determined by:

$$k_n = 1000 * \frac{E_c}{L}$$

$$k_t = 1000 * \frac{G_c}{L}$$

Where 'L' is the element size used in the mesh.

The settings for the updated crack dilatancy models are shown in Table 22 and are used instead.

Table 22 crack dilatancy settings used for experiment 1

Normal stiffness modulus	6.8e14 N/m^3
Shear stiffness modulus	3e14 N/m^3
Cubic compressive strength	6e7 N/m^2
Tensile strength	3e6 N/m^2
Maximum aggregate size	0.012 m
Fracture energy	137 N/m

Discrete crack settings

The settings required for the discrete crack are given in Table 23**.**

Table 23 Discrete crack settings used for experiment 1

Normal stiffness modulus	6.8e14 N/m^3
Shear stiffness modulus	3e14 N/m^3
Tensile strength	2.6e6 N/m^2
Fracture energy	137 N/m

Truss-bond slip settings

The values used for the truss-bond slip are based on (CEB-FIP Model code 1990, 1993) and are shown in Table 24**.**

Table 24 Truss-bond slip settings used for experiment 1

Normal stiffness modulus	2.2e12 N/m^3
Shear stiffness modulus	2.2e11 N/m^3
TAUmax	1.5e7 N/m^2
TAUf	2.3e6 N/m^2
S0	1e-6 m
S1	6e-4 m
S2	6e-4 m
S3	1e-3 m
Exponent alpha	0.4

Experiment 3

The tables containing settings of the different models are shown in Table 25

Crack dilatancy

Table 25 crack dilatancy settings used for experiment 3

Normal stiffness modulus	1.4e15 N/m^3
Shear stiffness modulus	7e14 N/m^3
Cubic compressive strength	6.95e7 N/m^2
Tensile strength	4.5e6 N/m^2
Maximum aggregate size	0.012 m
Fracture energy	154 N/m

Discrete crack

The settings for the Discrete crack are shown in Table 26

Table 26 Discrete crack settings used for experiment 3

Normal stiffness modulus	1.4e15 N/m^3
Shear stiffness modulus	7e14 N/m^3
Tensile strength	4.5e6 N/m^2
Fracture energy	154 N/m

Truss-bond slip

For this model, the CEB-Fib bond slip models have convergence issues, for which reason the Doerr model is used with the following settings:

Table 27 Truss-bond slip settings used for experiment 3

Normal stiffness modulus	3.75e12 N/m^3
Shear stiffness modulus	3.75e11 N/m^3
Parameter c	9e6 N/m^2
Shear slip at plateau	6e-5 m

Appendix D. Plasticity approach

The following tables contain the angles found using the plasticity approach. The base values are found in option 2. Only one variable can deviate from the base values at a time. As example, when the effect of the shear span a is investigated (for sigma=0), the angles are 22.4°, 16.5° and 13.1° for a=2, a=5 and a=10 respectively, while all other variables remain at their base values (found as option 2).

Over-reinforced

Table 28 the effect of changing a single variable on the crack angle of a simply supported beam, in case where sigma =0

Changed variable	Option 1	Option 2 (base values)	Option 3	θ1 [°]	θ2 [°]	θ3 [°]
a [m]	2	5	10	22.4	16.5	13.1
h [m]	0.2	0.5	1.0	12.0	16.5	20.1
d [m]	0.135	0.4	0.3	16.5	16.5	16.5
f_c [MPa]	30	60	80	15.9	16.5	16.0
ρ [%]	1	2	5	17.6	16.5	14.6

Table 29 the effect of changing a single variable on the crack angle of a simply supported beam, in case where sigma = 10

Changed variable	Option 1	Option 2 (base values)	Option 3	θ1 [°]	θ2 [°]	θ3 [°]
a [m]	2	5	10	33.9	19.6	14.0
h [m]	0.2	0.5	1.0	14.4	19.6	22.2
d [m]	0.135	0.4	0.3	16.3	19.6	18.3
f_c [MPa]	30	60	80	19.0	19.6	18.4
ρ [%]	1	2	5	21.7	19.6	16.4

Table 30 the effect of changing a single variable on the crack angle of a simply supported beam (uniform load), in case where sigma = 0

Changed variable	Option 1	Option 2 (base values)	Option 3	θ1 [°]	θ2 [°]	θ3 [°]
a [m]	2	5	10	27.9	20.0	15.9
h [m]	0.2	0.5	1.0	14.5	20.0	24.9
d [m]	0.135	0.4	0.3	20.0	20.0	20.0
f_c [MPa]	30	60	80	19.3	20.0	19.4
ρ [%]	1	2	5	21.4	20.0	17.8

Table 31 the effect of changing a single variable on the crack angle of a simply supported beam (uniform load), in case where sigma = 10

Changed variable	Option 1	Option 2 (base values)	Option 3	θ1 [°]	θ2 [°]	θ3 [°]
a [m]	2	5	10	53.8	27.4	18.5
h [m]	0.2	0.5	1.0	20.0	27.4	32.9
d [m]	0.135	0.4	0.3	20.7	27.4	24.6
f_c [MPa]	30	60	80	27.5	27.4	24.9
ρ [%]	1	2	5	30.9	27.4	22.2

Table 32 the effect of changing a single variable on the crack angle of a continuous beam, in case where sigma =0

Changed variable	Option 1	Option 2 (base values)	Option 3	θ1 [°]	θ2 [°]	θ3 [°]
L [m]	4	10	20	28.0	20.4	16.1
h [m]	0.2	0.5	1.0	14.9	20.4	24.9
d [m]	0.135	0.4	0.3	20.4	20.4	20.4
f_c [MPa]	30	60	80	19.6	20.4	19.7
ρ [%]	1	2	5	21.7	20.4	18.1

Table 33 the effect of changing a single variable on the crack angle of a continuous beam, in case where sigma =10

Changed variable	Option 1	Option 2 (base values)	Option 3	θ1 [°]	θ2 [°]	θ3 [°]
L [m]	4	10	20	54.4	28.2	18.9
h [m]	0.2	0.5	1.0	20.8	28.2	32.9
d [m]	0.135	0.4	0.3	21.1	28.2	25.2
f_c [MPa]	30	60	80	28.4	28.2	25.6
ρ [%]	1	2	5	31.9	28.2	22.8

Table 34 the effect of changing a single variable on the crack angle of a continuous beam (uniform load), in case where sigma = 0

Changed variable	Option 1	Option 2 (base values)	Option 3	θ1 [°]	θ2 [°]	θ3 [°]
L [m]	4	10	20	28.7	21.4	17.2
h [m]	0.2	0.5	1.0	15.9	21.4	25.6
d [m]	0.135	0.4	0.3	21.4	21.4	21.4
f_c [MPa]	30	60	80	20.5	21.4	20.7
ρ [%]	1	2	5	22.9	21.4	18.8

Table 35 the effect of changing a single variable on the crack angle of a continuous beam (uniform load), in case where sigma = 10

Changed variable	Option 1	Option 2 (base values)	Option 3	θ1 [°]	θ2 [°]	θ3 [°]
L [m]	4	10	20	63.1	32.0	21.2
h [m]	0.2	0.5	1.0	24.4	32.0	35.6
d [m]	0.135	0.4	0.3	22.5	32.0	27.9
f_c [MPa]	30	60	80	32.7	32.0	28.5
ρ [%]	1	2	5	36.7	32.0	25.0

Not over-reinforced

Table 36 the effect of changing a single variable on the crack angle of a simply supported beam, in case where sigma =0 for a non-over-reinforced beam

Changed variable	Option 1	Option 2 (base values)	Option 3	θ1 [°]	θ2 [°]	θ3 [°]
a [m]	2	5	10	27.2	20.0	15.9
h [m]	0.2	0.5	1.0	14.6	20.0	24.4
d [m]	0.135	0.4	0.3	20.0	20.0	20.0
f_c [MPa]	30	60	80	16.5	20.0	21.0
ρ [%]	1	2	5	26.0	20.0	14.8

Table 37 the effect of changing a single variable on the crack angle of a simply supported beam, in case where sigma =10 for a non-over-reinforced beam

Changed variable	Option 1	Option 2 (base values)	Option 3	θ1 [°]	θ2 [°]	θ3 [°]
a [m]	2	5	10	48.7	27.1	18.5
h [m]	0.2	0.5	1.0	20.17	27.1	31.5
d [m]	0.135	0.4	0.3	20.6	27.1	24.4
f_c [MPa]	30	60	80	20.3	27.1	28.3
ρ [%]	1	2	5	43.7	27.1	16.6

Table 38 the effect of changing a single variable on the crack angle of a simply supported beam (uniform load), in case where sigma =0 for a non-over-reinforced beam

Changed variable	Option 1	Option 2 (base values)	Option 3	θ1 [°]	θ2 [°]	θ3 [°]
a	2	5	10	33.8	24.3	19.3
h	0.2	0.5	1.0	17.7	24.3	30.2
d	0.135	0.4	0.3	24.3	24.3	24.3
fc	30	60	80	20.0	24.3	25.5
ρ	1	2	5	31.6	24.3	17.9

Table 39 the effect of changing a single variable on the crack angle of a simply supported beam (uniform load), in case where sigma =10 for a non-over-reinforced beam

Changed variable	Option 1	Option 2 (base values)	Option 3	θ1 [°]	θ2 [°]	θ3 [°]
a	2	5	10	72.2	39.2	25.3
h	0.2	0.5	1.0	29.4	39.2	45.8
d	0.135	0.4	0.3	26.6	39.2	34.0
fc	30	60	80	29.7	39.2	40.2
ρ	1	2	5	61.1	39.2	22.5

Table 40 the effect of changing a single variable on the crack angle of a continuous beam, in case where sigma =0 for a non-over-reinforced beam

Changed variable	Option 1	Option 2 (base values)	Option 3	θ1 [°]	θ2 [°]	θ3 [°]
L [m]	4	10	20	34.0	24.7	19.6
h [m]	0.2	0.5	1.0	18.1	24.7	30.2
d [m]	0.135	0.4	0.3	24.7	24.7	24.7
f_c [MPa]	30	60	80	20.4	24.7	25.9
ρ [%]	1	2	5	32.1	24.7	18.2

Table 41 the effect of changing a single variable on the crack angle of a continuous beam, in case where sigma =10 for a non-over-reinforced beam

Changed variable	Option 1	Option 2 (base values)	Option 3	θ1 [°]	θ2 [°]	θ3 [°]
L [m]	4	10	20	72.7	40.5	26.0
h [m]	0.2	0.5	1.0	30.7	40.5	45.8
d [m]	0.135	0.4	0.3	27.3	40.5	35.1
f_c [MPa]	30	60	80	30.7	40.5	41.4
ρ [%]	1	2	5	62.7	40.5	23.1

Table 42 the effect of changing a single variable on the crack angle of a continuous beam (uniform load), in case where sigma = 0 for a non-over-reinforced beam

Changed variable	Option 1	Option 2 (base values)	Option 3	θ1 [°]	θ2 [°]	θ3 [°]
L [m]	4	10	20	35.0	26.2	21.0
h [m]	0.2	0.5	1.0	19.4	26.2	31.3
d [m]	0.135	0.4	0.3	26.2	26.2	26.2
f_c [MPa]	30	60	80	21.4	26.2	27.5
ρ [%]	1	2	5	34.3	26.2	19.0

Table 43 the effect of changing a single variable on the crack angle of a continuous beam (uniform load), in case where sigma = 10 for a non-over-reinforced beam

Changed variable	Option 1	Option 2 (base values)	Option 3	θ1 [°]	θ2 [°]	θ3 [°]
L [m]	4	10	20	83.8	47.3	30.1
h [m]	0.2	0.5	1.0	37.1	47.3	51.6
d [m]	0.135	0.4	0.3	29.7	47.3	40.2
f_c [MPa]	30	60	80	35.7	47.3	48.0
ρ [%]	1	2	5	71.6	47.3	25.5

Appendix E. Lattice models

Lattice models were considered as an alternative method of modelling concrete and its cracking behaviour. The lattice models used in this chapter are like those found in (Aydin, Tuncay, & Binici, 2019). Explicit time integration is used, which is inherently stable and will, unlike FEA, not show convergence problems.

The model was designed for reinforced concrete and does not have a built-in function to apply prestressing. To make it possible to investigate prestressed beams, prestress is added to the model as a pair of external axial forces. It should be noted that this is merely an attempt to imitate the prestressing behaviour. Due to the nature of the model, the external forces will cause a 2nd order effect, causing additional moments. As prestressing is applied externally, the prestressing 'tendon' is also not loaded and behaves like regular reinforcement. For these reasons it is questioned whether the lattice models could be applied to prestressed beams.

Due to the time constraints of this thesis no detailed analysis was performed and only two different beams are investigated. The first beam is a fictional, simply supported, rectangular prestressed beam. The second beam is based on the experiment done on a prestressed T-beam found in (Huber, Huber, & Kollegger, 2018). The capacities found with the lattice models are compared to the shear capacity estimated using FprEN 1992-1-1, as well as the experimental value for the second beam. The crack patterns are also investigated, as the critical crack location is of high importance in this thesis.

The input parameters of the model other than the geometric properties are: The concrete tensile strength f_t, concrete Young's modulus E_c, concrete fracture energy G_F, steel yield strength f_y, steel ultimate strength f_t, steel Young's modulus E_s, and the ultimate steel strain ε_u.

The author of this thesis did not create the models himself due to time and copyright constraints. Instead, the Lattice Models investigated have been setup by Beyazit Aydin, who shared the results of the analysis.

Fictional beam

Unlike FEM, the lattice model requires that the geometry and reinforcement locations coincide with the mesh nodes. This also means that tendons cannot be modelled as a curve. To prevent high computational costs, or beam properties that do not coincide with the mesh, a fictional beam was modelled with a small span of 4m.

The fictional beam has a span of 4m with a concentrated load in the centre of the beam. The height of the beam is 400 mm, and it has a 320 mm width. Longitudinal reinforcement, with $A_{sl,bot}$=$A_{sl,top}$= 760 mm^2, is present at both the top and bottom of the beam, located at 40mm from the upper and lower fibre of concrete. Central prestressing steel is also added with an area of A_p=300 mm^2. The amount of shear reinforcement is d6/320.

Table 44 Material properties fictional beam

E_c	(Youngs modulus concrete)	35220	[Mpa]
E_s	(Youngs modulus steel)	200000	[Mpa]
f_{ct}	(concrete tensile strength)	3.51	[Mpa]
f_y	(steel yield strength)	500	[Mpa]
f_t	(steel ultimate strength)	650	[Mpa]
G_f	(concrete fracture energy)	141	[N/mm]
ε_t	(steel ultimate strain)	5	[%]

Three prestressing levels are investigated; P=0 kN, P=300 kN and P=405 kN with a mesh size of 40mm and external axial prestressing loads. The crack patterns of the models are shown below in Figure 111**.**

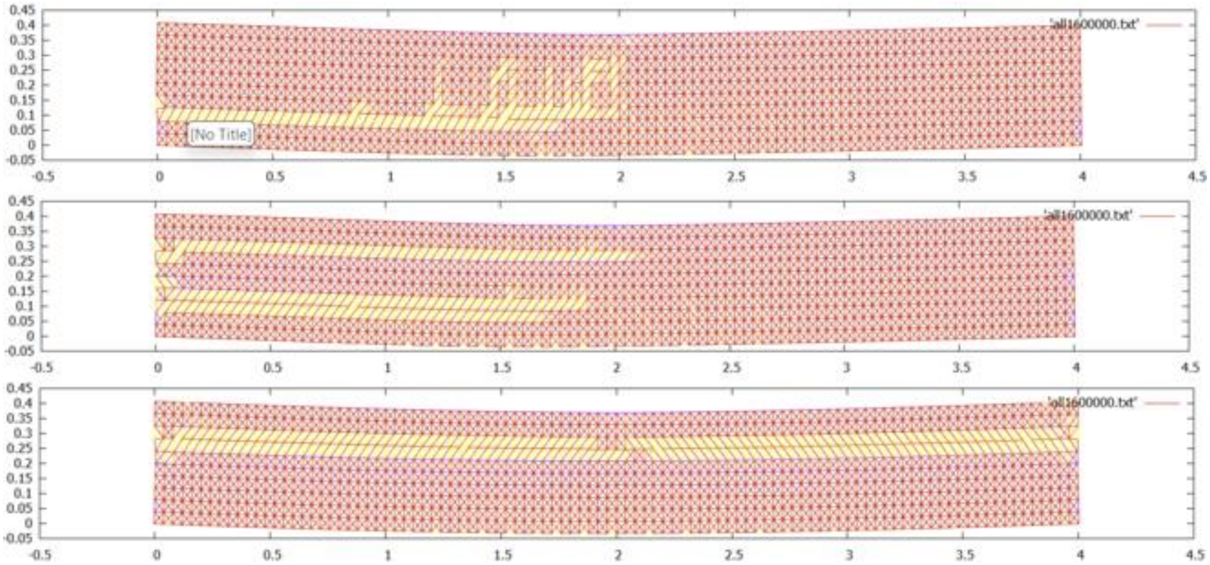

Figure 111 Crack patterns lattice models P= 0 (top), P=300 kN (middle) and P=405 kN (bottom) for mesh size of 40mm and concentrated external prestressing

It is observed that for the prestressed beams, large horizontal cracks occur instead of the expected shear cracks. In an attempt to prevent the unexpected horizontal cracks from forming, the mesh size is reduced to 20mm, and the calculations are repeated. The crack patterns of the model with the refined mesh size and concentrated prestressing are show in Figure 112.

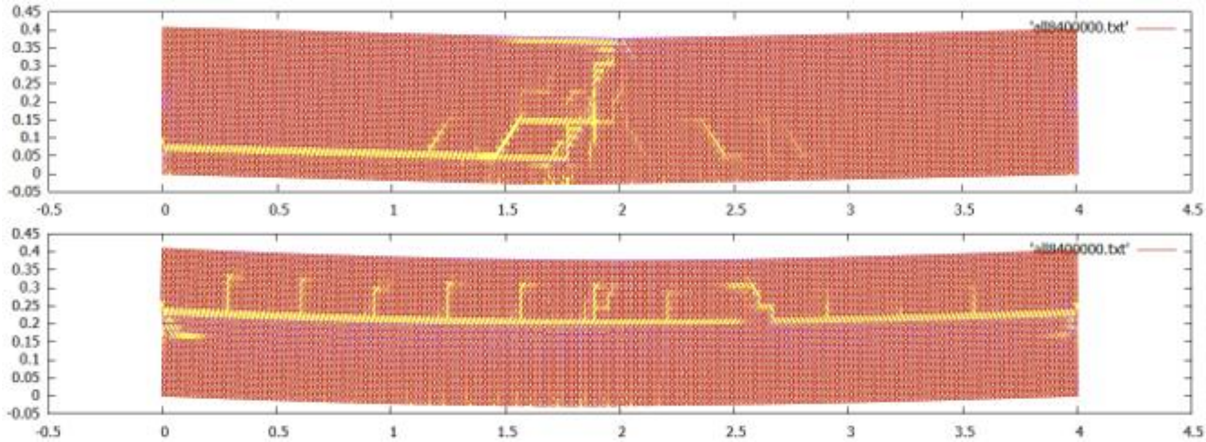
Figure 112 Crack patterns lattice models P=300 kN (top), P=405 kN (bottom) for mesh size of 20mm and concentrated external prestressing

It is found that using a smaller mesh did improve the crack patterns for P=300 kN, but the model with P=405 kN still shows unexpected behaviour. For this reason, another change has been made to improve the results. As the horizontal cracks are likely caused by the external concentrated prestressing loads, a distributed prestressing along the edges of the beam may provide better results. Crack patterns found using a distributed prestressing load instead of a concentrated prestressing load for P=405 kN are shown in Figure 113**.**

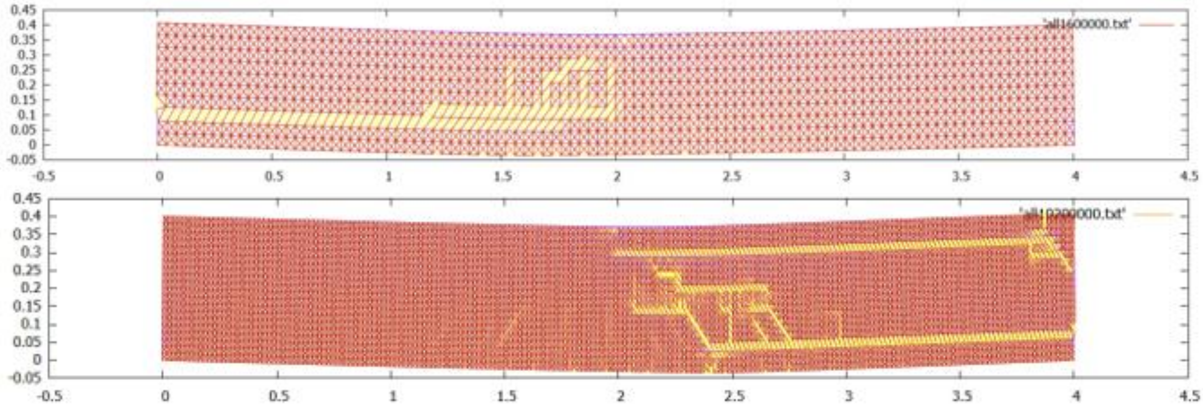

Figure 113 Crack patterns lattice models P=405 kN, for mesh size 40mm (top) and 20mm (bottom)

It was found that the crack patterns using distributed prestressing are much more realistic and clearly show shear cracks. For the most accurate results it is therefore concluded that prestressing should be applied in a distributed manner and with a small enough mesh.

The capacities found with the lattice models, have been compared to the capacities found using FprEN 1992-1-1 in Table 45. It is found that the FprEN 1992-1-1 predicts lower capacities, which is expected as it is a conservative model. The capacities in the table indicated with * are likely inaccurate as they are found in the models where the unexpected crack patterns occurred.

Table 45 Shear capacities found with the lattice models and FprEN 1992-1-1

Load Capacity for:	P=0	P=300 kN	P=405 kN	P=405 kN (distributed)
Mesh 40 mm	345 kN	375 kN*	310 kN*	360 kN
Mesh 20 mm	290 kN	300 kN	110 kN*	340 kN
FprEN 1992-1-1	238	254	260	(260)

The load-displacement curves for a mesh size of 40 mm and with a concentrated axial load are given below, in Figure 114.

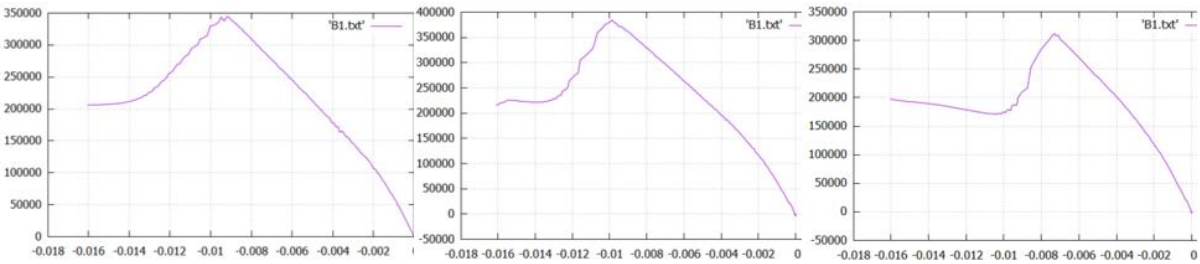

Figure 114 Load-Displacement curves lattice models P=0 (left), P=300 kN (middle), P=405 kN (right) for a mesh of 40 mm and concentrated prestressing.

The load-displacement curves for a mesh size of 20mm with a concentrated axial load are given in Figure 115.

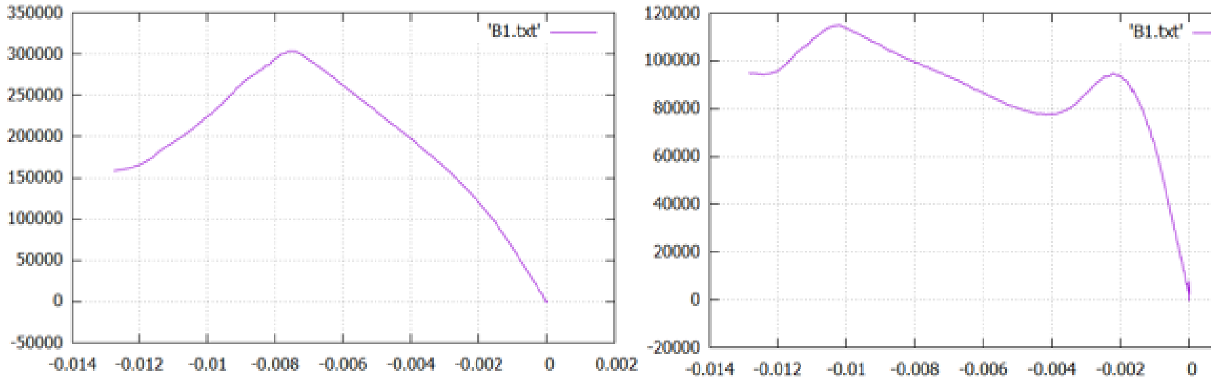

Figure 115 Load-Displacement curves lattice models P=300 kN (left) and P=405 kN (right) for a mesh of 20 mm

The load-displacement curves for P=405 kN with a distributed prestressing is shown in the figure below, Figure 116**.**

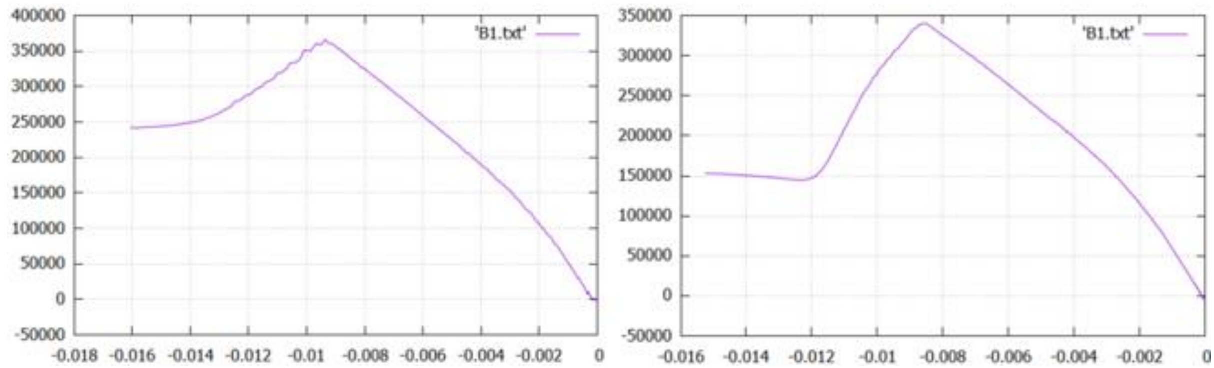

Figure 116 Load-Displacement curves lattice models P=405 kN, mesh size of 40 mm (left), and 20 mm (right) and distributed prestressing

Experiment 2

To investigate if the lattice models can estimate accurate capacities and crack patterns for prestressed beams, an experiment from (Huber, Huber, & Kollegger, 2018) has been modelled. The beam properties have been discussed in '4.3 Experiment 2 modelling simply supported prestressed T-beam' and are not repeated here. The curved prestressing tendon has been approximated by linear elements in the lattice models.

The crack patterns of two models are compared to the cracks found in the experiment. The first model uses a distributed prestress along the entire edge of the beam. The second model distributes the prestressing forces over the bottom half of the edge. The crack patterns are as shown in Figure 117. Although similar cracks can be observed between the experiment and the lattice models around the load point, the models were unable to find the critical shear crack observed in the experiment.

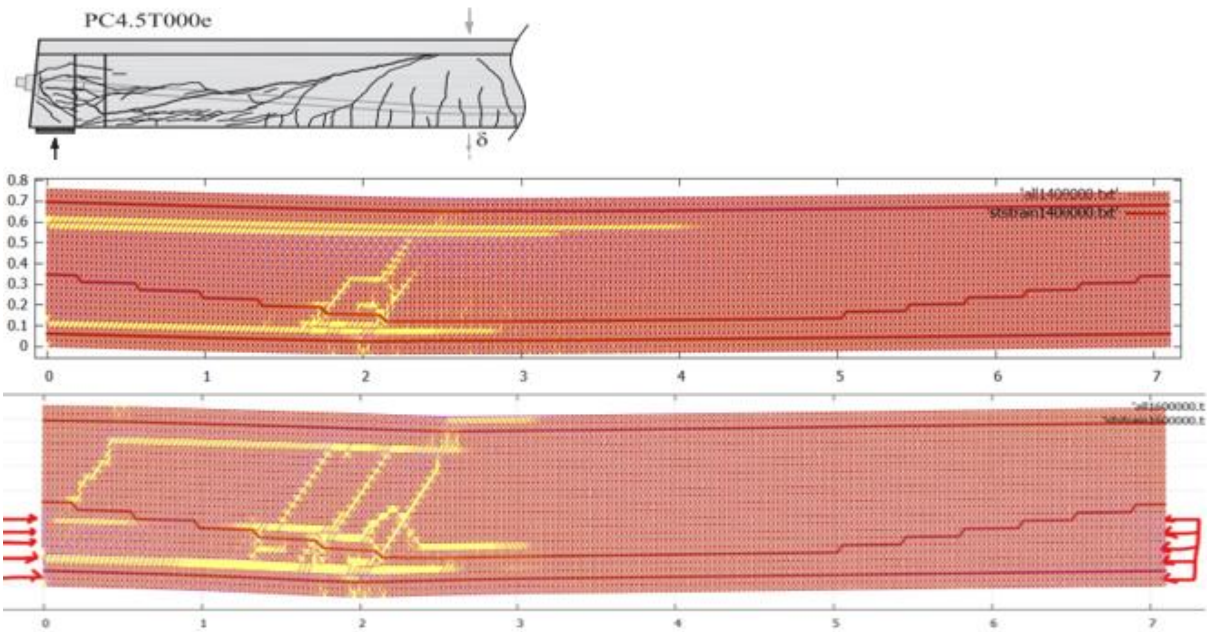

Figure 117 Crack patterns experiment (Huber, Huber, & Kollegger, 2018) (top) and lattice models, distributed prestress over full edge (middle), distributed prestress over bottom edge (bottom), for mesh size of 20 mm

The capacities found using the lattice models are compared with the experimental value and the estimate from FprEN 1992-1-1 in Table 46. The lattice models seem to perform reasonably well and estimate a capacity between the experimental value and the Eurocode estimate.

Table 46 Shear capacities found with the lattice models, FprEN 1992-1-1 and the experiment

Model	Shear capacity
Lattice model (distributed along full edge)	510 kN
Lattice model (distributed along bottom half of the edge)	600 kN
FprEN 1992-1-1	484 kN
Experiment	709 kN

The load-displacement curves for the lattice models are given below, in Figure 118**.**

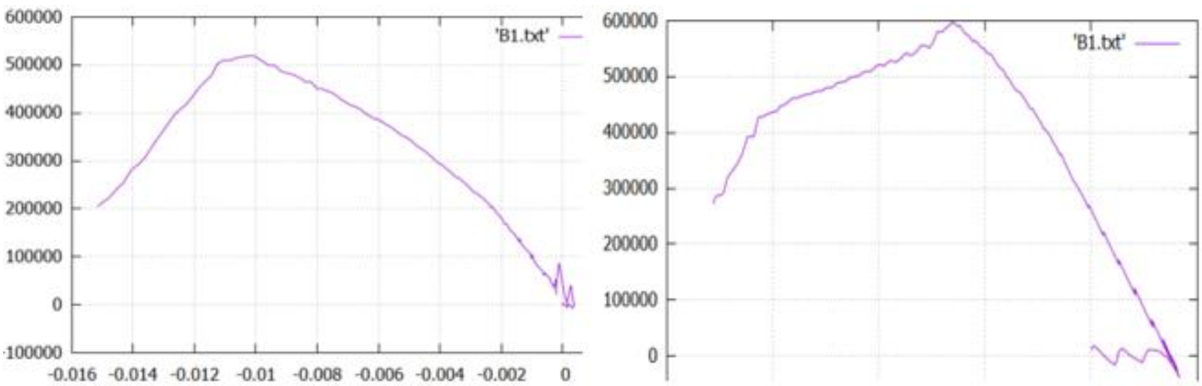

Figure 118 Load-Displacement curves lattice models; distributed prestress over full edge (left) and distributed prestress over bottom edge (right) for a mesh size of 20mm

Concluding remarks lattice models

Although reasonable capacities were obtained using lattice models for prestressed beams, the crack patterns found, using distributed or concentrated axial loads as prestress, were not deemed adequate for the purpose of this thesis. However, only a limited number of alternatives is investigated, and it may be possible to get better results if different assumptions are used.